UNIVERSITÀ DEGLI STUDI DI MILANO

SCUOLA DI DOTTORATO
FISICA, ASTROFISICA E FISICA APPLICATA

DIPARTIMENTO
FISICA

CORSO DI DOTTORATO DI RICERCA IN
FISICA, ASTROFISICA E FISICA APPLICATA
CICLO XXIII

Quantum Estimation and Discrimination in Continuous Variable and Fermionic Systems

Settore Scientifico Disciplinare FIS/03

Tesi di Dottorato di:
Carmen Invernizzi

Supervisore:
Prof. Matteo G. A. Paris

Coordinatore:
Prof. Marco BERSANELLI

Anno Accademico 2010 - 2011

Contents

Introduction

In quantum information and quantum computing the information of a quantum system is encoded in its state [1]. The knowledge of the state is equivalent to know the results of the measurements performed on the system. In particular, the state of a quantum system encodes the values of some quantities that are not directly accessible either in principle or due to experimental impediments. This is the case of relevant quantities like the entanglement and purity that cannot correspond to any observable [2] or the coupling constant of a many-body Hamiltonian [3] and the noise parameter in open quantum systems [4]. In all these cases, one has to resort to indirect measurement and infer the value of the quantity of interest from its influence on a given probe. Indeed, when estimating an unknown parameter in a quantum system, we typically prepare a probe, let it interact with the system, and then measure the probe. If the physical mechanism which governs the system dynamics is known, we can deduce the value of the parameter by comparing the input and output states of the probe [5]. This process is known as quantum parameter estimation and it can be properly addressed in the framework of the quantum estimation theory (QET) or quantum discrimination theory (QDT) according to the parameter belongs to a continuous or to a discrete set of values.

The powerful theoretical framework of quantum information can be applied to very different physical systems, to discrete and continuous variable systems as for example simple qubits or light modes, as well as to many-body systems either bosonic or fermionic.

The aim of this thesis is to characterize quantum states and parameters of systems that are of particular interest for quantum technologies. In the first part of the thesis, we will consider infinite-dimensional systems, the so-called continuous variable systems, and in particular Gaussian states that are a very significant class of quantum states for two reasons. First, they have a very simple mathematical characterization that allows for the derivation of otherwise highly nontrivial results and second, they describe accurately states of light that are realized with current technology. In this framework, we address the

estimation of quantities characterizing single-mode Gaussian states as the displacement and squeezing parameter and we study the improvement in the parameter estimation by introducing a Kerr nonlinearity. Moreover, we address the discrimination of noisy channels by means of Gaussian states as probe states and consider two problems: the detection of a lossy channel against the alternative hypothesis of an ideal lossless channel and the discrimination of two Gaussian noisy channels.

In the last part of the thesis, we consider a paradigmatic example of a many-body system which undergoes a second order quantum phase transition: the quantum Ising model in a transverse magnetic field. We will exploit the recent results about the geometric approach to quantum phase transitions to derive the optimal estimator of the coupling constant of the model at zero temperature in both cases of few spins and in the thermodynamic limit. We also analyze the effects of temperature and the scaling properties of the estimator of the coupling constant. Finally, we consider the discrimination problem for two ground states or two thermal states of the model.

The thesis is organized in three chapters. In the first chapter we introduce the basic notions that we need to proceed with the quantum state estimation and discrimination. The second and third chapters are devoted to continuous variable systems and to fermionic systems respectively. In both we address the estimation of some quantities of interest for those systems and the discrimination between quantum states.

List of publications

1. C. Invernizzi, M. Korbman, L. Campos Venuti, and M. G. A. Paris, *Optimal quantum estimation in spin systems at criticality*, Phys. Rev. A **78**, 042106 (2008).

2. P. Facchi, G. Florio, C. Invernizzi, and S. Pascazio, *Entanglement of two blocks of spins in the quantum Ising model*, Phys. Rev. A **78**, 052302 (2008).

3. M. G. Genoni, C. Invernizzi, and M. G. A. Paris, *Enhancement of parameter estimation by Kerr interaction*, Phys. Rev. A **80**, 033842 (2009).

4. C. Invernizzi and M. G. A. Paris, *The discrimination problem for two ground states or two thermal states of the quantum Ising model*, J. Mod. Opt. **57**, 198 (2010).

5. C. Invernizzi, M. G. A. Paris and S. Pirandola, *Improved detection of lossy channels by two-mode correlated probes*, to be submitted.

6. C. Invernizzi, M. G. A. Paris and S. Pirandola, *Quantum discrimination of Gaussian noise channels*, to be submitted.

1

Estimation and discrimination of quantum states

In this chapter we introduce the basic concepts and notations used throughout the thesis. We start in section 1.1, by reviewing the fundamental postulates of quantum mechanics given in terms of density matrices, positive operator valued measures and completely positive maps. We then consider some distinguishability measures for quantum states that are widely used in quantum information. In section 1.3 we introduce the fundamental notions about local quantum estimation theory, in particular we review the classical and quantum Cramer-Rao bound along with the definition of the classical and quantum Fisher information. Estimability of a parameter will be then defined in terms of the quantum signal-to-noise ratio and the number of measurements needed to achieve a given relative error. We also discuss the relation existing between quantum estimation and the geometric properties of the Hilbert space, by showing the connections between the quantum Fisher information and the Bures distance. Finally, in section 1.4, we present the main concepts of quantum state discrimination theory and we concentrate on the Bayes minimum error probability strategy by defining the error probability. We review the classical and quantum Chernoff bound and then consider the connections between the quantum Chernoff bound and some distance measures as the fidelity and the trace distance. We also address the Naiman-Pearson strategy as an alternative approach of quantum state discrimination which basically consists into maximizing the detection probability at fixed false alarm.

1.1 Basics of quantum mechanics

Quantum theory is a mathematical model of the physical world. It does provide a mathematical and conceptual framework for the development of the laws to which a physical system must obey through some postulates [1, 6, 7]. They, for example, assign an operational meaning to the concept of *quantum system* that is a useful abstraction, but it does not really exist in nature [8]. In general a quantum system is defined by an *equivalence class of preparations*. For example, there are many equivalent macroscopic procedures for producing what we call a photon, or a free hydrogen atom, etc. The equivalence of different preparations procedures should be verifiable by suitable tests. Quantum states can be given a clear operational definition, based on the notion of test. A state is characterized by the probabilities of the various outcomes of every conceivable test.

1.1.1 The postulates

The following postulates give a connection between the physical world and the mathematical formalism of quantum mechanics.

1. Each quantum mechanical system is associated to a Hilbert space $\mathcal{H}$.

   A Hilbert space is a complex vector space whose vectors are denoted with $|\psi\rangle$. It has an inner product $\langle\psi|\phi\rangle$ that maps a pair of vectors to $\mathbb{C}$ with the following properties:

   - Positivity: $\langle\psi|\psi\rangle > 0$ for $|\psi\rangle = 0$
   - Linearity: $|\phi\rangle(a|\psi_1\rangle + b|\psi_2\rangle) = a\langle\phi|\psi_1\rangle + b\langle\phi|\psi_2\rangle$
   - Skew symmetry:$\langle\phi|\psi\rangle = \langle\psi|\phi\rangle^*$

   Moreover, it is complete in the norm $\|\psi\| = \langle\psi|\psi\rangle^{1/2}$.

2. The physical states of a quantum mechanical system are described by statistical operators acting on the Hilbert space.

3. An observable is a property of the physical system that in principle can be measured. It is described by a self-adjoint operator acting on the Hilbert space.

   A self-adjoint operator A on a Hilbert space $\mathcal{H}$ is a linear operator $\mathcal{H} \to \mathcal{H}$ which satisfies

   $$\langle Ax|y\rangle = \langle x|Ay\rangle \tag{1.1}$$

for $x, y \in \mathcal{H}$. Self-adjoint operators on a finite dimensional Hilbert space $\mathbb{C}^n$ are $n \times n$ self-adjoint matrices. A self-adjoint matrix admits a spectral decomposition $A = \sum_i \lambda_i |x_i\rangle\langle x_i|$, where λ_i are the different eigenvalues of A and $E_i = |x_i\rangle\langle x_i|$ the orthogonal projection onto the subspace spanned by the eigenvectors corresponding to the eigenvalue λ_i. The E_i's satisfy

$$\begin{aligned} E_i E_j &= \delta_{ij} E_i \\ E_i^\dagger &= E_i \end{aligned} \tag{1.2}$$

Any density matrix ϱ can be written in the form

$$\varrho = \sum_i \lambda_i |x_i\rangle\langle x_i| \tag{1.3}$$

by means of unit vectors $|x_i\rangle$ and coefficients $\lambda_i \geq 0$, $\sum_i \lambda_i = 1$.

Quantum mechanics is not deterministic. If we prepare two identical systems in the same state and we measure the same observable on each, then the result of the *measurement* may not be the same. This indeterminism or stochastic feature is fundamental.

4. In quantum mechanics, the numerical outcome of a measurement of the observable A is an eigenvalue of A; right after the measurement, the quantum state is an eigenstate of A with the measured eigenvalue. If the quantum state just prior to the measurement is $|\psi\rangle$, then the outcome λ_i is obtained with probability

$$p(\lambda_i) = \langle\psi|E_i|\psi\rangle \tag{1.4}$$

and the state after the measurement becomes

$$|\psi_i\rangle = \frac{E_i|\psi\rangle}{\sqrt{p(\lambda_i)}} \tag{1.5}$$

5. The time evolution U_t of a quantum state is unitary; it acts on a quantum state $|\psi\rangle$ as:

$$|\phi(t)\rangle = U_t|\psi\rangle$$

and it is generated by a self-adjoint operator H called the Hamiltonian of the system $U_t = \exp\{-iHt\}$. The evolution of the state is given by the Schrodinger equation

$$\frac{d}{dt}|\psi(t)\rangle = -iH|\psi(t)\rangle. \tag{1.6}$$

These axioms provide a perfectly acceptable formulation of the quantum theory when we consider a close quantum system. Most of the time the quantum system is not close but it interacts with an environment and then the measurements are not orthogonal projections and the evolution is not unitary.

The density operator

The formalism of the density operator provides convenient means for describing quantum systems whose state is not completely known. Suppose a quantum system is in one of a number of states $\{|\psi_i\rangle\}$, where i is an index, with respective probabilities p_i. We shall call $\{p_i, |\psi_i\rangle\}$ an *ensemble* of pure states. The density operator for the system is defined by the equation (1.3) as $\varrho = \sum_i p_i |\psi_i\rangle\langle\psi_i|$ and it has the following properties

- ϱ is self-adjoint
- ϱ is positive
- $\mathrm{Tr}[\varrho] = 1$.

If the system is in a pure state $|\psi\rangle$, then $\varrho = |\psi\rangle\langle\psi|$ and we have that $\varrho^2 = \varrho$. If the state of the system is not pure (mixed state), then ϱ describes an ensemble of pure states and $\varrho^2 \neq \varrho$.

1.1.2 Generalized measurement

Let us examine the properties of a generalized measurement that can be realized on the system A by performing orthogonal measurements on a larger system that contains A. Consider that the system A is extended to a tensor product $\mathcal{H}_A \otimes \mathcal{H}_B$ and that the system A and B are described by the density operators ϱ_A and σ_B respectively. Suppose that the two states are coupled with the unitary evolution U and that after the interaction a measurement on the system B is performed by the operator $\mathbb{I}_A \otimes E$. The probability for the outcome i of such a measurement in given by

$$\begin{aligned} p_i =& \mathrm{Tr}_{AB}[U(\varrho_A \otimes \sigma_B)U^\dagger \mathbb{I}_A \otimes E_i] \\ =& \mathrm{Tr}_{AB}[(\varrho_A \otimes \sigma_B)U^\dagger \mathbb{I}_A \otimes E_i U] \\ =& \mathrm{Tr}_A[\varrho_A \Pi_i] \end{aligned} \tag{1.7}$$

where we have introduced the operator Π_i

$$\Pi_i = \mathrm{Tr}_B[\mathbb{I}_A \otimes \sigma_B U^\dagger \mathbb{I}_A \otimes E_k U] \tag{1.8}$$

which is an operator that acts on the Hilbert space of the system A only, allowing us to obtain the statistic of a measure without considering the whole quantum system. Here Tr_A and Tr_B denote the partial traces over the two subsystems. The operators Π_i are positive operators, i.e. Hermitian operators with nonnegative eigenvalues

$$\Pi_i \geq 0, \tag{1.9}$$

because they are obtained from the partial trace of two positive operators. Moreover they satisfy the relation

$$\sum_i \Pi_i = \mathbb{I}. \tag{1.10}$$

These two properties are the defining properties of a POVM (Positive Operator-Valued Measure). Note that as opposed to the case of a projective measurement (1.2), the set of operators satisfying (1.9) and (1.10) do not need to commute with each other.

There exists a theorem which assures that any POVM can be realized by considering orthogonal measurements in a space larger that $\mathcal{H}_A$.

Theorem 1 Naimark [9]: For any given POVM $\sum_x \Pi_x = \mathbb{I}$, $\Pi_x \geq 0$ on a Hilbert space $\mathcal{H}_A$, there exists a Hilbert space $\mathcal{H}_B$, a state $\varrho_B = |\omega_B\rangle\langle\omega_B|$, a unitary operaration U in $\mathcal{H}_A \otimes \mathcal{H}_B$ and a projective measurement P_x, $P_x P_{x'} = \delta_{xx'} P_x$ on $\mathcal{H}_\mathcal{B}$ such that

$$\Pi_x = \mathrm{Tr}_B[\mathbb{I} \otimes \varrho_B U^\dagger \mathbb{I} \otimes P_x U] \tag{1.11}$$

The meaning of the theorem is the following: in measuring a quantity of interest on a physical system, one generally deals with a larger system that involves additional degrees of freedom besides those of the system itself. These additional physical objects are usually referred to as the apparatus or the ancilla. The measured quantity may be always described by a standard observable on a larger Hilbert space describing both the system and the apparatus. When we trace out the degrees of freedom of the apparatus, we are generally left with a POVM rather than a projective measurement. Conversely, any POVM, i.e. a set of positive operators providing a resolution of the identity, describes a generalized measurement which may be always implemented as a standard measurement in a larger Hilbert space.

1.1.3 Completely positive map

Completely positive maps arise naturally in quantum information theory and in other situations in which one wishes to restrict attention to a quantum system that should properly be considered a subsystem of a larger system with which it interacts. In such situations, the system of interest is described by a Hilbert space $\mathcal{H}_\mathcal{A}$ and the larger system by $\mathcal{H}_\mathcal{A} \otimes \mathcal{H}_\mathcal{B}$. The state of the system is described by $\varrho \otimes |\phi\rangle\langle\phi|$ and it evolves by means of a unitary evolution U. We are interested in the system A alone, therefore after the

interaction, the density matrix of system A will be

$$\begin{aligned}\varrho'_A =& \mathrm{Tr}_B[U\varrho\otimes|\phi\rangle\langle\phi|U^\dagger] \\ =& \sum_s \langle s|U\varrho\otimes|\phi\rangle\langle\phi|U^\dagger|s\rangle \\ =& \sum_s \langle s|U|\phi\rangle\varrho_A\langle\phi|U^\dagger|s\rangle \\ =& \sum_s M_s\varrho_A M_s^\dagger \\ =& \mathcal{E}(\varrho) \end{aligned} \tag{1.12}$$

where $\{|s\rangle\}$ is an orthonormal basis for $\mathcal{H}_\mathcal{B}$ and $M_s = \langle s|U|\phi\rangle$ is an operator acting on $\mathcal{H}_\mathcal{A}$. From the unitarity of U it follows that

$$\sum_s M_s^\dagger M_s = \mathbb{I}. \tag{1.13}$$

Eq. (1.12) defines a linear map that takes linear operators to linear operators and it is called a *quantum operation*. Then we define a quantum operation a map $\mathcal{E} : \varrho \to \mathcal{E}(\varrho)$ which satisfies the following properties:

- $\mathcal{E}$ is linear
- $\mathcal{E}$ is trace preserving: $\mathrm{Tr}[\mathcal{E}(\varrho)] = \mathrm{Tr}\left[\sum_s M_s\varrho M_s^\dagger\right] = \mathrm{Tr}[\varrho\sum_s M_s^\dagger M_s] = \mathrm{Tr}[\varrho]$
- $\mathcal{E}$ preserves the hermiticity: if ϱ is self-adjoint then $\mathcal{E}(\varrho)$ is self-adjoint
- $\mathcal{E}$ is completely positive: considering any possible extension of $\mathcal{H}_\mathcal{A}$ to a tensor product $\mathcal{H}_\mathcal{B}$, then $\mathcal{E}$ is completely positive on $\mathcal{H}_\mathcal{A}$ if $\mathcal{E}\otimes\mathbb{I}_\mathcal{B}$ is positive for all such extensions.

Such maps are called the Kraus operator [10, 11] and they are important because they provide a formalism to discuss the theory of decoherence, the evolution of pure states into mixed states. Unitary evolution of ϱ_A is the special case in which there is only one term in the operator sum (1.12) and this is the only case where the operator $\mathcal{E}$ is invertible.

1.2 Distinguishability measures for quantum states

In this section we briefly review the notion of distance between quantum states or *statistical distance* [12], i.e. a distance measure that consider in its definition the statistical fluctuations associated with a sample of measurement. Because of this statistical error, one cannot distinguish between quantum preparations that have a difference in the probabilities smaller than the statistical fluctuations. Wootters first introduced this idea of

distinguishability in [13]: "If a finite ensemble of identically prepared quantum systems is analyzed by some fixed measuring device, the observed frequencies of occurrence of the various outcomes typically differ somewhat from the actual probabilities".

Classical theory gives us several ways to distinguish between two probability distributions and the idea of determining a quantum distinguishability measure is to start with the one specified by the classical theory. The probabilities are assumed to be the result of a measurement on the system described by the quantum states we want to distinguish and then quantum distinguishability is defined by varying over all the possible measurement on the system in order to find the one that makes the classical distinguishability the best it can be. This is the most natural way to discriminate between quantum states and it leads to the definition of the distance measures reviewed in what follows.

The distance $\mathcal{D}(\varrho_1, \varrho_2)$ between two arbitrary elements ϱ_1 and ϱ_2 of an Hilbert space has to satisfy the following properties:

- positive semi-definiteness

$$\mathcal{D}(\varrho_1, \varrho_2) \geq 0 \qquad \forall \varrho_1, \varrho_2 \tag{1.14}$$

$$\mathcal{D}(\varrho_1, \varrho_2) = 0 \qquad \varrho_1 = \varrho_2 \tag{1.15}$$

- symmetry

$$\mathcal{D}(\varrho_1, \varrho_2) = \mathcal{D}(\varrho_2, \varrho_1) \tag{1.16}$$

- triangular inequality

$$\mathcal{D}(\varrho_1, \varrho_2) \leq \mathcal{D}(\varrho_1, \varrho) + \mathcal{D}(\varrho, \varrho_2) \tag{1.17}$$

These three properties are always satisfied by an arbitrary norm $\|A\|$ and defining a distance as

$$\mathcal{D}(\varrho_1, \varrho_2) = K\|(\varrho_1 - \varrho_2)\|$$

where K is a multiplying constant.

Here we review the definitions and the properties of some distance measures that are widely used in quantum information: the *trace distance*, the *fidelity*, the *Bures distance* and the *quantum relative entropy* that is not a proper distance but it is widely used in the literature for its relevant properties.

1.2.1 Trace distance

The trace distance (also called the Kolmogorov distance) [1] is one of the most natural distance measures. It is intimately related to the problem of distinguishing two states in the following way: the value $\frac{1}{2} + \frac{1}{2}\mathcal{D}_{\mathrm{Tr}}(\varrho_0, \varrho_1)$ is the average success probability when distinguishing with a measurement two states ϱ_1 and ϱ_2 with equal a priori probability. The trace distance is defined by

$$\begin{aligned}\mathcal{D}_{\mathrm{Tr}}(\varrho_0, \varrho_1) =& \frac{1}{2}\Big\|(\varrho_0 - \varrho_1)\Big\| \\ =& \frac{1}{2}\mathrm{Tr}|(\varrho_0 - \varrho_1)|\end{aligned} \tag{1.18}$$

where $\|A\|$ is the trace norm defined as as

$$\|A\| = \mathrm{Tr}|A| = \mathrm{Tr}[\sqrt{A^\dagger A}] \tag{1.19}$$

The trace distance besides satisfying the three properties of a norm, has these additional properties

- $0 \leq \mathcal{D}_{\mathrm{Tr}}(\varrho_1, \varrho_2) \leq 1$
- subadditivity under tensor product, i.e.

$$\mathcal{D}_{\mathrm{Tr}}(\varrho_1 \otimes \sigma_1, \varrho_2 \otimes \sigma_2) \leq \mathcal{D}_{\mathrm{Tr}}(\varrho_1, \varrho_2) + \mathcal{D}_{\mathrm{Tr}}(\sigma_1, \sigma_2)$$

As we will see in the following, the connection between the definition (1.18) and the problem of distinguishing between two quantum states is provided by Helstrom [14] who solved a more general problem known as the binary decision problem in the theory of quantum hypothesis testing.

1.2.2 Fidelity

The *quantum fidelity* (or Uhlmann fidelity) between two arbitrary mixed quantum states ϱ_1 and ϱ_2 is defined in [16, 17] as

$$\mathcal{F}(\varrho_1, \varrho_2) = \left(\mathrm{Tr}\left[\sqrt{\sqrt{\varrho_1}\varrho_2\sqrt{\varrho_1}}\right]\right)^2. \tag{1.20}$$

It is a symmetric, non-negative, continuous, concave function of both states ϱ_1, ϱ_2 and also unitarily invariant. For pure states $\varrho_1 = |\psi_1\rangle\langle\psi_1|$ and $\varrho_2 = |\psi_2\rangle\langle\psi_2|$, the fidelity reduces to their overlap

$$\begin{aligned}\mathcal{F}(|\psi_1\rangle, |\psi_2\rangle) =& \left(\mathrm{Tr}\left[\sqrt{|\psi_1\rangle\langle\psi_1||\psi_2\rangle\langle\psi_2||\psi_1\rangle\langle\psi_1|}\right]\right)^2 \\ =& |\langle\psi_1|\psi_2\rangle|^2 \mathrm{Tr}\left[\sqrt{|\psi_1\rangle\langle\psi_1|}\right]^2 \\ =& |\langle\psi_1|\psi_2\rangle|^2,\end{aligned} \tag{1.21}$$

so it coincides with the standard distance given by the angle between rays in the Hilbert space, i.e. the so called *Fubini-Study distance* [18, 19]

$$\mathcal{D}_{FS}(|\psi_1\rangle, |\psi_2\rangle) = \cos^{-1}\sqrt{|\langle\psi_1|\psi_2\rangle|^2}. \tag{1.22}$$

Another function of the fidelity is the *Bures angle* or the *Bures length* [20] defined as

$$\mathcal{D}_A(\varrho_1, \varrho_2) = \cos^{-1}\sqrt{\mathcal{F}(\varrho_1, \varrho_2)}. \tag{1.23}$$

For pure states Eq. (1.23) reduces to the (1.22) one. In the following the Bures distance and the Quantum Chernoff Bound are considered which are strictly related to the fidelity. Moreover, as it will be explained in the next chapters, they are also endowed with a deep physical meaning and thanks to some theorems they will provide the means for the best estimation of physical parameters.

1.2.3 Bures distance

The Bures distance has been defined by Uhlmann as a natural extension of the Fubiny-Study metric to impure density matrices. Here we give an account of Uhlmann's results following [17] in a way that does not involve the theory of C^*-algebras as in [20].

Let be ϱ any mixed state in the Hilbert space $\mathcal{H}_1$. A purification of ϱ is any pure state $|\phi\rangle$ in any extended Hilbert space $\mathcal{H}_1 \otimes \mathcal{H}_2$ with the property that $\varrho = \mathrm{Tr}_2[|\phi\rangle\langle\phi|]$, i.e. a purification is any pure state having ϱ as the reduced density matrix for the subsystem.

Theorem 2 $\mathcal{F}(\varrho_1, \varrho_2) = \max|\langle\phi_1||\phi_2\rangle|^2$ *where the maximum is taken over all the purifications* $|\phi_1\rangle$ *and* $|\phi_2\rangle$ *of* ϱ_1 *and* ϱ_2 *respectively.*

Theorem 2 provides a kind of physical interpretation of Eq. (1.20) if we adopt the decoherence point of view, in which any mixed state is really describing the reduced state of a subsystem S entangled with an environment E, the total system $S + E$ being in a pure state. Then the fidelity that is also called *transition probability* provides a measure of distinguishability of the two mixed states in the case that we have no further information about the entanglement with E. By looking for the minimal distance between the purifications of ϱ_1 and ϱ_2 and solving the parallelity condition (that is a condition on the relative phase between the two states, see [20, 21] for details) one obtains [20, 22] the Bures distance [23] given in terms of the fidelity by

$$\begin{aligned}\mathcal{D}_B(\varrho_1, \varrho_2) =& \sqrt{2\left(1 - \mathrm{Tr}\left[\sqrt{\sqrt{\varrho_1}\varrho_2\sqrt{\varrho_1}}\right]\right)} \\ =& \sqrt{2\left(1 - \sqrt{\mathcal{F}(\varrho_1, \varrho_2)}\right)}\end{aligned} \tag{1.24}$$

while the infinitesimal Riemaniann metric resulting from this distance is given by ds_B^2 where

$$ds_B^2 = \mathcal{D}_B^2(\varrho, \varrho + d\varrho) = \mathrm{Tr}\, G^2 \varrho = \frac{1}{2}\mathrm{Tr}\, G\, d\varrho \tag{1.25}$$

where

$$d\varrho = G\,\varrho + \varrho\, G \tag{1.26}$$

and G is related to the solution $\dot{W} = GW$ to the extremization of $W(\lambda))$ where λ is an affine parameter and $\dot{} = d/d\lambda$.

The Bures metric

The Bures distance between two infinitesimally close density matrices of size N is computed in [24].

Let us set $\varrho_1 = \varrho$ and $\varrho_2 = \varrho + d\varrho$; then

$$\sqrt{\varrho_1^{1/2}\varrho_2\varrho_1^{1/2}} = \varrho + X + Y \tag{1.27}$$

where the matrix X is of order 1 in $d\varrho$ and Y of order 2. Squaring the precedent equation we obtain

$$\varrho^2 + \varrho^{1/2}d\varrho\varrho^{1/2} = \varrho^2 + X^2 + Y^2 + \varrho X + X\varrho + \varrho Y + Y\varrho + XY + YX \tag{1.28}$$

The terms Y^2, XY and YX are equal to zero because they are of order 3 and 4 in $d\varrho$ and we obtain to first and second order

$$\varrho^{1/2}d\varrho\varrho^{1/2} = X\varrho + \varrho X \qquad -X^2 = Y\varrho + \varrho Y \tag{1.29}$$

and in the basis $\varrho = \sum_n p_n |n\rangle\langle n|$ it becomes

$$X_{n,m} = d\varrho_{n,m}\frac{p_n^{1/2}p_m^{1/2}}{p_n + p_m} \qquad Y_{n,m} = -(X^2)_{n,m}\frac{1}{p_n + p_m} \tag{1.30}$$

where $O_{n,m} = \langle m|O|n\rangle$. Since $\mathrm{Tr}[\varrho] = 1$, hence $\mathrm{Tr}[d\varrho] = 0$ and $\mathrm{Tr}[X] = \mathrm{Tr}[d\varrho/2] = 0$, while

$$\mathrm{Tr}Y = -\sum_{n,m}\frac{1}{2p_n}|X_{n,m}|^2 = -\sum_{n,m}\frac{1}{4}\frac{|d\varrho_{n,m}|^2}{p_n + p_m} \tag{1.31}$$

and then we arrive to the Bures metric that is given by the square of Eq. (1.24), [24]

$$ds_B^2 = (\mathcal{D}_B(\varrho, \varrho + d\varrho))^2 = \frac{1}{2}\sum_{n,m}\frac{|d\varrho_{n,m}|^2}{p_n + p_m} = \frac{1}{2}\sum_{m,n}\frac{|\langle n|d\varrho|m\rangle|^2}{p_m + p_n}. \tag{1.32}$$

Eq.(3.96) can be cast in a form suitable for future elaborations by differentiating the density matrix: $d\varrho = \sum_n (dp_n|n\rangle\langle n| + p_n|dn\rangle\langle n| + p_n|n\rangle\langle dn|)$. Since $\langle n|m\rangle = \delta_{n,m}$, we have $d\langle n|m\rangle = \langle dn|m\rangle + \langle n|dm\rangle = 0$ and therefore $\langle dn|m\rangle = -\langle n|dm\rangle$. Using the above identities we have that $\langle n|d\varrho|m\rangle = \delta_{n,m}dp_n + (p_m - p_n)\langle n|dm\rangle$ and Eq. (3.96) becomes

$$ds_B^2 = \frac{1}{4}\sum_n \frac{dp_n^2}{p_n} + \frac{1}{2}\sum_{n\neq m} \frac{(p_m - p_n)^2}{p_n + p_m}|\langle n|dm\rangle|^2. \tag{1.33}$$

This relation is interesting because it tells apart the classical and the quantum correlations. The first term in Eq. (1.33) is the *Fisher-Rao* distance between the probability distributions $\{p_n\}_n$ and $\{p_n + dp_n\}_n$, whereas the second term takes into account the generic noncommutativity of ϱ and $\varrho' = \varrho + d\varrho$. Then we will refer to these two term as the classical and nonclassical one, respectively. When $[\varrho, \varrho'] = 0$, the problem becomes effectively classical and the Bures metric collapses to the Fisher-Rao one being this latter in general just a lower bound [13, 24]. Relevant papers about the relation of the Bures metric with the quantum information theory are due to Braunstein and Caves [25], Vedral and Plenio [26] and more recently a lot of work has been devoted to clarify the role of the Bures metric to characterize quantum phase transitions and to estimate Hamiltonian parameters. In the next chapters we will be more exhaustive about this subject.

1.2.4 Quantum relative entropy

Given two quantum states ϱ_1 and ϱ_2, the quantum relative entropy (QRE) is defined as

$$S(\varrho_1\|\varrho_2) = \mathrm{Tr}[\varrho_1(\log\varrho_1 - \log\varrho_2)] \tag{1.34}$$

As for its classical counterpart, the Kullback-Leibler divergence, it can be demonstrated that $0 < S(\varrho_1\|\varrho_2) < \infty$ if the support of the first state is contained in that of the second one $\mathrm{supp}\,\varrho_1 \leq \mathrm{supp}\,\varrho_2$ [6]. In particular, $S(\varrho_1\|\varrho_2) = 0$ iff $\varrho_1 = \varrho_2$. The quantum relative entropy is not a symmetric function of the two arguments.

In the following we will provide some motivation to study this quantity through the quantum Stein lemma which basically affirms that considering two states ϱ_1 and ϱ_2, the probability of confusing the two states after N measurements performed on ϱ_1 is given by

$$P_N(\varrho_1 \to \varrho_2) \sim \exp\{-NS(\varrho_1\|\varrho_2)\}. \tag{1.35}$$

1.3 Quantum state estimation

A state estimation technique is a method that provides the complete description of a system, i.e. it achieves the maximum possible knowledge of the state, thus allowing one to make the best predictions on the results of any measurement that may be performed on the system. Linearity of quantum mechanics [27] and the Heisemberg uncertainty principle [28] forbid one to devise a procedure consisting of multiple measurements that fully recovers the state of the system. Therefore it is not possible, even in principle, to determine the quantum state of a single system without having some prior knowledge about it [29]. This is consistent with the very definition of a quantum state which prescribes how to gain information of the state: many identical preparations taken from the same statistical ensemble are needed and different measurements should be performed on each of the copies. In the last decade an increasing interest has been devoted to the problem of inferring the state of a quantum system from measurements due to new developments in experimental techniques and to the progresses in quantum information technologies. Since the results of the measurements are subjected to fluctuations, one would like to eliminate or at least to minimize the corresponding errors. However, the precision of any measurement procedure is bounded by fundamental law of statistics and quantum mechanics, and in order to optimally estimate the value of some parameter, one has to exploit the tools provided by quantum estimation theory (QET) [6, 14, 30].

As a matter of fact, many quantities of interest do not correspond to quantum observables. Relevant examples are given by the entanglement or the purity of a quantum state [2] or the coupling constant of an interacting Hamiltonian. In these situations one needs to infer the value of the parameter through indirect measurements. There are two main paradigms in QET: *global* QET looks for the POVM minimizing a suitable cost functional, averaged over all possible values of the parameter to be estimated. The result of a global optimization is thus a single POVM, independent on the value of the parameter. On the other end, *local* QET looks for the POVM maximizing the Fisher information, thus minimizing the variance of the estimator, at a fixed value of the parameter [25, 31, 32]. Roughly speaking, one may expect local QET to provide better performances since the optimization concerns a specific value of the parameter, with some adaptive or feedback mechanism assuring the achievability of the ultimate bound.

Local QET has been successfully exploited to the estimation of quantum phase [33] and to estimation problems with open quantum systems: to optimally estimate the noise parameter of depolarizing [34] and for continuous variable systems to estimate the loss parameter of a quantum channel [35, 36, 37] as well as the position of a single photon [31].

Recently, the geometric structure induced by the Fisher information itself has been exploited to give a quantitative operational interpretation for multipartite entanglement [38] and to assess quantum criticality as a resource for quantum estimation [39]. In estimating the value of a parameter, one is led to define the Fisher information which represents an infinitesimal distance among probability distributions, and gives the ultimate precision attainable by an estimator via the Cramer-Rao theorem. Its quantum counterpart, the quantum Fisher information (QFI), is related to the degree of statistical distinguishability of a quantum state from its neighbours, and it turns out to be proportional to the *Bures metric* between quantum states [13, 17, 20, 23, 25, 40].

In the next section 1.3.1 we review the Cramer-Rao bound and in 1.3.2 the local QET. In particular we introduce classical and quantum Fisher information. We are interested in the ultimate bound on precision i.e. the smallest value of the parameter that can be discriminated, and to determine the optimal measurement achieving those bounds. Estimability of a parameter will be then defined in terms of the quantum signal-to-noise ratio and the number of measurements needed to achieve a given relative error. General formulas for the symmetric logarithmic derivative and the quantum Fisher information will be derived. In section 1.3.3 we present explicit formulas for sets of pure states and the generic unitary family. Finally in 1.3.4 we will consider the connections between estimability of a set of parameters, the optmization procedure and the geometry of quantum statistical models and review the general ideas advocated in [39], i.e. to exploit the geometrical theory of quantum estimation to derive the ultimate quantum bounds to the precision of any estimation procedure thus assessing quantum criticality as a resource for quantum estimation.

1.3.1 Cramer-Rao bound

Suppose one wants to know the value λ of a quantity Λ that characterize a physical system S, and also suppose that this quantity cannot be accessed directly by experiments, either in principle (as it happens for any field) or due to some technical impedements. In this case one should resort to indirect measurement, i.e an estimation procedure, which consists in measuring a differect quantity X somehow connected to the quantity of interest and infer the value λ by a suitable processing of the experimental sample $\chi = \{x_1, ..., x_M\}$. The solution of an estimation problem thus amounts to seek for a suitable quantity to measure and to choose an estimator, i.e a mapping $\hat{\lambda} = \hat{\lambda}(\chi)$ from the set of measurement outcomes to the space of parameters. The same situation occurs when one wants to characterize a device Γ, whose action depends on the value of an unknown quantity. In this case one prepares the system in a given known state S_0 and aims to estimate λ upon measuring

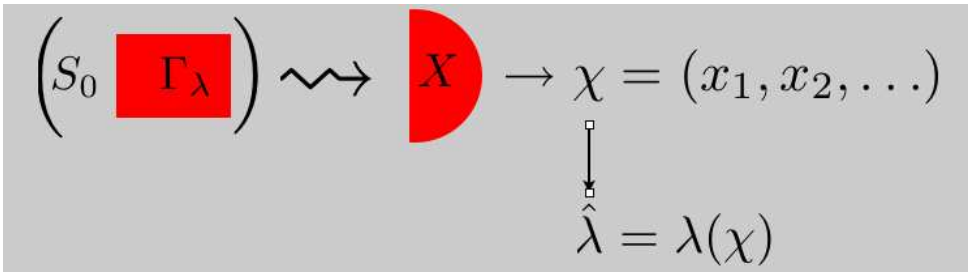

Figure 1.1: Schematic diagram of a generic estimation problem.

the system after the action with the device (see Fig. 1.1). Classically, optimal estimators are those saturating the Cramer-Rao inequality [41]

$$\mathrm{Var}(\lambda) \geq \frac{1}{MF(\lambda)}\,, \tag{1.36}$$

which establishes a lower bound on the variance $\mathrm{Var}(\lambda) = E[\hat{\lambda}^2] - E[\hat{\lambda}]^2$ of any unbiased estimator of the parameter λ, i.e. such that $\int dx \hat{\lambda}(x) p(x|\lambda = \lambda$. In the above inequality M is the number of independent measurements and $F(\lambda)$ the Fisher Information (FI) *i.e.*

$$F(\lambda) = \int dx\, p(x|\lambda) \left(\frac{\partial \ln p(x|\lambda)}{\partial \lambda} \right)^2 , \tag{1.37}$$

$p(x|\lambda)$ being the conditional probability of obtaining the value x when the parameter has the value λ. The proof of the Cramer-Rao bound is obtained by observing that given two functions $f_1(x)$ and $f_2(x)$, the average

$$\langle f_1, f_2 \rangle = \int dx\, p(x|\lambda) f_1(x) f_2(x) \tag{1.38}$$

defines a scalar product. Upon choosing $f_1(x) = \hat{\lambda} - \lambda$ and $f_2(x) = \partial_\lambda \ln p(x|\lambda)$, we have

$$\begin{aligned} \|f_1\|^2 &= \mathrm{Var}(\lambda) \\ \|f_2\|^2 &= F(\lambda) \\ \langle f_1, f_2 \rangle &= 1 \end{aligned} \tag{1.39}$$

where we have used that $\int dx\, \partial_\lambda p(x|\lambda) = 0$ and $\int dx\, \hat{\lambda}(x) p(x|\lambda) = 1$ assuming that derivative and integrals may be exchanged. The Cramer-Rao bound for a single measurement thus corresponds to the Cauchy-Schwartz inequality and the general relation from the additivity of Fisher information, i.e. from the fact that being the random variables $x_1, x_2, \ldots, x_M$ independent, we have $p(x_1, x_2, \ldots, x_M|\lambda) = \prod_{k=1}^{M} \log p(x_k|\lambda)$ and, in turn,

$$\begin{aligned} F_M(\lambda) =& \int dx_1 \ldots dx_M\, p(x_1, x_2, \ldots, x_M|\lambda) [\partial_\lambda \ln p(x_1, x_2, \ldots, x_M|\lambda)]^2 \\ =& M \int dx\, p(x|\lambda) [\partial_\lambda \ln p(x|\lambda)]^2 = MF(\lambda). \end{aligned} \tag{1.40}$$

According to the Cramer-Rao bound the optimal measurement to estimate the quantity Λ is the one with conditional distribution $p(x|\lambda)$ that maximizes the Fisher information. On the other hand, for any fixed measurement an efficient estimator is an estimator that saturares the Cramer-Rao inequality. The optimal estimation of a quantity Λ thus consists in choosing a measurement maximizing the Fisher information and then process the data by an efficient estimator. A question arises on whether such an estimator exists for any measurement. The answer is positive, at least when the sample data is large enough, as an efficient asymptotic ($M \gg 1$) estimator is provided by the maximum-likelihood principle, which will be briefly described in the following.

Maximum likelihood estimator

Let $p(x|\lambda)$ the probability density of a random variable x, conditioned to the value of the parameter λ. The form of p is known , but the true value of the parameter λ is unknown, and it will be estimated from the result of a measurement of x. Let $\{x_1, x_2, \ldots, x_M\}$ be a random sample of size M. The joint probability density of the independent random variable $x_1, x_2, \ldots, x_M$ (i.e. the global probability of the sample) is given by

$$\mathcal{L}(x_1, x_2, \ldots, x_M|\lambda) = \prod_{k=1}^{M} p(x_k|\lambda), \tag{1.41}$$

and is called the likelihood function of the given data sample. The maximum-likelihood estimator (MLE) of the parameter λ is defined as the quantity $\lambda_{ml} \equiv \lambda_{ml}(\{x_k\})$ that minimizes $\mathcal{L}(\lambda)$ for variations of λ, is given by the solution of the equations

$$\frac{\partial \mathcal{L}(\lambda)}{\partial \lambda} = 0; \quad \frac{\partial^2 \mathcal{L}(\lambda)}{\partial \lambda^2} < 0. \tag{1.42}$$

The meaning of the maximum-likelihood principle is that the observed data have been observed because the overall probability of the sample (the likelihood function) was larger than that for other samples. Thus the value of the parameter that most likely has generated the sample is that one maximizing this function. Since the likelihood is positive, the first equation is equivalent to $\partial L/\partial \lambda = 0$ where $L(\lambda) = \log \mathcal{L}(\lambda) = \sum_{k=M} \log p(x_k|\lambda)$ is the so-called log-likelihood function. In order to obtain a measure for the confidence interval in the determination of λ_{ml} we consider the variance

$$\mathrm{Var}(\lambda_{ml}) = \int \left[\prod_k dx_k p(x_k|\lambda) \right] [\lambda_{ml}(\{x_k\}) - \lambda]^2, \tag{1.43}$$

which, in the limit of large M, saturates the Cramer-Rao bound.

1.3.2 Local quantum estimation theory

We now illustrate the fundamental ingredients of local QET following [42]. Any estimation problem that involves quantum systems may be stated by considering a family of quantum states ϱ_λ which are defined on a given Hilbert space $\mathcal{H}$ and labeled by a parameter λ living on a d-dimensional manifold $\mathcal{M}$, with the mapping $\lambda \to \varrho_\lambda$ providing a coordinate system. This is sometimes referred to as a quantum statistical model. The parameter λ does not, in general, correspond to a quantum observable and our aim is to estimate its value through the measurement of some observable on ϱ_λ. In turn, a quantum estimator O_λ for λ is a selfadjoint operator, which describe a quantum measurement followed by any classical data processing performed on the outcomes. The indirect procedure of parameter estimation implies an additional uncertainty for the measured value, that cannot be avoided even in optimal conditions. The aim of quantum estimation theory is to optimize the inference procedure by minimizing this additional uncertainty. In quantum mechanics, according to the Born rule we have $p(x|\lambda) = \mathrm{Tr}[\Pi_x \varrho_\lambda]$ where $\{\Pi_x\}$, $\int dx\, \Pi_x = \mathbb{I}$, are the elements of a positive operator-valued measure (POVM) and ϱ_λ is the density operator parametrized by the quantity we want to estimate. Introducing the Symmetric Logarithmic Derivative (SLD) L_λ as the selfadjoint operator satistying the equation

$$\frac{L_\lambda \varrho_\lambda + \varrho_\lambda L_\lambda}{2} = \frac{\partial \varrho_\lambda}{\partial \lambda} \tag{1.44}$$

we have that $\partial_\lambda p(x|\lambda) = \mathrm{Tr}[\partial_\lambda \varrho_\lambda \Pi_x] = \mathrm{ReTr}[\varrho_\lambda \Pi_x L_\lambda]$. The Fisher Information (1.37) is then rewritten as

$$F(\lambda) = \int dx\, \frac{\mathrm{Re}(\mathrm{Tr}[\varrho_\lambda \Pi_x L_\lambda])^2}{\mathrm{Tr}[\varrho_\lambda \Pi_x]}. \tag{1.45}$$

For a given quantum measurement, i.e. a POVM $\{\Pi_x\}$, Eqs. (1.36) and (1.45) establish the classical bound on precision, which may be achieved by a proper data processing, i.e. by maximum likelihood, which is known to provide an asymptotically efficient estimator. On the other hand, in order to evaluate the ultimate bounds to precision we have now to maximize the Fisher information over the quantum measurements. We will find a bound and then prove it is achievable:

$$\begin{aligned} F(\lambda) &\leq \int dx \left| \frac{\mathrm{Tr}[\varrho_\lambda \Pi_x L_\lambda]}{\sqrt{\mathrm{Tr}[\varrho_\lambda \Pi_x]}} \right|^2 && (1.46) \\ &= \int dx \left| \mathrm{Tr}\left[\frac{\sqrt{\varrho_\lambda}\sqrt{\Pi_x}}{\sqrt{\mathrm{Tr}[\varrho_\lambda \Pi_x]}} \sqrt{\Pi_x} L_\lambda \sqrt{\varrho_\lambda} \right] \right|^2 \\ &\leq \int dx\, \mathrm{Tr}[\Pi_x L_\lambda \varrho_\lambda L_\lambda] && (1.47) \\ &= \mathrm{Tr}[L_\lambda \varrho_\lambda L_\lambda] = \mathrm{Tr}[\varrho_\lambda L_\lambda^2] && (1.48) \end{aligned}$$

The above chain of inequalities prove that the Fisher information $F(\lambda)$ of any quantum measurement is bounded by the so-called Quantum Fisher Information (QFI)

$$F(\lambda) \leq G(\lambda) \equiv \mathrm{Tr}[\varrho_\lambda L_\lambda^2] = \mathrm{Tr}[\partial_\lambda \varrho_\lambda L_\lambda] \tag{1.49}$$

that leads to a more general bound on the variance of the estimator of a quantum parameter, the quantum Cramer-Rao bound

$$\mathrm{Var}(\lambda) \geq \frac{1}{MG(\lambda)}. \tag{1.50}$$

The quantum version of the Cramer-Rao theorem provides an ultimate bound: it does depend on the geometrical structure of the quantum statistical model and does not depend on the measurement. Optimal quantum measurements for the estimation of λ thus correspond to POVM with a Fisher information equal to the quantum Fisher information, i.e those saturating both inequalities (1.46) and (1.47). The first one is saturated when $\mathrm{Tr}[\varrho_\lambda \Pi_x L_\lambda]$ is a real number $\forall\lambda$. The Ineq. (1.47) is based on the Schwartz inequality $|\mathrm{Tr}[A^\dagger B]|^2 \leq \mathrm{Tr}[A^\dagger A]\mathrm{Tr}[B^\dagger B]$ applied to $A^\dagger = \sqrt{\varrho_\lambda}\sqrt{\Pi_x}/\sqrt{\mathrm{Tr}[\varrho_\lambda \Pi_x]}$ and $B = \sqrt{\Pi_x} L_\lambda \sqrt{\varrho_\lambda}$ and it is saturated when

$$\frac{\sqrt{\Pi_x}\sqrt{\varrho_\lambda}}{\sqrt{\mathrm{Tr}[\varrho_\lambda \Pi_x]}} = \frac{\sqrt{\Pi_x} L_\lambda \sqrt{\varrho_\lambda}}{\sqrt{\mathrm{Tr}[\varrho_\lambda \Pi_x L_\lambda]}} \quad \forall\lambda. \tag{1.51}$$

This last equation is satisfied iff the POVM operators $\{\Pi_x\}$ correspond to projectors over the eigenstates of L_λ, which thus represents itself the optimal POVM to estimate the parameter λ. Notice, however, that L_λ itself may not represent the optimal observable to be measured. In fact, Eq. (1.51) determines the POVM and not the estimator i.e. the function of the eigenvalues of L_λ. As we have already mentioned above, this corresponds to a classical post-processing of data aimed to saturate the Cramer-Rao inequality (1.36) and may be pursued by maximum likelihood, which is known to provide an asymptotically efficient estimator. Using the fact that $\mathrm{Tr}[\varrho_\lambda L_\lambda] = 0$, an explicit form for the optimal quantum estimator is given by

$$O_\lambda = \lambda \mathbb{I} + \frac{L_\lambda}{G(\lambda)} \tag{1.52}$$

for which indeed we have

$$\mathrm{Tr}[\varrho_\lambda O_\lambda] = \lambda, \quad \mathrm{Tr}[\varrho_\lambda O_\lambda^2] = \lambda^2 + \frac{\mathrm{Tr}[\varrho_\lambda L_\lambda^2]}{G^2(\lambda)}, \tag{1.53}$$

and thus

$$\langle \Delta O_\lambda^2 \rangle = \frac{1}{G(\lambda)}.$$

The general solution for the SLD L_λ is

$$L_\lambda = 2\int_0^\infty dt \exp\{-\varrho_\lambda t\}\partial_\lambda\varrho_\lambda \exp\{-\varrho_\lambda t\} \tag{1.54}$$

which, upon writing ϱ_λ in its diagonal basis $\varrho_\lambda = \sum_n \varrho_n|\psi_n\rangle\langle\psi_n|$, leads to

$$L_\lambda = 2\sum_{nm}\frac{\langle\psi_m|\partial_\lambda\varrho_\lambda|\psi_n\rangle}{\varrho_n+\varrho_m}|\psi_m\rangle\langle\psi_n| \tag{1.55}$$

where the sums include only terms with $\varrho_m + \varrho_n \neq 0$. The quantum Fisher information is thus given by

$$G(\lambda) = 2\sum_{nm}\frac{|\langle\psi_m|\partial_\lambda\varrho_\lambda|\psi_n\rangle|^2}{\varrho_n+\varrho_m}, \tag{1.56}$$

or, in a basis independent form,

$$G(\lambda) = 2\int_0^\infty dt\,\mathrm{Tr}[\partial_\lambda\varrho_\lambda \exp\{-\varrho_\lambda t\}\partial_\lambda\varrho_\lambda \exp\{-\varrho_\lambda t\}]. \tag{1.57}$$

Notice that both the eigenvalues ϱ_n and the eigenvectors $|\psi_n\rangle$ may depend on the parameter. In order to separate the two contributions to the QFI, we explicitly evaluate $\partial_\lambda\varrho_\lambda$

$$\partial_\lambda\varrho_\lambda = \sum_p \partial_\lambda\varrho_p|\psi_p\rangle\langle\psi_p| + \varrho_p|\partial_\lambda\psi_p\rangle\langle\psi_p| + \varrho_p|\psi_p\rangle\langle\partial_\lambda\psi_p| \tag{1.58}$$

The symbol $|\partial_\lambda\psi_p\rangle$ denotes the ket $|\partial_\lambda\psi_p\rangle = \sum_k \partial_\lambda\psi_{nk}|k\rangle$, where ψ_{nk} are obtained expanding $|\psi_n\rangle$ in arbitrary basis $\{|k\rangle\}$ independent on λ. Since $\langle\psi_n|\psi_m\rangle = \delta_{nm}$, we have that $\partial_\lambda\langle\psi_n|\psi_m\rangle \equiv \langle\partial_\lambda\psi_n|\psi_m\rangle + \langle\psi_n|\partial_\lambda\psi_m\rangle = 0$ and therefore

$$\mathrm{Re}\langle\partial_\lambda\psi_n|\psi_m\rangle = 0 \quad \langle\partial_\lambda\psi_n|\psi_m\rangle = -\langle\psi_n|\partial_\lambda\psi_m\rangle = 0. \tag{1.59}$$

Using Eq. (1.58) and the above identities we have

$$L_\lambda = \sum_p \frac{\partial_\lambda\varrho_p}{\varrho_p}|\psi_p\rangle\langle\psi_p| + 2\sum_{n\neq m}\frac{\varrho_n-\varrho_m}{\varrho_n+\varrho_m}\langle\psi_n|\partial_\lambda\psi_m\rangle|\psi_m\rangle\langle\psi_n| \tag{1.60}$$

and in turn

$$G(\lambda) = \sum_p \frac{(\partial_\lambda\varrho_p)^2}{\varrho_p} + 2\sum_{n\neq m}\sigma_{nm}|\langle\psi_m|\partial_\lambda\psi_n\rangle|^2 \tag{1.61}$$

where

$$\sigma_{nm} = \frac{(\varrho_n-\varrho_m)^2}{\varrho_n+\varrho_m} + \text{any antisymmetric term}, \tag{1.62}$$

as for example,

$$\sigma_{nm} = 2\varrho_n \frac{\varrho_n - \varrho_m}{\varrho_n + \varrho_m} \quad \text{or} \quad \sigma_{nm} = 2\varrho_n \left(\frac{\varrho_n - \varrho_m}{\varrho_n + \varrho_m} \right)^2 \tag{1.63}$$

The first term in Eq. (1.61) represents the classical Fisher information of the distribution $\{\varrho_p\}$ whereas the second term contains the truly quantum contribution. When the eigenvectors of ϱ_λ do not depend on the parameter λ, the second term vanishes. In this case $[\varrho_\lambda, \partial_\lambda \varrho_\lambda] = 0$ and Eq. (1.54) reduces to $L_\lambda = \partial_\lambda \log \varrho_\lambda$. Finally, upon substituting the above Eqs. in (1.52), we obtain the optimal quantum estimator

$$O_\lambda = \sum_p \left(\lambda + \frac{\partial_\lambda \varrho_p}{\varrho_p} \right) |\psi_p\rangle\langle\psi_p| + \frac{2}{G(\lambda)} \sum_{n \neq m} \frac{\varrho_n - \varrho_m}{\varrho_n + \varrho_m} \langle\psi_m|\partial_\lambda \psi_n\rangle |\psi_m\rangle\langle\psi_n|. \tag{1.64}$$

Estimability of a parameter

A large signal is easily estimated whereas a quantity with a vanishing value may be inferred only if the corresponding estimator is very precise i.e characterized by a small variance. This intuitive statement indicates that in assessing the performances of an estimator and, in turn, the overall estimability of a parameter the relevant figure of merit is the scaling of the variance with the mean value rather than its absolute value. This feature may be quantified by means of the signal-to-noise ratio (for a single measurement)

$$R_\lambda = \frac{\lambda^2}{\mathrm{Var}(\lambda)} \tag{1.65}$$

which is larger for better estimators. Using the quantum Cramer-Rao bound, one easily derives that the signal-to-noise ratio of any estimator is bounded by the quantity

$$R_\lambda \leq Q_\lambda \equiv \lambda^2 G(\lambda) \tag{1.66}$$

which we refer to as the quantum signal-to-noise ratio. We say that a given parameter λ is effectively estimable quantum-mechanically when the corresponding Q_λ is large. Upon taking into account repeated measurements we have that the number of measurements leading to a 99.9% (3σ) confidence interval corresponds to a relative error

$$\delta^2 = \frac{9\mathrm{Var}(\lambda)}{M\lambda^2} = \frac{9}{M} \frac{1}{Q_\lambda}. \tag{1.67}$$

Therefore, the number of measurements needed to achieve a 99.9% confidence interval with a relative error δ scales as

$$M_\delta = \frac{9}{\delta^2} \frac{1}{Q_\lambda} \tag{1.68}$$

In other words, a vanishing Q_λ implies a diverging number of measurements to achieve a given relative error, whereas a finite value allows estimation with arbitrary precision at finite number of measurements.

1.3.3 Example: unitary families and pure states

Let us consider the case where the parameter of interest is the amplitude of a unitary perturbation imposed to a given initial state ϱ_0. The family of quantum states we are dealing with may be expressed as $\varrho_\lambda = U_\lambda \varrho_0 U_\lambda^\dagger$ where $U_\lambda = \exp\{-i\lambda A\}$ is a unitary operator and A is the corresponding Hermitian generator. Upon expanding the unperturbed state in its eigenbasis $\varrho_0 = \sum_n \varrho_n |\phi_n\rangle\langle\phi_n|$ we have $\varrho_\lambda = \sum_n \varrho_n |\psi_n\rangle\langle\psi_n|$ where $|\psi_n\rangle = U_\lambda |\phi_n\rangle$. As a consequence we have

$$\partial_\lambda \varrho_\lambda = i U_\lambda [A, \varrho_0] U_\lambda^\dagger \tag{1.69}$$

and the SLD may be written as $L_\lambda = U_\lambda L_0 U_\lambda^\dagger$ where L_0 is given by

$$\begin{aligned} L_0 =& 2i \sum_{nm} \frac{\langle\phi_m|[A, \varrho_0]|\phi_n\rangle}{\varrho_n + \varrho_m} |\phi_n\rangle\langle\phi_m| \\ =& 2i \sum_{n\neq m} \langle\phi_m|A|\phi_n\rangle \frac{\varrho_n - \varrho_m}{\varrho_n + \varrho_m} |\phi_n\rangle\langle\phi_m|. \end{aligned} \tag{1.70}$$

The corresponding quantum Fisher information is independent on the value of the parameter and may be written as

$$G = \mathrm{Tr}[\varrho_0 L_0^2] = \mathrm{Tr}[\varrho_0 [L_0, A]] = \mathrm{Tr}[L_0 [A, \varrho_0]] = \mathrm{Tr}[A[\varrho_0, L_0]] \tag{1.71}$$

or, more explicitly as

$$G = 2 \sum_{n\neq m} \sigma_{nm} A_{nm}^2 \tag{1.72}$$

where the σ_{nm}'s are given in Eq. (1.62) and $A_{nm} = \langle\phi_n|A|\phi_m\rangle = \langle\psi_n|A|\psi_m\rangle$ denotes the matrix element of the generator A in either the eigenbasis of ϱ_0 or ϱ_λ.

For a generic family of pure states, we have $\varrho_\lambda = |\psi_\lambda\rangle\langle\psi_\lambda|$. Since $\varrho_\lambda^2 = \varrho_\lambda$, we have that $\partial_\lambda \varrho_\lambda = \partial_\lambda \varrho_\lambda \varrho_\lambda + \varrho_\lambda \partial_\lambda \varrho_\lambda$ and thus $L_\lambda = 2\partial_\lambda \varrho_\lambda = |\partial_\lambda \psi_\lambda\rangle\langle\psi_\lambda| + |\psi_\lambda\rangle\langle\partial_\lambda \psi_\lambda|$. Finally we have

$$G(\lambda) = 4[\langle\partial_\lambda \psi_\lambda|\partial_\lambda \psi_\lambda\rangle + (\langle\partial_\lambda \psi_\lambda|\psi_\lambda\rangle)^2]. \tag{1.73}$$

For a unitary family of pure states $|\psi_\lambda\rangle = U_\lambda |\psi_0\rangle$, we have

$$\begin{aligned} |\partial_\lambda \psi_\lambda\rangle =& -iAU_\lambda|\psi_0\rangle = -iA|\psi_\lambda\rangle \\ \langle\partial_\lambda \psi_\lambda|\partial_\lambda \psi_\lambda\rangle =& \langle\psi_0|A^2|\psi_0\rangle \\ \langle\partial_\lambda \psi_\lambda|\psi_\lambda\rangle =& -i\langle\psi_0|A|\psi_0\rangle. \end{aligned} \tag{1.74}$$

The quantum Fisher information thus reduces to the form

$$G = 4\langle\psi_0|\Delta A^2|\psi_0\rangle \tag{1.75}$$

which is independent on λ and proportional to the fluctuations of the generator on the unperturbed state $\langle\psi_0|\Delta A^2|\psi_0\rangle = \langle\psi_0|A^2|\psi_0\rangle - (\langle\psi_0|A|\psi_0\rangle)^2$. The quantum Cramer-Rao bound can be rewritten in the form

$$\mathrm{Var}(\lambda)\langle\Delta A^2\rangle \geq \frac{1}{4M}, \tag{1.76}$$

which represents a parameter based uncertainty relation which applies also when the shift parameter in the unitary $U_\lambda = e^{-i\lambda A}$ does not correspond to the observable canonically conjugate to A.

1.3.4 Geometry of quantum estimation

The estimability of a set of parameters labelling the family of quantum states $\{\varrho_\lambda\}$ is naturally related to the distinguishability of the states within the quantum statistical model i.e. with the notions of distance. On the manifold of quantum states, however, different distances may be defined and a question arises on which of them captures the notion of estimation measure. As it can be easily proved it turns out that the Bures distance [17, 20, 23, 43, 44, 45, 46] is the proper quantity to be taken into account. This may be seen as follows: the Bures metric tensor $g_{\mu\nu}$ is obtained upon considering the distance between two infinitesimally close states which differ for slightly different values of the parameter

$$ds_B^2 = \mathcal{D}_B^2(\varrho_\lambda, \varrho_{\lambda+d\lambda}) = \sum_{\mu\nu} g_{\mu\nu} d\lambda_\mu d\lambda_\nu \tag{1.77}$$

where ds_B^2 is the Bures metric which has been explicitly calculated in Eq. (1.33). Then by comparing Eqs. (1.33) and (1.61), one arrives at

$$g_{\mu\nu} = \frac{1}{4} G_{\mu\nu}, \tag{1.78}$$

that is the Bures tensor metric is simply proportional to the quantum Fisher information, which itself is symmetric, real and positive semidefinite, i.e. represents a metric for the manifold underlying the quantum statistical model. Indeed, a large value of the QFI for a given λ implies that the quantum states ϱ_λ and $\varrho_{\lambda+d\lambda}$ should be statistically distinguishable more effectively than the analogue states for a value of λ corresponding to a smaller QFI. In other words, optimal estimability (that corresponds to a diverging QFI) corresponds to quantum states that are sent far apart upon infinitesimal variations of the parameters.

1.4 Quantum state discrimination

Consider that we have a quantum system prepared in a state chosen from a discrete set, rather than from the whole set of quantum states as in the quantum estimation case. We want to discriminate the state starting from the results of certain measurements performed on the system. To the extent that the quantum states are nonorthogonal, the problem is highly nontrivial and of practical importance. Moreover, a fundamental theorem of quantum theory tells us that it is not possible to distinguish perfectly between non-orthogonal quantum states. Then the relevant figure of merit is the error rate in discriminating between quantum states and the task of quantum state discrimination is to develop some techniques that keep the error as low as possible.

In this framework, two main strategies have been suggested: the unambiguous quantum discrimination and the (ambiguous) minimum error discrimination. In the first approach, whenever a definite answer is returned after a measurement on the state, the result should be unambiguous, at the expense of allowing inconclusive outcomes to occur. In the second case, one considers that the errors are unavoidable when the states are non-orthogonal. Then, based on the outcome of the measurement on the state in each single case, a guess has to be made as to what the state of the quantum system was. This procedure is known as *quantum hypothesis testing*. The problem consists into finding the optimum measurement strategy that minimizes the probability of errors. The classical version of this problem was solved about fifty years ago by Herman Chernoff, who proved his famous bound which characterizes the asymptotic behavior of the minimal probability of errors when discriminating two hypothesis given a large number of observations [47]. Its quantum analog, the quantum Chernoff bound (QCB), was recently proven in [48, 49]. The use of QCB in quantum state discrimination is fundamental in several areas of quantum information and it has been exploited as a distinguishability measure between qubits and single-mode Gaussian states [48, 50, 51], to evaluate the degree of nonclassicality for one mode Gaussian states [52] or the polarization of a two-mode state [53]. It has also been applied in the theory of quantum phase transitions to distinguish between different phases of the XY model at finite temperature [54], and to the discrimination of two ground states or two thermal states of the quantum Ising model [55].

In the following we first review the unambiguous state discrimination according to [56], then, in 1.4.2, we address the strategy of quantum hypothesis testing in which we are mostly interested and study both the classical and the quantum Chernoff bounds. We start with the classical hypothesis testing upon defining the error probability and then by reviewing the classical Chernoff bound. We discuss the quantum hypothesis testing both

in the single copy case and in the case when many copies of the two states are given. We consider the connections between the quantum Chernoff bound and some distinguishability measures for quantum states as the fidelity. Moreover we address the discrimination problem for two infinitesimally close quantum states by calculating the quantum Chernoff metric. Finally we consider a different strategy of discrimination between two quantum states, namely the Nayman-Pearson strategy, giving an important result for optimal discrimination in the case of N measurements performed on one of the two states.

1.4.1 Unambiguous state discrimination

In this section we review schemes for unambiguous discrimination following [56]. We mention that the two main discrimination strategies evolved rather differently from the very beginning. On the one hand, unambiguous discrimination started with pure states and only very recently turned its attention to discriminating among mixed quantum states. On the other hand, minimum-error discrimination addressed the problem of discriminating among two mixed quantum states from the very beginning and the results for two pure states followed as special cases.
Each strategy has its own advantages and drawbacks. While unambiguous discrimination is relatively straightforward to generalize for more than two states, it is difficult to treat mixed states. The error-minimizing approach instead, initially developed for two mixed states, is hard to generalize for more than two states.

Unambiguous discrimination started with the work of Ivanovic [57] who studied the following problem. A collection of quantum systems is prepared so that each single system is equally likely to be prepared in one of two known states, $|\psi_1\rangle$ or $|\psi_2\rangle$. Furthermore, the states are not orthogonal, $\langle\psi_1|\psi_2\rangle \neq 0$. The preparer then hands the systems over to an observer one by one whose task is to determine which one of the two states has actually been prepared in each case. All the observer can do is to perform a single measurement or perhaps a series of measurements on the individual system. Ivanovic came to the conclusion that if one allows inconclusive detection results to occur then in the remaining cases the observer can conclusively determine the state of the individual system. A simple von Neumann measurement can accomplish this task. Let us introduce the projector P_1 for $|\psi_1\rangle$ and $\overline{P}_1$ for the orthogonal subspace such that $P_1 + \overline{P}_1 = \mathbb{I}$. Then we know that the state $|\psi_2\rangle$ was prepared if a click in the $\overline{P}_1$ detector occurs. A similar conclusion can be reached for $|\psi_1\rangle$ by inverting the roles of $|\psi_1\rangle$ and $|\psi_2\rangle$. When a click along P_1 (or P_2) occurs, we can say nothing about the state of the system thus corresponding to inconclusive results. The probability of the inconclusive outcome, or failure, is $R_{IDP} = |\langle\psi_1|\psi_2\rangle|$ and

the probability of success is then given by the so called Ivanovich-Dieks-Peres (IDP) limit

$$P_{IDP} = 1 - R_{IDP} = 1 - |\langle\psi_1|\psi_2\rangle|. \tag{1.79}$$

This result can be generalized for the case when the a priori probabilities of the states, η_1 and η_2 are different, i.e. $\eta_1 \neq \eta_2$. The result of Eq. (1.79) corresponds to the case $\eta_1 = \eta_2 = 1/2$.

The von Neumann projective measurement described above has two outcomes. It can correctly identify one of the two states at the expense of missing the other completely and occasionally missing the identifiable one, as well. If we want to do the best prediction we would like to have a measurement with three outcomes: $|\psi_1\rangle$, $|\psi_2\rangle$ and the failure. We introduce the operators Π_1, Π_2 and Π_0 such that: $\langle\psi_1|\Pi_1|\psi_1\rangle = p_1$ is the probability of successfully identifying $|\psi_1\rangle$, $\langle\psi_2|\Pi_2|\psi_2\rangle = p_2$ is the probability of successfully identifying $|\psi_2\rangle$, $\langle\psi_1|\Pi_0|\psi_1\rangle = q_1$ is the probability of failing to identify $|\psi_1\rangle$ (and similarly for $|\psi_2\rangle$). For unambiguous discrimination we require that $\langle\psi_1|\Pi_2|\psi_1\rangle = \langle\psi_2|\Pi_1|\psi_2\rangle = 0$. The operators $\{\Pi_i\}$ form a POVM

$$\Pi_1 + \Pi_2 + \Pi_0 = \mathbb{I} \tag{1.80}$$

These operators can be determined explicitly upon introducing $|\psi_i^\perp\rangle$ that is the vector orthogonal to $|\psi_j\rangle$ $(i \neq j)$ and the final expression is

$$\begin{aligned} \Pi_1 &= \frac{p_1}{\sin^2\theta}|\psi_1^\perp\rangle\langle\psi_1^\perp|, \\ \Pi_2 &= \frac{p_2}{\sin^2\theta}|\psi_2^\perp\rangle\langle\psi_2^\perp|, \end{aligned} \tag{1.81}$$

where $\sin\theta = |\langle\psi_1|\psi_1^\perp\rangle|$ and $\cos\theta = |\langle\psi_1|\psi_2\rangle|$. The positivity of the inconclusive operator

$$\Pi_0 = \mathbb{I} - \Pi_1 - \Pi_2 \tag{1.82}$$

leads to the additional condition

$$q_1 q_2 \geq |\langle\psi_1|\psi_2\rangle|^2, \tag{1.83}$$

where $q_1 = 1 - p_1$ and $q_2 = 1 - p_2$ are the failure probabilities for the corresponding input states. The last inequality represents the constraint imposed by the positivity requirement on the optimum detection operators. Let

$$R = \eta_1 q_1 + \eta_2 q_2 \tag{1.84}$$

denotes the average failure probability for unambiguous discrimination. Due to the relation $P = \eta_1 p_1 + \eta_2 p_2 = 1 - R$, the minimization of R, subject to the constraint (1.84), gives

the maximum probability of success. We express $q_2 = \cos^2\theta/q_1$ and then insert this expression in (1.84). Optimization of R with respect to q_1 gives $q_1^{POVM} = \sqrt{\eta_2/\eta_1}\cos\theta$ and $q_2^{POVM} = \sqrt{\eta_1/\eta_2}\cos\theta$ and

$$R_{POVM} = 2\sqrt{\eta_1\eta_2}\cos\theta. \tag{1.85}$$

For $\eta_1 = \eta_2 = 1/2$ it reproduces the result of Eq. (1.79). Let us next see how this result compares to the average failure probabilities of the two possible unambiguously discriminating von Neumann measurements that were described at the beginning of this section. The average failure probability for the first von Neumann measurement, with its failure direction along $|\psi_1\rangle$ can be written by simple inspection as

$$R_1 = \eta_1 + \eta_2|\langle\psi_1|\psi_2\rangle|^2 \tag{1.86}$$

and he average failure probability for the second von Neumann measurement, with its failure direction along $|\psi_2\rangle$ is given by

$$R_2 = \eta_1|\langle\psi_1|\psi_2\rangle|^2 + \eta_2. \tag{1.87}$$

The optimum failure probability given by the POVM does perform better than R_1 and R_2 when it exists. Indeed, it is subject to the condition for the existence of the POVM solution given by $q_1^{POVM} \leq 1$ and $q_2^{POVM} \leq 1$ which corresponds to $\cos^2\theta/(1+\cos^2\theta) \leq \eta_1 \leq 1/(1+\cos^2\theta)$. If $\eta_1 < \cos^2\theta/(1+\cos^2\theta)$ then the optimum failure probability is given by R_1 and if $\eta_1 > 1/(1+\cos^2\theta)$ the optimum failure probability is R_2.

1.4.2 Bayes strategy: the quantum Chernoff bound

One of the most basic tasks in information theory is the discrimination of two different probability distributions: given a source that outputs variables according one of the two probability distributions, determine which one it is with the minimal possible error. Here we state the problem of classical hypothesis testing by defining the error probability according to the Bayes approach and give the solution found by Chernoff [47].

The probability of error

A way of defining a notion of statistical distinguishability concerns the following scenario. Consider an observer that has to choose between two hypotheses H_0 and H_1 with probability π_0 and π_1 and his decision is based on a set of data collected from the measurement outcomes $b = 1, \ldots, n$ he performs on the system. These measurements have probability distributions $p_0(b)$ and $p_1(b)$ depending upon the hypothesis that he tests. A notion

of distinguishability should give to the observer some method to distinguishing between the two distributions, for example, a Bayesian-like approach consists in minimizing the two error probabilities i.e. the probability of guessing 1 when the true hypothesis is H_0 and the probability of say 0 when the hypothesis is H_1. This latter approach which is known as hypothesis testing gives rise to a measure of distinguishability associated with the exponential decreasing of the error probability that is the Chernoff Bound.

A decision function is any function

$$\delta : \{1, \ldots, n\} \to \{0, 1\} \tag{1.88}$$

representing the method of guess the observer might use in the problem. The probability that such a guess will be in error is

$$P_e(\delta) = \pi_0 P(\delta = 1|0) + \pi_1 P(\delta = 0|1), \tag{1.89}$$

where π_0 and π_1 denote the a priori probabilities assigned to the occurrence of each hypothesis, $P(\delta = 1|0)$ denotes the probability that the guess is $p_1(b)$ when, in fact the distribution is really $p_0(b)$. Similarly $P(\delta = 0|1)$ denotes the probability that the guess is $p_0(b)$ when the distribution is $p_1(b)$. A natural decision function is the Bayes' decision function δ_B that chooses 0 or 1 according to which has the highest posterior probability given the outcome b. The posterior probability according the Bayes rule is

$$p(i|b) = \frac{\pi_i p_i(b)}{\pi_0 p_0(b) + \pi_1 p_1(b)}, \tag{1.90}$$

where $i = 0, 1$ and $p(b) = \pi_0 p_0(b) + \pi_1 p_1(b)$ is the total probability for the outcome b. Then the Bayes' decision function gives

$$\delta_B(b) = \begin{cases} 0 & \text{if} \quad \pi_0 p_0(b) > \pi_1 p_1(b) \\ 1 & \text{if} \quad \pi_1 p_1(b) > \pi_0 p_0(b) \\ \text{anything} & \text{if} \quad \pi_0 p_0(b) = \pi_1 p_1(b) \end{cases} \tag{1.91}$$

In the following we demonstrate that this decision function is optimal as far as the error probability is concerned [58]. Note that for any decision procedure δ, the error probability of Eq. (1.89) can be written as

$$P_e(\delta) = \pi_0 \sum_b \delta(b) p_0(b) + \pi_1 \sum_b [1 - \delta(b)] p_1(b), \tag{1.92}$$

because $\sum_b \delta(b) p_0(b)$ is the total probability of guessing 1 when the answer is 0 and $\sum_b [1 - \delta(b)] p_1(b)$ is the total probability of guessing 0 when the answer is 1. Then it follows that

$$P_e(\delta) - P_e(\delta_B) = \sum_b \left(\delta(b) - \delta_B(b)\right) \left(\pi_0 p_0(b) - \pi_1 p_1(b)\right). \tag{1.93}$$

Suppose that $\delta \neq \delta_B$. Then the nonzero terms in the sum occur when $\delta(b) \neq \delta_B(b)$ and $\pi_0\, p_0(b) \neq \pi_1\, p_1(b)$. When $\delta(b) = 0$ and $\delta_B(b) = 1$, $\pi_0\, p_0(b) - \pi_1\, p_1(b) < 0$ and the term in the sum is positive; when $\delta(b) = 1$ and $\delta_B(b) = 0$, $\pi_0\, p_0(b) - \pi_1\, p_1(b) > 0$ and again the term in the sum is positive. Then it follows that

$$P_e(\delta) > P_e(\delta_B), \tag{1.94}$$

for any decision function and therefore the Bayes' decision function is optimal. For the outcome b is measured with prior probability $p(b)$, the probability of a correct decision is just the $\max\{p(0|b), p(1|b)\}$. Therefore the error probability associated to the Bayes decision function can be expressed as follows

$$\begin{aligned} P_e &= \sum_b p(b)\,(1 - \max\{p(0|b), p(1|b)\}) \\ &= \sum_b p(b)\min\{p(0|b), p(1|b)\} \qquad (1.95) \\ &= \sum_{b=1}^{n} \min\{\pi_0\, p_0(b), \pi_1\, p_1(b)\} \qquad (1.96) \end{aligned}$$

where Eq. (1.95) follows from the relation $p(0|b) + p(1|b) = 1$. Notice that Eq. (1.96) depends on the prior state of knowledge through π_0 and π_1 and is not only a function of the probability distributions that have to be distinguished. This depends on the definition of Bayesian probabilities that are always defined with respect to someone's state of knowledge. The latter Eq. gives a simple operational definition of P_e as we can see in the following example due to Cover [59].

Consider the following four different probability distributions over two outcomes: $p_0 = \{.96, .04\}$, $p_1 = \{.04, .96\}$, $q_0 = \{.90, .10\}$ and $q_1 = \{0, 1\}$. Let us compare the distinguishability of p_0 and p_1 via Eq. (1.96) to that of q_0 and q_1 by assuming equal a priori probabilities

$$P_e(p_0, p_1) = \frac{1}{2}\min\{.96, .04\} + \frac{1}{2}\min\{.04, .96\} = .04 \tag{1.97}$$

$$P_e(q_0, q_1) = \frac{1}{2}\min\{0.9, 0\} + \frac{1}{2}\min\{.1, 1\} = .05 \tag{1.98}$$

Therefore

$$P_e(p_0, p_1) < P_e(q_0, q_1) \tag{1.99}$$

and so the distributions p_0 and p_1 are more distinguishable form each other that the distributions q_0 and q_1. Now consider that two samples of outcomes are taken before a

guess and therefore we have four possible outcomes. Then the error probability will be

$$P_e(p_0^2, p_1^2) = \frac{1}{2}\min\{.96 \times .96, .04 \times .04\} + \frac{1}{2}\min\{.96 \times .04, .04 \times .96\} + \frac{1}{2}\min\{.04 \times .04, .96 \times .96\} + \frac{1}{2}\min\{.04 \times .96, .96 \times .04\} = .04 \quad (1.100)$$

$$P_e(q_0^2, q_1^2) = \frac{1}{2}\min\{.9 \times .9, 0 \times 0\} + \frac{1}{2}\min\{.9 \times .1, 0 \times 1\} + \frac{1}{2}\min\{.1 \times .1, 1 \times 1\} + \frac{1}{2}\min\{.1 \times .9, 1 \times 0\} = .005 \quad (1.101)$$

Therefore

$$P_e(q_0^2, q_1^2) < P_e(p_0^2, p_1^2) \quad (1.102)$$

the distributions q_0 and q_1 are more distinguishable from each other than p_0 and p_1 when one samples two sets of outcomes in the decision problem. This example suggests that the probability of error, though it is a good measure of distinguishability for the problem of making a decision after one sampling, does not adapt to further data acquisition. Therefore we need a measure that it is not explicitly tied with the number N of samplings.

The Chernoff bound

The optimal probability of error in the decision problem must decrease to zero when the number of samplings increases. It turns out that it decreases asymptotically as an exponential in the number of samplings N [47]. This exponential is called the *Chernoff bound* and the formal statement is given in the following [59]

Theorem 3 *Let $P_e(N)$ be the probability of error for Bayes' decision rule after sampling N times one of the two distributions $p_0(b)$ or $p_1(b)$. Then*

$$P_e(N) \leq \frac{1}{2}\min_{s\in[0,1]}\left(\sum_{b=1}^{n} p_0(b)^s p_1(b)^{1-s}\right)^N \quad (1.103)$$

Moreover the bound is approached asymptotically in the large N limit.

The quantum Chernoff bound

In the quantum hypothesis testing problem, one has to decide between two states of a system. The decision is performed by a two-valued measurement. A single copy of the quantum system is not enough for a good decision and one should make independent measurements on several identical copies. Let us address the quantum scenario. Suppose that a quantum system is prepared in two possible states (pure or mixed) ϱ_0 and ϱ_1. The states are known, as well as the *a priori* probabilities π_0 and $\pi_1 = 1-\pi_0$ but we don't know

which state has been actually sent to the observer. We are given n copies of the state ϱ with the promise that it has been prepared either by the source 0 (with prior probability π_0) or 1 (with prior probability π_1) which generate ϱ_0 and ϱ_1 respectively. We formulate two hypotheses H_0 and H_1 about the identity of the source (0 or 1 respectively) and we have to define the minimal error probability to determine which hypothesis better explains the nature of the n copies. The protocol develops in two stages. First, to obtain information about the states we must necessarily make a quantum measurement. Second, one has to provide a classical algorithm which processes the measurement outcomes and produces the best answer (H_0 or H_1). Quantum mechanics allows for a convenient description of this two-step process by assigning to each answer H_0 and H_1 an element E_0 and E_1 respectively, of a two-outcomes POVM $\{E_0, E_1\}$ on the system, where $E_0 + E_1 = \mathbb{I}$ and $E_k \geq 0\ \forall k$. After observing the outcome j the observer infers that the state of the system is ρ_j. The probability of giving the answer H_b conditioned by the state $\varrho = \varrho_i$ is thus given by $p_i(b) = \mathrm{Tr}\left[\varrho_i^{\otimes n} E_b\right]$ and the problem reduces to find the optimal POVM $\{E_b\}_{b=0}^{1}$ for the discrimination problem that is the one minimizing the overall probability of a misidentification given in Eq. (1.96) i.e.

$$P_e = \pi_0\, p_0(1) + \pi_1\, p_1(0). \tag{1.104}$$

In the simplest case of a single copy $n = 1$ and two equiprobable hypotheses $\pi_0 = \pi_1 = 1/2$, we have

$$P_e = \frac{1}{2}(\mathrm{Tr}[\varrho_0 E_1] + \mathrm{Tr}[\varrho_1 E_0]) \tag{1.105}$$

that is to say that the error probability is just the probability that ϱ_0 is the true state times the conditional probability that the guess is wrong summed to the similar term for ϱ_1. The minimization of the error probability in the single copy case is due to Helstrom [14]. Since $E_0 = \mathbb{I} - E_0$, we can introduce the Helstrom matrix $\Upsilon \equiv \varrho_1 - \varrho_0$ and write

$$P_e = \frac{1}{2}\left(1 - \mathrm{Tr}\left[E_1 \Upsilon\right]\right) \tag{1.106}$$

which only needs to be optimized with respect to E_1. Since $\mathrm{Tr}\Upsilon = 0$, the matrix Υ has some negative eigenvalues. This necessarily implies that the minimum error probability is attained if E_1 is the projector over the subspace of positive eigenvalues of Υ that we denote with Υ_+. Assuming this optimal operator we have $\mathrm{Tr}[E_1\Upsilon] = \mathrm{Tr}\Upsilon_+ = \frac{1}{2}\mathrm{Tr}|\Upsilon|$ where $|A|$ is the trace norm defined in (2.133) and

$$A_+ = (|A| + A)/2. \tag{1.107}$$

We arrive at the final result [14]

$$P_e = \frac{1}{2}\left(1 - \frac{1}{2}\mathrm{Tr}\,|\varrho_1 - \varrho_0|\right). \tag{1.108}$$

Let us now suppose that N copies of both ϱ_0 and ϱ_1 are available for the discrimination. The problem may be addressed using the above formulas upon replacing ϱ with $\varrho^{\otimes N}$ [48]. We thus need to analyze the quantity

$$P_e(N) = \frac{1}{2}\left(1 - \frac{1}{2}\mathrm{Tr}|\varrho_1^{\otimes N} - \varrho_0^{\otimes N}|\right). \tag{1.109}$$

The computation of the trace norm of the Helstrom matrix is rather difficult. Moreover it provides a little information about the large n behavior of the error probability, which is what the Chernoff bound is about. The quantum Chernoff bound Q gives an upper bound to the probability of error P_e [48, 50]

$$P_e \leq \frac{Q}{2} \tag{1.110}$$

where

$$Q = \min_{0\leq s\leq 1} \mathrm{Tr}\left[\varrho_0^s \varrho_1^{1-s}\right]. \tag{1.111}$$

Q is a very efficient quantity to be computed and it holds for arbitrary density matrices. In the case of N copies ,

$$P_e(N) \leq \frac{Q^N}{2} = \frac{1}{2}\exp\{-N(-\min_{s\in[0,1]} \log \mathrm{Tr}[\varrho_0^s \varrho_1^{1-s}])\}. \tag{1.112}$$

In the limit $N \to \infty$, the probability of error behaves as

$$P_e(N) \sim \exp\{-N\xi_{QCB}\} \tag{1.113}$$

where we called ξ_{QCB} the quantum Chernoff information

$$\xi_{QCB} = -\lim_{N\to\infty} \frac{1}{N} P_e(N) = -\min_{s\in[0,1]} \log \mathrm{Tr}[\varrho_0^s \varrho_1^{1-s}]. \tag{1.114}$$

This equality holds because of the asymptotical attainability of bound (1.112) as follows from the results in [49].

The bound (1.111) can be inferred by the following

Theorem 4 *Let A and B two positive operators, then for all $0 \leq s \leq 1$,*

$$\mathrm{Tr}[A^s B^{1-s}] \geq \frac{1}{2}\mathrm{Tr}[A + B - |A - B|]. \tag{1.115}$$

The proof of this theorem is given in Ref. [48]. Because $\mathrm{Tr}[A \otimes B] = \mathrm{Tr}[A]\mathrm{Tr}[B]$, the upper bound in the case of N copies immediately follows from Eq.(1.110).

Several comments about Eq. (1.110) are in order.

- If the two matrices ϱ_0 and ϱ_1 commute, the bound reduces to the classical Chernoff bound (1.103) where the two probability distributions are given by the spectrum of the two density matrices.
- The function $Q_s = \mathrm{Tr}[\varrho^s \sigma^{1-s}]$ (whose minimum gives the best bound) is a convex function of s in $[0, 1]$ which means that a stationary point will automatically be a global minimum. Indeed the function $s \mapsto x^s y^{1-s}$ is convex for positive scalars x and y as one confirms by calculating the second derivative $x^s y^{1-s}(\log x - \log y)^2$, which is non-negative. Consider then a basis in which ϱ is diagonal $\varrho = \mathrm{diag}(\lambda_1, \lambda_2, \ldots)$. Let the eigenvalue decomposition of σ in that basis given by $\sigma = U\mathrm{diag}(\mu_1, \mu_2, \ldots)U^\dagger$, where U is a unitary matrix. Then $\mathrm{Tr}[\varrho^s \sigma^{1-s}] = \sum_{ij} \lambda_i^s \mu_j^{1-s} |U_{ij}|^2$. As this is a sum with positive weights of convex terms $\lambda_i^s \mu_j^{1-s}$, the sum itself is convex.
- Q is jointly concave in (ϱ_1, ϱ_2), unitarily invariant, and non-decreasing under trace preserving quantum operations.

Relation to the trace distance

One may think that, though its difficult computation, the trace distance (1.18) to which is related the definition of the error probability P_e, has a more natural operational meaning that the QCB. In spite of this, it does not adapt to the case of many copies; indeed, one can find examples of states $\rho, \sigma, \rho', \sigma'$ such that $\mathrm{Tr}[\rho - \sigma] < \mathrm{Tr}[\rho' - \sigma']$ but $\mathrm{Tr}[\rho'^N - \sigma'^N] < \mathrm{Tr}[\rho^N - \sigma^N]$. By contrast, the QCB does resolve this problem since $Q(\rho, \sigma) < Q(\rho', \sigma')$ implies $Q(\rho^N, \sigma^N) < Q(\rho'^N, \sigma'^N)$. Because of this property, the minimization of the QCB over single-copy states (ρ and σ) implies the minimization over multi-copy states (ρ^N, σ^N). However, the following upper and lower bounds on Q in terms of the trace norm distance $\mathcal{D}_{\mathrm{Tr}}$ have been demonstrated in [12].

Theorem 5 *Let ϱ_0 and ϱ_1 be density matrices. Then the following relation holds:*

$$\sqrt{1 - Q} \leq \mathcal{D}_{\mathrm{Tr}}[\varrho_0, \varrho_1] \leq \sqrt{1 - Q^2}. \tag{1.116}$$

The first inequality is proved by defining a POVM E_Q^* that optimizes Q and E_D^* likewise

$$1 - Q(\varrho_0, \varrho_1) = 1 - Q(p_0(E_Q^*), p_1(E_Q^*)) \tag{1.117}$$

$$\leq \mathcal{D}_{\mathrm{Tr}}[p_0(E_Q^*), p_1(E_Q^*)] \tag{1.118}$$

$$\leq \mathcal{D}_{\mathrm{Tr}}[p_0(E_D^*), p_1(E_D^*)] = \mathcal{D}_{\mathrm{Tr}}[\varrho_0, \varrho_1] \tag{1.119}$$

The second inequality follows from

$$\begin{aligned}\mathcal{D}_{\mathrm{Tr}}[\varrho_0,\varrho_1] =& \mathcal{D}_{\mathrm{Tr}}[p_0(E_D^*),p_1(E_D^*)] && (1.120)\\ \leq& \sqrt{1-1-Q(p_0(E_D^*),p_1(E_D^*))^2} && (1.121)\\ \leq& \sqrt{1-1-Q(p_0(E_Q^*),p_1(E_Q^*))^2} && (1.122)\\ =& \sqrt{1-Q(\varrho_0,\varrho_1)^2}. && (1.123)\end{aligned}$$

Relation to fidelity

The fidelity is always an upper bound to Q

$$P_e \leq \frac{Q}{2} \leq \frac{\mathrm{Tr}[\varrho_0^{1/2}\varrho_1^{1/2}]}{2} \leq \frac{\mathrm{Tr}|\varrho_0^{1/2}\varrho_1^{1/2}|}{2} = \frac{\sqrt{\mathcal{F}(\varrho_0,\varrho_1)}}{2} \tag{1.124}$$

where $\mathcal{F}(\varrho_0,\varrho_1) = \left(\mathrm{Tr}[\sqrt{\varrho_0^{1/2}\varrho_1\varrho_0^{1/2}}]\right)^2 = \left(\mathrm{Tr}|\varrho_0^{1/2}\varrho_1^{1/2}|\right)^2$ and it also provides a lower bound to P_e [12]

$$\frac{1-\sqrt{1-\mathcal{F}(\varrho_0,\varrho_1)}}{2} \leq P_e \tag{1.125}$$

These inequalities translate in the following bounds to the quantum Chernoff information

$$-\frac{1}{2}\log\mathcal{F}(\varrho_0,\varrho_1) \leq \xi_{QCB}(\varrho_0,\varrho_1) \leq -\log\mathcal{F}(\varrho_0,\varrho_1). \tag{1.126}$$

When one of the states is pure, the minimum of the $\mathrm{Tr}[\varrho_0^s\varrho_1^{1-s}]$ is attained for $s=0$ and we have

$$\begin{aligned}Q(\varrho_0,\varrho_1) =& \mathcal{F}(\varrho_0,\varrho_1) && (1.127)\\ \xi_{QCB}(\varrho_0,\varrho_1) =& -\log\mathcal{F}(\varrho_0,\varrho_1). && (1.128)\end{aligned}$$

Relation to the relative entropy

The connection between the QCB and the relative entropy can be seen as follows. By differentiating the quantity $\mathrm{Tr}[\varrho^s\sigma^{1-s}]$ with respect to s, one observes that the minimum, which is unique due to convexity, is obtained when

$$\mathrm{Tr}[\varrho^s\sigma^{1-s}\log\varrho] = \mathrm{Tr}[\varrho^s\sigma^{1-s}\log\sigma]. \tag{1.129}$$

One easily verifies that this is equivalent to the condition that

$$S(\tau_s\|\varrho) = S(\tau_s\|\sigma) \tag{1.130}$$

with $S(A\|B)$ the quantum relative entropy as defined in (1.34) and

$$\tau_s = \frac{\varrho^s \sigma^{1-s}}{\mathrm{Tr}[\varrho^s \sigma^{1-s}]}. \tag{1.131}$$

Notice that τ_s is not a state because it is not even self-adjoint (except in the commuting case). Nevertheless, it has positive spectrum and the its entropy and the relative entropies used in (1.130) are well-defined.

Discriminating infinitesimally close states

Let us call ds^2 the distance between two infinitesimally close density matrices ϱ and $\varrho + d\varrho$. In this case the distinguishability measure defined in Eq. (1.111) defines a metric on the manifold of density operators, i.e. a symmetric nonnegative function that satisfies the triangle inequality, and it has been computed in [50]. It can be demonstrated that, when the difference between the two states is $d\varrho \simeq 0$, the s that minimizes ds^2_{QCB} is given by $s^* = 1/2$ and the distance becomes (see for example [50])

$$ds^2_{QCB} = \frac{1}{2} \sum_{n,m} \frac{|\langle \psi_n | d\varrho | \psi_m \rangle|^2}{(\sqrt{p_m} + \sqrt{p_n})^2}. \tag{1.132}$$

that can also be written as

$$ds^2_{QCB} = \frac{1}{8} \sum_n \frac{(dp_n)^2}{p_n} + \frac{1}{2} \sum_{n \neq m} \frac{|\langle \psi_n | d\psi_m \rangle|^2 (p_n - p_m)^2}{(\sqrt{p_n} + \sqrt{p_m})^2}. \tag{1.133}$$

The choice of Eq. (1.132) as a definition of a distinguishability measure between two infinitesimally close states is then motivated by the underlying description of the measure process as provided by the QCB given in terms of the upper bound to the error probability. The same argument is valid for the choice of the Bures metric in the theory of parameter estimation. A remarkable example of this relation is given in a seminal paper of Braunstein and Caves [25] when they first use the theory of quantum parameter estimation for distinguishing neighboring quantum states. Although the definitions of the QCB in Eq. (1.111) and the Bures distance $\mathcal{D}(\varrho_0, \varrho_1)$ given in Eq. (1.24) look quite different, their infinitesimal versions given by the metrics are strictly related. Indeed for neighboring matrices, by expanding the density matrix $\varrho = \sum_n p_n |\psi_n\rangle\langle\psi_n|$, we can put in evidence the relation existing between the Bures metric and the metric induced by the Chernoff bound. In fact recalling the Eq. (3.96) and using the inequalities $(\sqrt{p_m} + \sqrt{p_n})^2 \geq (p_m + p_n)$ and $2(p_m + p_n) \geq (\sqrt{p_m} + \sqrt{p_n})^2$, one sees that

$$\frac{ds^2_B}{2} \leq ds^2_{QCB} \leq ds^2_B \tag{1.134}$$

For pure states we have that $p_j = \sqrt{p_j} = 1$ and therefore $ds^2_B = ds^2_{QCB}$.

1.4.3 Neyman-Pearson strategy: the quantum relative entropy

Hypothesis testing refers to a general set of tools in statistics and probability theory for making decisions based on experimental data from random variables. In a typical scenario, an experimentalist is faced with two possible hypotheses and must decide based on experimental observation which one was actually realized. There are two types of errors in this process, corresponding to mistakenly identifying one of the two options when the other should have been detected. A central task in hypothesis testing is the development of optimal strategies for minimizing such errors and the determination of compact formulae for the minimum error probabilities. Here we consider a null hypothesis H_0 and an alternative hypothesis H_1. The alternative hypothesis is the one of interest and states that "something significant is happening" as for example some case of flu is the avian one, or an e-mail attachment is a computer virus [60]. In contrast, the null hypothesis corresponds to this not being the case: the flu can be treated with an aspirin, and the attachment is just a nice picture. Neyman and Pearson introduced the idea of making a distinction between type I and type II errors. The type I error, or false positive, denoted by α, is the error of accepting the alternative hypothesis when in reality the null hypothesis holds and the results can be attributed merely to chance. The type II error or false negative, denoted by β, is the error of accepting the null hypothesis when the alternative hypothesis is the true state of nature. The cost associated to the the two types of error can be widely different, or even incommensurate. In the previous section we considered a symmetric hypothesis testing, where no essential distinction is made between the two kinds of errors. To wit, in symmetric hypothesis testing, one considers the average, or Bayesian, error probability P_e, defined as the average of α and β weighted by the prior probabilities of the null and the alternative hypothesis, respectively. Here, we consider the asymmetric hypothesis approach which consists in minimizing the probability of mistakenly identifying ϱ_0 instead of ϱ_1 i.e. the type II error probability, while requiring that the false-alarm probability, that is the probability that ϱ_1 is identified instead of ϱ_0, is bounded by a small number.

Suppose that $N \gg 1$ copies of a quantum system are prepared identically in the state ϱ_1. In order to learn the identity of the state the observer measures a two outcome POVM $\{\Pi_1, \mathbb{I} - \Pi_1\}$ is measured on each of these. If he obtains the outcome associated to Π_1 ($\mathbb{I} - \Pi_1$), then he concludes that the state was ϱ_1 (ϱ_0). The state ϱ_0 is seen as the null hypothesis, while ϱ_1 is the alternative hypothesis. There are two types of errors:

- Type I: the observer finds that the state was ϱ_1 when in reality it was ϱ_0. This

happens with probability

$$\alpha = \mathrm{Tr}[\varrho_0^{\otimes N}\Pi_1] \tag{1.135}$$

- Type II: the the observer finds that the state was ϱ_0 when in reality it was ϱ_1. This happens with probability

$$\beta = \mathrm{Tr}[\varrho_1^{\otimes N}(\mathbb{I} - \Pi_1)]. \tag{1.136}$$

The Neyman-Pearson approach consists into prescribing a bound ϵ for the probability of type I error while the probability of type II error is minimized, i.e. the detection probability is maximized. The relevant error quantity in this case can be written as

$$\beta(\epsilon) = \min_{0\leq\Pi_1\leq\mathbb{I}}\{\beta(\mathbb{I} - \Pi_1) : \alpha(\Pi_1) \leq \epsilon\} \tag{1.137}$$

and the quantum Stein's lemma [61, 62] states that for every $0 < \epsilon < 1$

$$\lim_{N\to\infty} -\frac{\log\beta(\epsilon)}{N} = S(\varrho_0\|\varrho_1) \tag{1.138}$$

where $S(\varrho_0||\varrho_1)$ is the quantum relative entropy (QRE) between the two states ϱ_0 with and ϱ_1 defined in Eq. (1.34). This fundamental result gives a rigorous operational interpretation for the quantum relative entropy and was proved by Hiai and Petz [61] and Ogawa and Nagaoka [62]. The relative entropy is also the asymptotic optimal exponent for the decay of β when we require that $\alpha \to 0$ for $N \to \infty$ [63]. Then, the probability of type II errors in discriminating the states ϱ_0 and ϱ_1 after performing N measurements on ϱ_1 is for $N \to \infty$ is

$$\beta_N(\varrho_1 \to \varrho_0) = \exp\{-NS(\varrho_0||\varrho_1)\} \tag{1.139}$$

It tells us how difficult it is to distinguish the state ϱ_0 from the state ϱ_1, in particular we have that $S(\varrho_0||\varrho_1) = 0$ iff $\varrho_0 = \varrho_1$. For a review of the important properties of the QRE we refer the reader to [64].

Neyman-Pearson strategy: discriminating infinitesimally close parameters

In the limit of $S(\varrho_{\theta+\epsilon}||\varrho_\theta)$, i.e. for two infinitesimally close density matrices, the quantum relative entropy can characterize the so-called Kubo-Mori-Bogoljubov (KMB) Fisher information $\tilde{G}(\theta)$ according to the following relation [65]

$$\tilde{G}(\theta) = \lim_{\epsilon\to 0}\frac{2}{\epsilon}S(\varrho_{\theta+\epsilon}||\varrho_\theta) \tag{1.140}$$

where the KMB Fisher information $\tilde{G}(\theta)$ is defined as [66]

$$\tilde{G}(\theta) = \mathrm{Tr}[\varrho_\theta \tilde{L}_\theta^2] \tag{1.141}$$

with

$$\tilde{L}_\theta = \frac{d \log \varrho_\theta}{d\theta}. \tag{1.142}$$

The KMB Fisher information provides an upper bound to the quantum Fisher information [65]

$$\tilde{G}(\theta) \geq G(\theta). \tag{1.143}$$

2

Estimation and discrimination in continuous variable systems

In this chapter we consider continuous variable systems and address the quantum estimation of parameters by the class of some probe Gaussian states. We also address the discrimination of noisy channels using Gaussian states as probing signals and in particular consider two problems: the detection of a lossy channel against the alternative hypothesis of an ideal lossless channel and the discrimination of Gaussian noisy channels. The chapter is structured as follows. In section 2.1 we briefly introduce the basic concepts and notation about continuous variable (CV) systems. In particular, Cartesian decomposition of mode operators in the phase space, as well as basic properties of displacement and squeezing operators [67]. Moreover we introduce characteristic functions and Wigner functions along with their basic properties [68]. In section 2.2 we introduce Gaussian states and their main properties. In particular the normal forms of the single-mode and two-mode covariance matrices are given. In 2.3 we describe some criteria to detect entanglement and both quantum and classical correlations whereas section 2.4 gives the evolution of a Gaussian state in a noisy channel and an example of evolution in a lossy channel of the covariance matrix of a single-mode and a two-mode Gaussian state. In section 2.5 we address quantum estimation of displacement and squeezing parameters by the class of probes made of Gaussian states undergoing Kerr interaction. In section 2.6 we evaluate the quantum Chernoff bound to discriminate lossy channels by means of single-mode and two mode Gaussian states. Finally, in 2.7 we address discrimination of Gaussian noise channels using both minimum error probality (Bayes) and maximum detection probability (Neyman-Pearson) strategies. We also consider the discrimination of channels with infinitesimally close values of the noise parameter and evaluate the metrics associated with the two distinguishability

notions.

2.1 Continuous variable systems

Let us consider a system of n bosons described by the mode operators a_k, $k = 1, \dots n$, satisfying the commutation relations $[a_k, a_j^\dagger] = \delta_{kj}\mathbb{I}$, where δ_{kj} is the kronecker delta and $\mathbb{I}$ is the identity operator over the Hilbert space $\mathcal{H} = \otimes_{k=1}^n \mathcal{H}_k$. The free Hamiltonian of the system is $H = \sum_{k=1}^n (a_k a_k^\dagger + \frac{1}{2}\mathbb{I})$ where from now on we set $\hbar\omega_k = 1$ and follow the notation of [67]. The position and momentum operators are defined through the Cartesian decomposition of the mode operators $a_k = \frac{1}{\sqrt{2}}(q_k + ip_k)$:

$$q_k = \frac{1}{\sqrt{2}}(a_k + a_k^\dagger), \qquad p_k = \frac{1}{i\sqrt{2}}(a_k - a_k^\dagger)$$

and the corresponding commutation relations are $[q_j, p_k] = i\delta_{jk}\mathbb{I}$. Introducing the vector $\boldsymbol{R} = (q_1, p_1, \dots, q_n, p_n)^T$, where $(\dots)^T$ denotes the transposition operation, the commutation relations become

$$[R_k, R_j] = i\Omega_{kj}\mathbb{I} \tag{2.1}$$

where Ω_{kj} are the elements of the symplectic matrix

$$\boldsymbol{\Omega} = \bigoplus_{k=1}^{n} \boldsymbol{\omega}, \qquad \boldsymbol{\omega} = \begin{pmatrix} 0 & 1 \\ -1 & 0 \end{pmatrix}. \tag{2.2}$$

For a quantum state ϱ of a system of n bosons, the covariance matrix $\boldsymbol{\sigma} = \boldsymbol{\sigma}[\varrho]$ of elements σ_{kj} is defined as follows

$$\sigma_{kj} = \frac{1}{2}\langle\{R_k, R_j\}\rangle - \langle R_k\rangle\langle R_j\rangle \tag{2.3}$$

where $\{A, B\} = AB + BA$ denotes the anticommutator and $\langle O\rangle = \mathrm{Tr}[\varrho O]$ is the expectation value of the operator O. The uncertainty relations among canonical operators impose a constraint to the covariance matrix

$$\boldsymbol{\sigma} + \frac{i}{2}\boldsymbol{\Omega} \geq 0, \tag{2.4}$$

thus expressing the positivity of the density matrix ϱ. The vacuum state of n bosons is a pure separable state $|\mathbf{0}\rangle$ characterized by the covariance matrix $\boldsymbol{\sigma} = \frac{1}{2}\mathbb{I}_{2n}$, where $\mathbb{I}_{2n}$ is the $2n \times 2n$ identity matrix. A state at thermal equilibrium is described by the density operator $\nu = \otimes_{k=1}^n \nu_k$ where

$$\nu_k = \frac{e^{-\beta a_k^\dagger a_k}}{\mathrm{Tr}[e^{-\beta a_k^\dagger a_k}]} = \frac{1}{n_{kT}+1}\sum_m \left(\frac{n_{kT}}{n_{kT}+1}\right)^m |m\rangle_{kk}\langle m|. \tag{2.5}$$

$n_{kT} = (e^{\beta} - 1)^{-1}$ is the average number of thermal quanta at equilibrium in the k-th mode and $\{|m\rangle_k\}_{m\in\mathbb{N}}$ are the eigenstates of the number operator $a_k^\dagger a_k$ which form a basis of each Hilbert space $\mathcal{H}_k$.

The covariance matrix of a thermal state ν is given by

$$\boldsymbol{\sigma}[\nu] = \mathrm{Diag}\left(n_{1T} + \frac{1}{2}, \ldots, n_{nT} + \frac{1}{2}\right) \tag{2.6}$$

where $\mathrm{Diag}(x_1, \ldots, x_n)$ denotes the diagonal matrix with elements x_k, $k = 1, \ldots n$.

2.1.1 Symplectic transformations

Let us first consider a classical system of n particles described by the canonical coordinates $(q_1, \ldots, q_n)$ and conjugated momenta $(p_1, \ldots, p_n)$. If H is the Hamiltonian of the system, the equations of motion are given by

$$\dot{q}_k = \frac{\partial H}{\partial p_k}, \qquad \dot{p}_k = -\frac{\partial H}{\partial q_k} \tag{2.7}$$

where $\dot{x}$ denotes the time derivative. For a system of n particles, the Equations (2.7) can be summarized as

$$\dot{R}_k = \Omega_{ks}\frac{\partial H}{\partial R_s} \tag{2.8}$$

where Ω_{ks} are the elements of the symplectic matrix (2.2) and $\boldsymbol{R}$ the vector of coordinates given in the section 2.1. The linear transformation of coordinates $\boldsymbol{R'} = \boldsymbol{F}\boldsymbol{R}$ is described by $F_{ks} = \frac{\partial R'_k}{\partial R_s}$ and leads to

$$\frac{\partial R'_k}{\partial t} = F_{ks}\Omega_{sp}F_{lp}\frac{\partial H}{\partial R'_l}. \tag{2.9}$$

Therefore the Hamilton equations remain unchanged if and only if $\boldsymbol{F}$ satisfies

$$F_{ks}\Omega_{sp}F_{lp} = \Omega_{kl} \quad \text{or} \quad \boldsymbol{F\Omega F^T} = \boldsymbol{\Omega} \tag{2.10}$$

which characterize symplectic transformations and describe the canonical transformations of coordinates. Let us now consider a quantum state of n bosons. A mode transformation $\boldsymbol{R'} = \boldsymbol{F}\boldsymbol{R}$ leaves the kinematics invariant if it preserves the canonical commutation relations (2.1) that means the $2n \times 2n$ matrix $\mathbf{F}$ should satisfy the symplectic condition (2.10). Since $\boldsymbol{\Omega}^T = \boldsymbol{\Omega}^{-1} = -\boldsymbol{\Omega}$, from (2.10) one obtains that $\mathrm{Det}[\mathbf{F}]^2 = 1$ and therefore $\mathbf{F}^{-1}$ exists. Moreover, it can be also showed that if $\mathbf{F}, \mathbf{F}_1$ and $\mathbf{F}_2$ are symplectic, then also $\mathbf{F}^{-1}$, $\mathbf{F}^T$ and $\mathbf{F}_1\mathbf{F}_2$ are symplectic, with $\mathbf{F}^{-1} = \boldsymbol{\Omega}\mathbf{F}^{\mathbf{T}}\boldsymbol{\Omega}^{-\mathbf{1}}$. Therefore the set of real matrices satisfying (2.10) form the *symplectic group* $\mathrm{Sp}(2n, \mathbb{R})$ with dimension $n(2n + 1)$. Together with the phase-space translation $\mathbf{R}' = \mathbf{R} + \boldsymbol{\Lambda}$ it forms the *affine (inhomogeneous) symplectic group* $\mathrm{ISp}(2n, \mathbb{R})$.

2.1.2 Linear and bilinear interactions of modes

The physical transformation which generates the whole group of symplectic transformations may be written in the most general form with an Hamiltonian of this type:

$$H = \sum_{k=1}^{n} g_k^{(1)} a_k^\dagger + \sum_{k>l=1}^{n} g_{kl}^{(2)} a_k^\dagger a_l + \sum_{k,l=1}^{n} g_{kl}^{(3)} a_k^\dagger a_l^\dagger + \text{h.c.}, \tag{2.11}$$

which is at most bilinear in the field modes. Transformations induced by the Hamiltonian (2.11) correspond to unitary representations of the affine symplectic group $\mathrm{ISp}(2n, \mathbb{R})$. The first term of the Hamiltonian (2.11) is linear in the field modes $\propto g^{(1)} a^\dagger + \text{h.c.}$ and the corresponding unitary transformations are the set of *displacement operators*. The second block contains terms of the form $\propto g^{(2)} a^\dagger b + \text{h.c.}$ and describes linear mixing of the modes. The third kind of interaction is represented by Hamiltonians of the form $\propto g^{(3)} {a^\dagger}^2 + \text{h.c.}$ and $g^{(3)} a^\dagger b^\dagger$ which describe single-mode and two-mode squeezing.

Displacement operator

The displacement operator for n bosons is defined as

$$D(\lambda) = \bigotimes_{k=1}^{n} D_k(\lambda_k) \tag{2.12}$$

where λ is the column vector $\lambda = (\lambda_1, \ldots, \lambda_n)^T$, $\lambda_k \in \mathbb{C}$, $k = 1, \ldots, n$ and

$$D_k(\lambda_k) = \exp\{\lambda_k a_k^\dagger - \lambda_k^* a_k\}$$

are single-mode displacement operators. Displacement operator takes its name after the action on the mode operators

$$D^\dagger(\lambda) a_k D(\lambda) = a_k + \lambda_k \quad (k = 1, \ldots, n). \tag{2.13}$$

For the single-mode displacement operator the following properties are immediate consequence of the definition

$$D^\dagger(\lambda) = D(-\lambda), \tag{2.14}$$

$$\mathrm{Tr}[D(\lambda)] = \pi \delta^{(2)}(\lambda), \tag{2.15}$$

$$D(\lambda_1) D(\lambda_2) = D(\lambda_1 + \lambda_2) \exp\{\frac{1}{2}(\lambda_1 \lambda_2^* - \lambda_1^* \lambda_2)\}. \tag{2.16}$$

The two-dimensional complex δ-function is defined as

$$\delta^{(2)}(z) = \int_{\mathbb{C}} \frac{d^2\lambda}{\pi^2} \exp\{\lambda^* z - z^* \lambda\} = \int_{\mathbb{C}} \frac{d^2\lambda}{\pi^2} \exp\{i(\lambda^* z + z^* \lambda)\} \tag{2.17}$$

Matrix elements in the Fock (number) basis are given by

$$\langle n+d|D(\alpha)|n\rangle = \sqrt{\frac{n!}{(n+d)!}} e^{-\frac{1}{2}|\alpha|^2} \alpha^d L_n^d(|\alpha|^2) \tag{2.18}$$

$$\langle n|D(\alpha)|n+d\rangle = \sqrt{\frac{n!}{(n+d)!}} e^{-\frac{1}{2}|\alpha|^2} (-\alpha^*)^d L_n^d(|\alpha|^2) \tag{2.19}$$

$$\langle n|D(\alpha)|n\rangle = e^{-\frac{1}{2}|\alpha|^2} L_n(|\alpha|^2), \tag{2.20}$$

$L_n^d(x)$ being the Laguerre polynomials. The displacement operator is strictly related to coherent states. The coherent state $|\alpha\rangle$ is defined as the eigenstate of the mode operator a, i.e.

$$a|\alpha\rangle = \alpha|\alpha\rangle \tag{2.21}$$

where $\alpha \in \mathbb{C}$ is a complex number. The expansion in terms of the Fock spaces reads

$$|\alpha\rangle = e^{-\frac{1}{2}|\alpha|^2} \sum_{k=0}^{\infty} \frac{\alpha^k}{\sqrt{k!}} |k\rangle. \tag{2.22}$$

Then, using (2.13) it can be shown that coherent states are generated by unitary evolution of the vacuum through the displacement operator, i.e. $|\alpha\rangle = D(\alpha)|0\rangle$. Properties of coherent states, i.e. overcompleteness and nonorthogonality, thus follow from that of displacement operator. The expansion (2.22) in the number state is recovered from the definition $|\alpha\rangle = D(\alpha)|0\rangle$ by the normal ordering of the displacement

$$D(\alpha) = e^{\alpha a^\dagger} e^{-\frac{1}{2}|\alpha|^2} e^{-\alpha^* a} \tag{2.23}$$

and by explicit calculations. Coherent states are *minimum uncertainty* states, i.e. they fulfill (2.4) with equality sign and, in addition, with uncertainties that are equal for position- and momentum-like operators. In other words the covariance matrix of a coherent state coincides with that of the vacuum state $\sigma = \frac{1}{2}\mathbb{I}$. Note that coherent states are not orthogonal and their overlap results

$$\langle \beta|\alpha\rangle = e^{-\frac{1}{2}(|\alpha|^2+|\beta|^2-2\beta^*\alpha)}. \tag{2.24}$$

However they satisfy the completeness relation

$$\int_{\mathbb{C}} \frac{d^2\alpha}{\pi} |\alpha\rangle\langle\alpha| = \mathbb{I}. \tag{2.25}$$

Two-mode mixing

The linear mixing described by the Hamiltonian $H \propto a^\dagger b + b^\dagger a$ is the simplest example of two-mode interaction. For two modes of the radiation field it corresponds to a beam splitter, i.e. to the interaction taking place in a linear optical medium such as a dielectric plate. The evolution operator can be recast in the form

$$U(\zeta) = \exp\{\zeta a^\dagger b - \zeta^* a b^\dagger\} \tag{2.26}$$

where $\zeta = \phi e^{i\theta} \in \mathbb{C}$ is proportional to the interaction time and to the linear susceptibility of the medium. We can use the two-mode boson representation of $SU(2)$ algebra to disentangle the evolution operator by identifying: $J_+ = a^\dagger b$, $J_- = (J_+)^\dagger = a b^\dagger$ and $J_3 = \frac{1}{2}[J_+, J_-] = \frac{1}{2}(a^\dagger a - b^\dagger b)$ thus obtaining

$$\begin{aligned} U(\zeta) &= \exp\{\zeta J_+ - \zeta^* J_-\} && (2.27)\\ &= \exp\{e^{i\theta}\tan\phi\, a^\dagger b\}(\cos^2\phi)^{b^\dagger b - a^\dagger a}\exp\{-e^{-i\theta}\tan\phi\, a b^\dagger\} && (2.28)\\ &= \exp\{-e^{-i\theta}\tan\phi\, a b^\dagger\}(\cos^2\phi)^{a^\dagger a - b^\dagger b}\exp\{e^{i\theta}\tan\phi\, a^\dagger b\}. && (2.29) \end{aligned}$$

Eq. (2.27) are often written introducing the quantity $\tau = \cos^2\phi$ which is referred as the transmissivity of the beam splitter. The total number of quanta of the two modes $a^\dagger a + b^\dagger b$ is a constant of motion; this is usually summarized by saying that the beam splitter is a *passive* device. It also implies that $U(\zeta)|\mathbf{0}\rangle = |\mathbf{0}\rangle$ where $|\mathbf{0}\rangle = |0\rangle \otimes |0\rangle$. The Heisemberg evolution of the modes a and b is obtained with the following Baker-Haussdorf formula

$$e^{\lambda A} B e^{-\lambda A} = B + \lambda[A,B] + \frac{\lambda^2}{2!}[A,[A,B]] + \ldots + \frac{\lambda^n}{n!}[A,[A,\ldots[A,B]]] \tag{2.30}$$

giving

$$\begin{pmatrix} a' \\ b' \end{pmatrix} = U^\dagger(\zeta)\begin{pmatrix} a \\ b \end{pmatrix}U(\zeta) = \mathbf{S}_\zeta \begin{pmatrix} a \\ b \end{pmatrix} \tag{2.31}$$

where

$$\mathbf{S}_\zeta = \begin{pmatrix} \cos\phi & e^{i\theta}\sin\phi \\ -e^{-i\theta}\sin\phi & \cos\phi \end{pmatrix}. \tag{2.32}$$

From (2.31) we obtain the symplectic matrix $\mathbf{F}_\zeta$, given by

$$\mathbf{F}_\zeta = \begin{pmatrix} \mathrm{Re}[\mathbf{S}_\zeta] & -\mathrm{Im}[\mathbf{S}_\zeta] \\ \mathrm{Im}[\mathbf{S}_\zeta] i & \mathrm{Re}[\mathbf{S}_\zeta] \end{pmatrix}. \tag{2.33}$$

Single-mode squeezing

Squeezing transformations correspond to Hamiltonians of the form $H \propto (a^\dagger)^2 + a^2$, the corresponding unitary evolution operator is the single-mode squeezing operator

$$S(\xi) = \exp\{\frac{1}{2}\xi(a^\dagger)^2 - \frac{1}{2}\xi^* a^2\} \tag{2.34}$$

corresponding to mode evolution given by

$$S^\dagger(\xi) a S(\xi) = \mu a + \nu a^\dagger, \qquad S^\dagger(\xi) a^\dagger S(\xi) = \mu a^\dagger + \nu^* a \tag{2.35}$$

where $\mu \in \mathbb{R}$, $\nu \in \mathbb{C}$, $\mu = \cosh r$, $\nu = e^{i\psi}\sinh r$, $\xi = re^{i\psi}$. Using the two-boson representation of the SU(1,1) algebra $K_+ = \frac{1}{2}{a^\dagger}^2$, $K_- = (K_+)^\dagger$, $K_3 = -\frac{1}{2}[k_+, K_-] = \frac{1}{2}(a^\dagger a + \frac{1}{2})$, it is possible to disentangle $S(\xi)$, achieving the normal orderings of mode operators

$$\begin{aligned} S(\xi) &= \exp\{\xi K_+ - \xi^* K_-\} \\ &= \exp\left\{-\frac{\nu}{2\mu}a^2\right\} \mu^{(a^\dagger a + \frac{1}{2})} \exp\left\{\frac{\nu^*}{2\mu}a^{\dagger 2}\right\}, \end{aligned} \tag{2.36}$$

from which one obtains the action of the squeezing operator on the vacuum state $|\xi\rangle = S(\xi)|0\rangle$. The state $|\xi\rangle$ is known as the *squeezed vacuum state* which expanded over the number basis reads

$$|\xi\rangle = \frac{1}{\sqrt{\mu}} \sum_{k=0}^{\infty} \left(\frac{\nu}{2\mu}\right)^k \frac{\sqrt{(2k)!}}{k!} |2k\rangle \tag{2.37}$$

Despite its name, the squeezed vacuum is not empty and the mean photon number is given by $\langle\xi|a^\dagger a|\xi\rangle = |\nu|^2 = \sinh^2 r$, which represents the squeezing energy. In general, if $\varrho' = S(\xi)\varrho S^\dagger(\xi)$ is the state after the squeezer, the mean number of photons is given by

$$\langle a^\dagger a\rangle_{\varrho'} = \sinh^2 r + (2\sinh r + 1)\langle a^\dagger a\rangle_\varrho + \sinh(2r)\langle a^2 e^{-i\psi} + a^{\dagger 2} e^{i\psi}\rangle_\varrho. \tag{2.38}$$

The symplectic matrix obtained from (2.35) is

$$\mathbf{\Sigma}_\xi = \begin{pmatrix} \mu + \mathrm{Re}[\nu] & \mathrm{Im}[\nu] \\ \mathrm{Im}[\nu] & \mu - \mathrm{Re}[\nu] \end{pmatrix} \tag{2.39}$$

which, in the case of real squeezing $\psi = 0$, reduces to $\mathbf{\Sigma}_\xi = \mathrm{Diag}(\mathrm{e}^{\mathrm{r}}, \mathrm{e}^{-\mathrm{r}})$.

Two-mode squeezing

Two-mode squeezing operations correspond to Hamiltonian of the form $H \propto a^\dagger b^\dagger + \mathrm{h.c.}$. The evolution operator is written as

$$S_2(\xi) = \exp\left\{\xi a^\dagger b^\dagger - \xi^* ab\right\} \tag{2.40}$$

where $\xi = re^{i\psi}$. The corresponding evolution of the modes is given by

$$S_2^\dagger(\xi) \begin{pmatrix} a \\ b^\dagger \end{pmatrix} S_2(\xi) = \mathbf{S} \begin{pmatrix} a \\ b^\dagger \end{pmatrix} \tag{2.41}$$

where

$$\mathbf{S} = \begin{pmatrix} \mu & \nu \\ \nu^* & \mu \end{pmatrix}. \tag{2.42}$$

As for single squeezing we have $\mu = \cosh r$, $\nu = e^{i\psi} \sinh r$. We can disentangle the operator considering a different realization of the SU(1, 1) algebra, namely $K_+ = a^\dagger b^\dagger$, $K_- = (K_+)^\dagger$, $K_3 = -\frac{1}{2}[K_+, K_-] = \frac{1}{2}(a^\dagger a + b^\dagger b + \frac{1}{2})$ thus obtaining

$$S_2(\xi) = \exp\left\{\frac{\nu^*}{\mu} a^\dagger b^\dagger\right\} \mu^{-(a^\dagger a + b^\dagger b)} \exp\left\{-\frac{\nu}{\mu} ab\right\} \tag{2.43}$$

The symplectic matrix associated to the squeezing operator is

$$\mathbf{\Sigma}_{2\xi} = \begin{pmatrix} \mu \mathbb{I}_2 & \mathbf{R}_\xi \\ \mathbf{R}_\xi & \mu \mathbb{I}_2 \end{pmatrix}, \tag{2.44}$$

with

$$\mathbf{R}_\xi = \begin{pmatrix} \mathrm{Re}[\nu] & \mathrm{Im}[\nu] \\ \mathrm{Im}[\nu] & -\mathrm{Re}[\nu] \end{pmatrix}. \tag{2.45}$$

The action of $S_2(\xi)$ on the vacuum $|\mathbf{0}\rangle = |0\rangle \otimes |0\rangle$ can be evaluated starting from (2.40). The resulting state is given by

$$S_2(\xi)|\mathbf{0}\rangle = |\xi\rangle\rangle = \frac{1}{\sqrt{\mu}} \sum_{k=0}^{\infty} \left(\frac{\nu}{\mu}\right)^k |k\rangle \otimes |k\rangle \tag{2.46}$$

and it is known as *two-mode squeezed vacuum* or *twin-beam state* (TWB). The second denomination refers to the fact that TWB shows perfect correlation in the photon number, i.e. it is an eigenstate of the photon number difference $a^\dagger a - b^\dagger b$ with eigenvalue zero:

$$(a^\dagger a - b^\dagger b)|\xi\rangle\rangle = 0.$$

The mean photon number of each mode is given by

$$\langle a^\dagger a \rangle = \langle b^\dagger b \rangle = \sinh^2 r. \tag{2.47}$$

2.1.3 Characteristic function and Wigner function

The set of displacement operators $D(\boldsymbol{\lambda})$ with $\boldsymbol{\lambda} \in \mathbb{C}$ is complete in the sense that any operator O that acts on a Hilbert space $\mathcal{H}$ can be written as

$$O = \int_{\mathbb{C}^n} \frac{d^{2n}\boldsymbol{\lambda}}{\pi^n} \chi[O](\boldsymbol{\lambda}) D^\dagger(\boldsymbol{\lambda}) \tag{2.48}$$

where $\chi[O](\boldsymbol{\lambda})$ is the characteristic function of an operator O

$$\chi[O](\boldsymbol{\lambda}) = \mathrm{Tr}[OD(\boldsymbol{\lambda})]. \tag{2.49}$$

The Eq. (2.48) is known as Glauber formula [69]. Using Eq. (2.48) and (2.15), it can be shown that for any pair of generic operators acting on the Hilbert space on n modes we have

$$\mathrm{Tr}[O_1 O_2] = \frac{1}{\pi^n} \int_{\mathbb{C}^n} d^{2n}\boldsymbol{\lambda} \chi[O_1](\boldsymbol{\lambda}) \chi[O_2](-\boldsymbol{\lambda}) \tag{2.50}$$

which allows to evaluate a quantum trace as a phase-space integral in terms of the characteristic function. Other properties of the characteristic function follow from the definition

$$\int_{\mathbb{C}^n} \frac{d^{2n}\boldsymbol{\lambda}}{\pi^{2n}} \chi[O](\boldsymbol{\lambda}) = \mathrm{Tr}[O\boldsymbol{\Pi}], \tag{2.51}$$

$$\int_{\mathbb{C}^n} \frac{d^{2n}\boldsymbol{\lambda}}{\pi^{2n}} |\chi[O](\boldsymbol{\lambda})|^2 = \mathrm{Tr}[O^2], \tag{2.52}$$

where we introduced the n-mode parity operator $\boldsymbol{\Pi} = \otimes_{k=1}^n (-)^{a_k^\dagger a_k} = (-)^{\sum_{k=1}^n a_k^\dagger a_k}$.

The so-called Wigner function of the operator O is defined as the Fourier transform of the characteristic function as follows [70]

$$W[O](\boldsymbol{\alpha}) = \int_{\mathbb{C}^n} \frac{d^{2n}\boldsymbol{\lambda}}{\pi^{2n}} \exp\left\{\boldsymbol{\lambda}^* \boldsymbol{\alpha} + \boldsymbol{\alpha}^\dagger \boldsymbol{\lambda}\right\} \chi[O](\boldsymbol{\lambda}). \tag{2.53}$$

The Wigner function of a density matrix ϱ is a quasiprobability distribution for the quantum state. Using Eq. (2.52), we have that $\chi[\varrho](\boldsymbol{\lambda})$ is a square integrable function for any quantum state.

2.2 Continuous variable Gaussian states

2.2.1 Definition and some properties

A state ϱ of a continuous variable system with n degrees of freedom is Gaussian if its Wigner function, or equivalently its characteristic function, is Gaussian, i.e.

$$W[\varrho](\mathbf{X}) = \frac{\exp\{-\frac{1}{2}(\mathbf{X}-\overline{\boldsymbol{X}})^T\boldsymbol{\sigma}^{-1}(\boldsymbol{X}-\overline{\boldsymbol{X}})\}}{(2\pi)^n\sqrt{\mathrm{Det}[\boldsymbol{\sigma}]}} \tag{2.54}$$

$$\chi[\varrho](\boldsymbol{\Lambda}) = \exp\left\{\frac{1}{2}\boldsymbol{\Lambda}^T\boldsymbol{\sigma}\boldsymbol{\Lambda} + \overline{\boldsymbol{X}}^T\boldsymbol{\Lambda}\right\} \tag{2.55}$$

where $\overline{\boldsymbol{X}}$ is the vector of the quadratures' average values and $\boldsymbol{\sigma}$ is the covariance matrix. The definitions (2.54) and (2.55) express that Gaussian states are completely characterized by the vector of first moments $\overline{\boldsymbol{X}}$ and the covariance matrix $\boldsymbol{\sigma}$. Pure Gaussian states are easily characterized with the *purity* $\mu = \mathrm{Tr}[\varrho^2]$ in terms of the overlap of the Wigner function:

$$\mu(\boldsymbol{\sigma}) = \frac{1}{2^n\sqrt{\mathrm{Det}[\boldsymbol{\sigma}]}} \tag{2.56}$$

and a Gaussian state is pure if and only if

$$\mathrm{Det}[\boldsymbol{\sigma}] = 2^{-2\mathrm{n}}.$$

Gaussian states are particularly important from an applicative point of view because they can be generated using only the linear and bilinear interactions introduced in Section 2.1.2. Moreover the following theorem ensures us that every covariance matrix can be diagonalized through a symplectic transformation.

Theorem 6 (Williamson) [71]: Given $\boldsymbol{\sigma}$, $\boldsymbol{\sigma}^T = \boldsymbol{\sigma}$ and $\boldsymbol{\sigma} > 0$, there exists $\mathbf{S} \in \mathrm{Sp}(2\mathrm{n},\mathbb{R})$ and $d_1,\ldots,d_n \in \mathbb{R}$ such that

$$\boldsymbol{\sigma} = \mathbf{S}^T\mathbf{W}\mathbf{S} \tag{2.57}$$

with $\mathbf{W} = \oplus_{k=1}^n d_k\mathbb{I}_2$. The elements d_k are called the symplectic eigenvalues of $\boldsymbol{\sigma}$, while we say that $\mathbf{S}$ performs a symplectic diagonalization of $\boldsymbol{\sigma}$. The physical statement implied by the theorem is that every Gaussian state ϱ can be obtained from a thermal state (with covariance matrix given by $\mathbf{W}$) by performing the unitary transformation $U_{\mathbf{S}}$ associated to the symplectic matrix $\mathbf{S}$, which in turn can be generated by linear and bilinear interactions. In formula,

$$\varrho = U_{\mathbf{S}}\nu U_{\mathbf{S}}^\dagger, \qquad U_{\mathbf{S}} = e^{-iH} \tag{2.58}$$

where H is an Hamiltonian of the type in Eq. (2.11) and the number of thermal photons n_{kT} is given by $n_{kT} = d_k - \frac{1}{2}$. The Williamson theorem allows to recast the uncertainty principle (2.4), which is invariant under symplectic transformations, into

$$\mathbf{S}^T\mathbf{W}\mathbf{S} + \frac{i}{2}\mathbf{\Omega} \geq 0 \Rightarrow \mathbf{W} + \frac{i}{2}(\mathbf{S}^T)^{-1}\mathbf{\Omega}\mathbf{S}^{-1} \geq 0. \tag{2.59}$$

Since if $\mathbf{S}$ is symplectic, then $(\mathbf{S}^T)^{-1}$ and $\mathbf{S}^{-1}$ are also symplectic, hence $(\mathbf{S}^T)^{-1}\mathbf{\Omega}\mathbf{S}^{-1} = \mathbf{\Omega}$ and

$$\mathbf{W} + \frac{i}{2}\mathbf{\Omega} \geq 0 \iff d_k \geq \frac{1}{2}. \tag{2.60}$$

Pure Gaussian states are obtained only if ν is pure, i.e. the vacuum state $\nu_k = |0\rangle\langle 0| \ \forall k$, with $\nu = \otimes_{k=1}^{n}\nu_k$ and covariance matrix $\boldsymbol{\sigma} = \frac{1}{2}\mathbf{S}^\mathbf{T}\mathbf{S}$. Furthermore from (2.60) we have that, pure Gaussian states, for which we have $d_k = \frac{1}{2}$, $\forall k$ are minimum uncertainty states.

2.2.2 Single-mode Gaussian states

The simplest class of Gaussian states involves a single mode. Decomposition (2.58) for single-mode Gaussian states reads as follows [72]

$$\varrho = D(\alpha)S(\xi)\nu S^\dagger(\xi)D^\dagger(\alpha) \tag{2.61}$$

that is a displaced squeezed thermal state (DSTS) with $\alpha = \frac{1}{2}(x + iy)$, $\xi = re^{i\phi}$ and ν a thermal state with average photon number n_T. A convenient parametrization of Gaussian states can be given expressing their covariance matrix $\boldsymbol{\sigma}$ as a function of n_T, r, ϕ. Indeed, by using the phase-space representation of the squeezing operator, we have that the covariance matrix for the state ϱ is $\boldsymbol{\sigma} = \mathbf{\Sigma}_\xi^T\boldsymbol{\sigma}_\nu\mathbf{\Sigma}_\xi$, where $\boldsymbol{\sigma}_\nu$ is the covariance matrix of the thermal state and $\mathbf{\Sigma}_\xi$ is given in (2.39). Explicitly, we have

$$\boldsymbol{\sigma} = \begin{pmatrix} a & c \\ c & b \end{pmatrix} \tag{2.62}$$

where

$$\begin{aligned} a &= (n_T + \frac{1}{2})\left[\cosh(2r) - \sinh(2r)\cos\phi\right] \\ b &= (n_T + \frac{1}{2})\left[\cosh(2r) + \sinh(2r)\cos\phi\right] \\ c &= (n_T + \frac{1}{2})\sinh(2r)\sin\phi\,. \end{aligned} \tag{2.63}$$

Examples of the most important families of single-mode Gaussian states are obtained from the definition (2.61). For $\alpha = r = \phi = 0$, we obtain thermal states. For $r = n_T = \phi = 0$ we obtain coherent states and squeezed vacuum for $\alpha = n_T = 0$. If also $\phi = 0$, we

have squeezed real vacuum with covariance matrix $\boldsymbol{\sigma} = \frac{1}{2}\mathrm{Diag}(\mathrm{e}^{-2\mathrm{r}}, \mathrm{e}^{2\mathrm{r}})$ and mean photon number given by

$$n_S = \sinh^2 r. \tag{2.64}$$

The average mean photon number of a DSTS is given by

$$\mathrm{Tr}[\varrho a^\dagger a] = N = \left(n_T + \frac{1}{2}\right)\cosh(2r) - \frac{1}{2} + |\alpha|^2. \tag{2.65}$$

For a STS ($\alpha = 0$) the last equation becomes

$$\begin{aligned} N =& (n_T + \frac{1}{2})\cosh(2r) - \frac{1}{2} \\ =& (n_T + \frac{1}{2})(1 + 2\sinh^2 r) - \frac{1}{2} \\ =& n_T + n_S + 2n_T n_S. \end{aligned} \tag{2.66}$$

From Eq. (2.56), it follows that

$$\mu = \frac{1}{(2n_T + 1)}$$

which means that the purity of a generic Gaussian state depends only on the average number of thermal photons and that since displacement and squeezing are unitary operators, hence they do not affect the trace involved in the definition of purity. The same is true when one considers the *von Neumann entropy* S_V of a generic single-mode Gaussian state

$$\begin{aligned} S_V =& -\mathrm{Tr}[\varrho \log \varrho] \\ =& h(\sqrt{\det[\boldsymbol{\sigma}[\varrho]]}) && (2.67) \\ =& (1 + n_T)\log(1 + n_T) - n_T \log n_T && (2.68) \\ =& \frac{1-\mu}{2\mu}\log\left(\frac{1+\mu}{1-\mu}\right) - \log\left(\frac{2\mu}{1+\mu}\right) && (2.69) \end{aligned}$$

where

$$h(x) = (x + \frac{1}{2})\log(x + \frac{1}{2}) - (x - \frac{1}{2})\log(x - \frac{1}{2}). \tag{2.70}$$

2.2.3 Two-mode Gaussian states

In the following we study bipartite $1+1$ Gaussian systems. The main concept to be introduced is that of *local equivalence* which allows us to introduce normal forms to represent them and in general it holds for $n+m$ modes Gaussian states. Two states ϱ_1 and ϱ_2 of a bipartite system $\mathcal{H}_A \otimes \mathcal{H}_B$ are locally equivalent if there exist two unitary transformations U_A and U_B acting on $\mathcal{H}_A$ and $\mathcal{H}_B$ respectively such that $\varrho_2 = U_A \otimes U_B \varrho_1 U_A^\dagger \otimes U_B^\dagger$. The extension to multipartite systems is straightforward. Let us consider the case of bipartite

$1+1$ modes system, then the covariance matrix $\boldsymbol{\sigma}$ of any quantum state ϱ can be written in the so called standard form $\boldsymbol{\sigma}_{sf}$ by means of solely local operations can be recast, upon the action of local symplectic operations, in the standard form [73]

$$\boldsymbol{\sigma} = \frac{1}{2}\begin{pmatrix} a & 0 & c_1 & 0 \\ 0 & a & 0 & c_2 \\ c_1 & 0 & b & 0 \\ 0 & c_2 & 0 & b \end{pmatrix} \tag{2.71}$$

where a, b, c_1 and c_2 are determined by the four local symplectic invariants $I_1 = a^2$, $I_2 = b^2$, $I_3 = c_1 c_2$. $I_4 = \det[\boldsymbol{\sigma}] = (ab - c_1^2)(ab - c_2^2)$. The normal form (2.71) allows us to rewrite the uncertainty principle

$$I_1 + I_2 + 2I_3 \leq 4I_4 + \frac{1}{4}. \tag{2.72}$$

Let us consider an arbitrary two-mode Gaussian state ϱ. Then it can be shown that the corresponding covariance matrix $\boldsymbol{\sigma}$ can be written as

$$\boldsymbol{\sigma} = A^T \boldsymbol{\nu}_{d_\pm} A \tag{2.73}$$

where $\boldsymbol{\nu}_{d_\pm} = \boldsymbol{\nu}_{d_-} \oplus \boldsymbol{\nu}_{d_+}$ is the covariance matrix of a tensor product of thermal states with average photon numbers $n_{T\pm} = d_\pm - 1/2$ in the two modes

$$\boldsymbol{\nu}_{d_\pm} = \mathrm{diag}(d_-, d_-, d_+, d_+) \tag{2.74}$$

and

$$A = \boldsymbol{\Sigma}_L(r_1, r_2) R(\phi_1) \boldsymbol{\Sigma}_L(r, -r) R(\phi_2) \mathbf{S}_{loc}. \tag{2.75}$$

$\mathbf{S}_{loc}$ is a local operation which brings $\boldsymbol{\sigma}$ in its standard form (2.71), $\boldsymbol{\Sigma}_L(r_1, r_2)$ is the local two mode squeezing operator given by the direct product of two single-mode squeezing operators with null phase

$$\boldsymbol{\Sigma}_L(r_1, r_2) = \boldsymbol{\Sigma}_{r_1} \oplus \boldsymbol{\Sigma}_{r_2},$$

and $R(\phi)$ is the non-local two-mode mixing with a real parameter ϕ. The symplectic eigenvalues can be evaluated from the local invariants

$$d_\pm = \sqrt{\frac{\Delta(\boldsymbol{\sigma}) \pm \sqrt{\Delta(\boldsymbol{\sigma})^2 - 4I_4}}{2}}, \tag{2.76}$$

where $\Delta(\boldsymbol{\sigma}) = I_1 + I_2 + 2I_3$. The uncertainty relation then reads

$$d_- \geq 1/2. \tag{2.77}$$

Eq. (2.76) allows us to express the von Neumann entropy (2.67) in a very simple form

$$S_V = h(d_-) + h(d_+) \tag{2.78}$$

where the function $h(x)$ has been defined in (2.70). A relevant subclass of two-mode Gaussian states is constituted by two-mode squeezed thermal states $\varrho = S_2(r)\nu_{n_1} \otimes \nu_{n_2} S_2^\dagger(r)$ with a real squeezing parameter $r \in \mathbb{R}$, which corresponds to a covariance matrix

$$\boldsymbol{\sigma} = \frac{1}{2}\begin{pmatrix} a\mathbb{I}_2 & c\sigma_z \\ c\sigma_z & b\mathbb{I}_2 \end{pmatrix} \tag{2.79}$$

with parameters

$$a = \cosh(2r) + 2n_{T_1}\cosh^2 r + 2n_{T_2}\sinh^2 r \tag{2.80}$$

$$b = \cosh(2r) + 2n_{T_1}\sinh^2 r + 2n_{T_2}\cosh^2 r \tag{2.81}$$

$$c = (1 + n_{T_1} + n_{T_2})\sinh 2r\,. \tag{2.82}$$

The mean total number of photons for this class of states in terms of the covariance matrix is given by [67]

$$\begin{aligned} N =& \frac{1}{2}(a+b) - 1 \\ =& \frac{1}{2}[1 + 2\sinh^2 r + 2n_{T_1}(1+\sinh^2 r) + 2n_{T_2}\sinh^2 r] \\ &+ \frac{1}{2}[1 + 2\sinh^2 r + 2n_{T_2}(1+\sinh^2 r) + 2n_{T_1}\sinh^2 r] - 1 \\ =& n_{T_1} + n_{T_2} + 2n_S(1 + n_{T_1} + n_{T_2}) \end{aligned} \tag{2.83}$$

where we used that $n_S = \sinh^2 r$. The TWB state (2.46) is recovered when the thermal states are vacuum states, i.e. $n_1 = n_2 = 0$, leading to $a = b = \cosh(2r)$, $c = \sinh(2r)$.

2.3 Some measures of correlations in Gaussian states

Entanglement

Quantum correlations have been the subject of intensive studies in the past two decades, mainly because they are believed to be the fundamental resource in quantum processing tasks. There have been many attempts to address the classification of quantum correlations and in particular, starting from [74], the concept of quantum entanglement has been put on a firm basis. A state of a bipartite quantum system is called *entangled* if it cannot be written as a separable state as follows

$$\varrho = \sum_k p_k \varrho_{Ak} \otimes \varrho_{Bk} \tag{2.84}$$

where $p_k \geq 0$, $\sum_k p_k = 1$ and ϱ_{Ak}, ϱ_{Bk} are generic density matrices describing the states of the two subsystems. The physical meaning of such a definition is that a separable state can be prepared by means of operations acting on the two subsystems separately (i.e. local operations) and classical communication. In the following we will restrict ourselves to the characterization of the entanglement and of some other measures of quantum correlations for two-mode Gaussian states.

The necessary and sufficient separability criterion for such states is the positivity of the partially transposed state $\tilde{\boldsymbol{\sigma}}$ (PPT) criterion [75]. In this last paper, Simon observed that the action of partial transposition amounts, in the phase space, to a mirror reflection of one of the four canonical variables. In terms of the symplectic invariants, this results in flipping the sign of I_3. Then we have that the symplectic invariants of the covariance matrix $\tilde{\boldsymbol{\sigma}}$ of the partially transposed state are

$$\tilde{I}_1 = I_1, \qquad \tilde{I}_2 = I_2, \qquad \tilde{I}_3 = -I_3, \qquad \tilde{I}_4 = I_4 \tag{2.85}$$

where I_j are the local invariants of $\boldsymbol{\sigma}$. Together with (2.72), a separable Gaussian two-mode state must obey to

$$I_1 + I_2 + 2|I_3| \leq 4I_4 + \frac{1}{4} \tag{2.86}$$

and the PPT criterion can be written in terms of $\tilde{d}_-$ the smallest symplectic eigenvalue of $\tilde{\boldsymbol{\sigma}}$ as

$$\tilde{d}_- \geq 1/2 \tag{2.87}$$

where

$$\tilde{d}_-^2 = \frac{1}{2}[\tilde{\Delta} - \sqrt{\tilde{\Delta}^2 - 4I_4}] \tag{2.88}$$

and $\tilde{\Delta} = I_1 + I_2 - 2I_3$. As regards the quantification of the entanglement, a measure that can be computed for arbitrary two-mode Gaussian states is provided by the negativity $\mathcal{N}$, introduced by Vidal end Werner for continuous variable systems [76]. The negativity of a quantum state ϱ is defined as

$$\varrho = \frac{\|\tilde{\varrho}\| - 1}{2} \tag{2.89}$$

where $\tilde{\varrho}$ is the partially transposed state and $||\hat{o}|| = \mathrm{Tr}\sqrt{\hat{o}^\dagger \hat{o}}$ is the trace norm of an operator $\hat{o}$. The quantity $\mathcal{N}(\varrho)$ is equal to the modulus of the sum of the negative eigenvalues of $\tilde{\varrho}$ and it quantifies to which $\tilde{\varrho}$ fails to be positive. Strictly related to $\mathcal{N}$ is the logarithmic negativity $E_{\mathcal{N}}$ defined as $E_{\mathcal{N}} = \log \|\tilde{\varrho}\|$. It can be shown that, for two-mode Gaussian states, it is a simple function of $\tilde{d}_-$, namely

$$E = \max\{0, -\log 2\tilde{d}_-\} \tag{2.90}$$

that is an entanglement monotone, more precisely it is a monotonic decreasing function of $\tilde{d}_-$, quantifying the amount by which Eq. (2.87) is violated.

Quantum discord

The quantum discord is defined as the mismatch between two quantum analogues of classically equivalent expressions of the mutual information. For pure quantum states, the quantum discord coincides with the entropy of entanglement. However, the quantum discord can be different from zero also for some separable (mixed) states. In other words, classical communication can give rise to quantum correlations. This can be understood by considering that the states ϱ_{Ak} and ϱ_{Bk} of a bipartite system may be physically nondistinguishable, i.e. nonorthogonal, and thus not all the information about them can be locally retrieved. This phenomenon has no classical counterpart, thus accounting for the quantumness of the correlations in a separable state with quantum discord.

Let us consider two classical random variables A and B with joint probability $p_{AB}(a, b)$; the total correlations between the two variables are measured by the mutual information. The latter can be defined by two equivalent expressions: $I(A;B) = H(A)+H(B)-H(A,B)$ and $I(A;B) = H(A) - H(A|B) \equiv H(B) - H(B|A)$, where $H(X) = -\sum_x p_X(x) \log p_X(x)$ is the Shannon entropy of the corresponding probability distribution and the conditional entropy is defined in terms of the conditional probability $p_{A|B}(a|b)$ as $H(A|B) = -\sum_{ab} p_{AB}(a,b) \log p_{A|B}(a|b)$. The idea of quantum discord grows up of the fact that the quantum version of the mutual information of a bipartite state ϱ_{AB} may be defined in two nonequivalent ways. The first is obtained by the straightforward quantization of $I(A;B)$, i.e. $I(\varrho_{AB}) = S(\varrho_A) + S(\varrho_B) - S(\varrho_{AB})$ where $S(\varrho)$ is the von Neumann entropy of the

state ϱ as defined in (2.67) and $\varrho_{A(B)} = \mathrm{Tr}_{B(A)}[\varrho_{AB}]$ are the partial traces over the two subsystems. The second is obtained with the quantization of the conditional entropy which involves the conditional state of a subsystem after a measurement performed on the other one, and this fact has the consequence that: i) the symmetry between the two subsystems is broken; ii) the quantity depends on the choice of the measurement; iii) the resulting expression is generally different from $I(\varrho_{AB})$. Let us denote by $\varrho_{Ak} = 1/p_b(k)\mathrm{Tr}_B[\varrho_{AB}\mathbb{I}\otimes\Pi_k]$, with $p_B(k) = \mathrm{Tr}_{AB}[\varrho_{AB}\mathbb{I}\otimes\Pi_k]$, the conditional state of the system A after having observed the outcome k from a measurement performed on the system B. In turn, $\{\Pi_k\}$, $\sum_k \Pi_k = \mathbb{I}$ denotes a POVM describing a generalized measurement. The quantum analogue of the mutual information defined via the conditional entropy is defined as the upper bound $J_A = \sup_{\{\Pi_k\}} S(\varrho_A) - \sum_k p_B(k)S(\varrho_{Ak})$ taken over all the possible measurements. Finally the quantum A discord is defined in terms of the mismatch $D(\varrho_{AB}) = I(\varrho_{AB}) - J_A(\varrho_{AB})$. Analogously one is led to define the quantum B discord through the entropy of conditional states of system B.

For a bipartite squeezed thermal state (STS) with covariance matrix as in Eq. (2.71) the quantum discord may be written as [77]

$$D = h(\sqrt{I_2}) - h(d_-) - h(d_+) + h(\frac{\sqrt{I_1} + 2\sqrt{I_1 I_2} + 2I_3}{1 + 2\sqrt{I_2}}) \tag{2.91}$$

where $h(x) = (x + \frac{1}{2})\log(x + \frac{1}{2}) - (x - \frac{1}{2})\log(x - \frac{1}{2})$.

Quantum mutual information

The quantum mutual information, which quantifies the amount of total, classical plus quantum, correlations, is given by $I = S(\rho_A) + S(\rho_B) - S(\rho_{AB})$, where $S(\rho)$ is the von Neumann entropy of the state ρ defined in Eq. (2.67). For a Gaussian bipartite state in the canonical form (2.71) the quantum mutual information reduces to

$$I = \frac{1}{2}\left[h(\sqrt{I_1}) + h(\sqrt{I_2}) - h(d_+) - h(d_-)\right] \tag{2.92}$$

where the symplectic eigenvalues $d_\pm$ are given in Eq. (2.76).

2.4 Gaussian quantum channels

We address the evolution of a Gaussian state in an open quantum system usually called quantum channel that is a completely positive trace-preserving map $\varrho \to \mathcal{E}(\varrho)$ as defined in (1.12) that takes states ϱ into states. We will restrict ourselves to Gaussian quantum channels that are defined as those that map Gaussian states into Gaussian states [78]. In section 2.1 we described all the unitary Gaussian channels, that correspond in the phase space to matrices S such that $S\Omega S^T = \Omega$ and comprise the displacement operator, the beam splitter evolutions and the single- and two-mode squeezing operations. The covariance matrix of a quantum state undergone this kind of unitary operations transforms as

$$\boldsymbol{\sigma} \to S^T \boldsymbol{\sigma} S. \tag{2.93}$$

It can be shown that the action of the most general Gaussian channel $\mathcal{E}$ in the Schrödinger picture $\varrho \to \mathcal{E}(\varrho)$ corresponds to a transformation of the covariance matrix

$$\boldsymbol{\sigma} \to X^T \boldsymbol{\sigma} X + Y. \tag{2.94}$$

X serves the purpose of amplification or attenuation and rotation in the phase space, whereas the Y contribution is a noise term which may consists of quantum as well as classical noise. Two important cases of Gaussian channels are:

- the *classical noise channel*, i.e. $X = \mathbb{I}$, $Y \geq 0$, that can be represented by a random displacement,
- the *lossy channel*, i.e. $X = \mathbb{G}^{1/2}$, $Y = (\mathbb{I} - \mathbb{G})(1/2 + N)\mathbb{I}$ where $\mathbb{G} = \bigoplus_{h=1}^{n} e^{-\Gamma t}\mathbb{I}_2$, Γ is the damping rate and N the mean number of photons in the bath.

The evolution of a Gaussian state in both these channels is described in the following. Let us consider the evolution of a Gaussian state in a dissipative channel $\mathcal{E}_\Gamma$ characterized by a damping rate Γ, which may result from the interaction of the system with an external environment, as for example a bath of oscillators, or from an absorption process. The propagation of a mode of radiation (the *system*) described by the Hamiltonian H_S in a lossy channel corresponds to the coupling of the mode a with a finite temperature T reservoir (bath) described by H_R made of large number of external modes. The reservoir may be for example the modes of the free electromagnetic field or phonon modes in a solid. There is a weak interaction between the system and the reservoir given by the Hamiltonian V. Thus we have that the total Hamiltonian is

$$H = H_S + H_R + V \tag{2.95}$$

The derivation of the Master equation is not dependent on the specific reservoir model. In the particular case of a damped harmonic oscillator we have

$$H_S = a^\dagger a + \frac{1}{2}, \tag{2.96}$$

$$H_R = \sum_j (b_j^\dagger b_j + \frac{1}{2}), \tag{2.97}$$

$$V = a^\dagger B(t) e^{i\omega_0 t} + a B^\dagger(t) e^{-i\omega_0 t}, \qquad \text{with} \quad B(t) = \sum_j g_j b_j e^{-i\omega_j t} \tag{2.98}$$

where $[a^\dagger, a] = \mathbb{I}$, $[b_j^\dagger, b_k] = \delta_{jk}\mathbb{I}$, ω_0 the frequency of the system and V is written in the interaction picture. By writing the evolution equation of the whole system and tracing out the bath we obtain the reduced density matrix of the system that is described by a Gaussian state. By assuming a Markovian reservoir i.e. $\langle b^\dagger(\omega_j) b(\omega_k)\rangle = N\delta(\omega_j - \omega_k)$ and weak coupling between the system and the reservoir the dynamics of the system is described by the Lindblad Master equation [79]

$$\dot{\varrho} = \frac{\Gamma}{2}\left\{(N+1)\mathcal{L}[a] + N\mathcal{L}[a^\dagger]\right\}\varrho \tag{2.99}$$

where $\mathcal{L}[a]\varrho = 2a\varrho a^\dagger - a^\dagger a\varrho - \varrho a^\dagger a$.

Lossy channels

The propagation of a mode of radiation in a lossy channel corresponds to the coupling of the mode a with a zero temperature reservoir made of large number of external modes. Then the Lindblad Master equation becomes

$$\dot{\varrho} = \frac{\Gamma}{2}\mathcal{L}[a]\varrho \tag{2.100}$$

The general solution of Eq. (2.100) may be expressed with the operator-sum representation of the associated CP-map i.e., upon writing $\eta = e^{-\Gamma t}$

$$\varrho(\eta) = \sum_m V_m \, \varrho \, V_m^\dagger$$

where

$$V_m = \sqrt{\frac{(1-\eta)^m}{m!}}\, a^m \, \eta^{\frac{1}{2}(a^\dagger a - m)},$$

and ϱ is the initial state. Let us now start with single-mode states. Eq. (2.99) can be recast into a Fokker-Planck equation for the Wigner function in terms of the quadrature variables q and p,

$$\dot{W} = \frac{\Gamma}{2}\left[\partial_{\boldsymbol{X}}^T \boldsymbol{X} + \partial_{\boldsymbol{X}}^T \boldsymbol{\sigma}_\infty \partial_{\boldsymbol{X}}^T\right] W \tag{2.101}$$

where $\boldsymbol{X} = (q,p)^T$, $\partial_{\boldsymbol{X}} = (\partial_q, \partial_p)^T$ and we introduced the diffusion matrix $\boldsymbol{\sigma}_\infty = \mathrm{diag}(1/2+N, 1/2+N)$. Solving the equation for the Wigner function of a single-mode Gaussian states one can obtain the evolution equation for $\boldsymbol{\sigma}$

$$\dot{\boldsymbol{\sigma}} = -\Gamma(\boldsymbol{\sigma} - \boldsymbol{\sigma}_\infty) \tag{2.102}$$

which yields to

$$\boldsymbol{\sigma}(t) = e^{-\Gamma t}\boldsymbol{\sigma}_0 + (1 - e^{-\Gamma t})\boldsymbol{\sigma}_\infty \tag{2.103}$$

which describes the evolution of an initial Gaussian state with CM $\boldsymbol{\sigma}_0$ towards the stationary state given by the Gaussian state of the environment with covariance matrix given by $\boldsymbol{\sigma}_\infty$. In terms of the matrices introduced in Eq. (2.94) we have

$$X = e^{-\Gamma t/2}\mathbb{I}_2, \qquad Y = (1 - e^{-\Gamma t})(\frac{1}{2} + N)\mathbb{I}_2. \tag{2.104}$$

For $\Gamma = 0$ we have a classical noise channel which corresponds to $X = \mathbb{I}$ and $Y = 0$, whereas $\Gamma \neq 0$ is the case of a lossy channel. We consider as input state a squeezed thermal state with an average number of thermal photons given by n_T and a real squeezing parameter r. The covariance matrix is given in Eq. (2.62) with $\phi = 0$ and the evolved CM of the single mode case, Eq. (2.103) reads

$$\boldsymbol{\sigma}' = e^{-\Gamma}\boldsymbol{\sigma} + (1 - e^{-\Gamma})\,\boldsymbol{\sigma}_\infty = \begin{pmatrix} a_\Gamma & 0 \\ 0 & b_\Gamma \end{pmatrix}, \tag{2.105}$$

where from now on we omit the index of $\boldsymbol{\sigma}_0$, replace $\boldsymbol{\sigma}(t) = \boldsymbol{\sigma}'$ and, since the loss parameter always appears as Γt, consider that the time t has been absorbed in Γ. The number of thermal photons n_Γ and the squeezing parameter r_Γ after the evolution in the lossy channel is obtained upon rewriting $\boldsymbol{\sigma}'$ in the standard form,

$$\begin{aligned} n_\Gamma &= \sqrt{\det[\boldsymbol{\sigma}']} - 1/2 \\ r_\Gamma &= 1/4 \log\left[\frac{e^{-\Gamma}a + (1 - e^{-\Gamma})/2}{e^{-\Gamma}b + (1 - e^{-\Gamma})/2}\right] \end{aligned} \tag{2.106}$$

with

$$\begin{aligned} a_\Gamma &= \frac{1}{2}\,(1 + 2n_\Gamma)\,e^{2r_\Gamma} \\ b_\Gamma &= \frac{1}{2}\,(1 + 2n_\Gamma)\,e^{-2r_\Gamma}\,. \end{aligned} \tag{2.107}$$

We now consider the evolution of a two-mode Gaussian state in two noisy channels characterized by the damping Γ_1 and Γ_2 respectively and described by the map $\mathcal{E}_{\Gamma_1} \otimes \mathcal{E}_{\Gamma_2}$.

At the level of the covariance matrix it corresponds to the following transformation

$$\begin{aligned}\boldsymbol{\sigma}_\Gamma = &\left(e^{-\Gamma_1/2}\mathbb{I}_2 \oplus e^{-\Gamma_2/2}\mathbb{I}_2\right)\boldsymbol{\sigma}\left(e^{-\Gamma_1/2}\mathbb{I}_2 \oplus e^{-\Gamma_2/2}\mathbb{I}_2\right)\\ &+ (\mathbb{I}_4 - e^{-\Gamma_1}\mathbb{I}_2 \oplus e^{-\Gamma_2/2}\mathbb{I}_2)\boldsymbol{\sigma}_\infty\end{aligned} \tag{2.108}$$

where we have used the same notation introduced for the single-mode case. If the input state is a two-mode squeezed thermal state of the form $\varrho_2 = S_2(r)\nu_1 \otimes \nu_2 S_2(r)^\dagger$ and covariance matrix given in Eq. (2.71), then also the output state belongs to the same class, with the replacements $r \to r_\Gamma$, $n_{T1} \to n_{\Gamma 1}$, $n_{T2} \to n_{\Gamma 2}$. The covariance matrix in Eq. (2.79) may be recast in the standard form as

$$\boldsymbol{\sigma}_\Gamma = \frac{1}{2}\begin{pmatrix} a_\Gamma \mathbb{I}_2 & b_\Gamma \sigma_z \\ c_\Gamma \sigma_z & b_\Gamma \mathbb{I}_2 \end{pmatrix} \tag{2.109}$$

and the explicit form of the parameters of the evolved state may be obtained from the very definition of the symplectic invariants. For two-mode squeezed thermal states we have

$$\begin{aligned} a_\Gamma - b_\Gamma &= n_{1\Gamma} - n_{2\Gamma},\\ \sqrt{\det \boldsymbol{\sigma}_\Gamma} &= \frac{1}{4}\left(2n_{1\Gamma}+1\right)\left(2n_{2\Gamma}+1\right),\\ c_\Gamma &= \left(n_{1\Gamma} + n_{2\Gamma} + 1\right)\sinh 2r_\Gamma. \end{aligned} \tag{2.110}$$

Gaussian Noise

We address the problem of discriminating between two single-mode Gaussian states ϱ_{Δ_1} and ϱ_{Δ_2} obtained by the evolution in channels characterized by two different additive Gaussian noises. We consider an initial state that evolves into a state ϱ_Δ through the mapping described by the so called Gaussian noise map $\mathcal{G}_\Delta$, [80, 81, 82]

$$\mathcal{G}_\Delta(\varrho_0) = \varrho_\Delta = \int_{\mathbb{C}} d^2\gamma \frac{e^{-|\gamma|^2/\Delta}}{\pi\Delta} D(\gamma)\varrho_0 D^\dagger(\gamma) \tag{2.111}$$

Δ being the thermal mean number of added photons and $\varrho_0 = D(\alpha_0)S(r_0)\nu(n_0)S^\dagger(r_0)D^\dagger(\alpha_0)$ a displaced squeezed thermal state (DSTS) with covariance matrix given by Eq. (2.62) with parameters n_0, r_0 and ϕ_0. The state ϱ_{Δ_i} is already a DSTS

$$\varrho_{\Delta_i} = D(\alpha_i)S(r_i)\nu(n_i)S^\dagger(r_i)D^\dagger(\alpha_i) \tag{2.112}$$

The only modification to the covariance matrix

$$\boldsymbol{\sigma}_\Delta = \begin{pmatrix} a' & c' \\ c' & b' \end{pmatrix}. \tag{2.113}$$

of the evolved state given by the mapping (2.111) is an addition of Δ to the diagonal elements of $\boldsymbol{\sigma}_0$: $a' \to a + \Delta$ and $b' \to b + \Delta$ whereas $c' = c$. In terms of the matrices introduced in Eq. (2.94) we have

$$X = \mathbb{I}_2, \qquad Y = \Delta \mathbb{I}_2. \tag{2.114}$$

Notice that for $\Delta = 0$, $Y = \mathbb{I}_2$ i.e. the additive Gaussian noise channel converges to the identity channel. The amplitude $\alpha_i = \alpha_0$ because $\mathrm{Tr}[\varrho_{\Delta_i} a] = \langle a \rangle_{\varrho_0}$, r_i is a rather involved function of r_0, n_0 and Δ_i and $n_i = \sqrt{\det[\sigma_{\Delta_i}]} - 1/2$. The entries a', b' and c' of $\boldsymbol{\sigma}_\Delta$ in Eq. (2.113) can be written in the standard form by solving the following

$$\begin{aligned} \phi_i &= \phi_0 \\ (n_i + 1/2)\sinh(2r_i) &= (n_0 + 1/2)\sinh(2r_0) \\ (n_i + 1/2)\cosh(2r_i) &= (n_0 + 1/2)\cosh(2r_0) + \Delta_i. \end{aligned} \tag{2.115}$$

2.5 Estimation of parameters in quantum optics

In this section we address quantum estimation of displacement and squeezing parameters by using two classes of probe states. We first consider displaced squeezed vacuum states and then squeezed vacuum states undergoing Kerr interaction. This last class of non-classical states of light represents a resource for high precision measurements. They are generally produced in active optical media, which couple one or more modes of the field through the nonlinear susceptibility of the matter. In particular, parametric processes in second order $\chi^{(2)}$ media correspond to Gaussian operations and are used to generate squeezing, hereafter *Gaussian* squeezing, and entanglement. Gaussian squeezing is the basic ingredient of quantum enhanced interferometry [83, 84, 85, 86, 87, 88, 89, 90] and found several applications in quantum metrology and communication [91, 92, 93, 94, 95, 96]. In addition, Gaussian squeezing is the key resource to achieve precise estimation of unitary [33, 97] and non unitary parameters [35]. In turn, squeezed vacuum state has been addressed as a universal optimal probe [98, 35, 97] within the class of Gaussian states.

On the other hand, the Kerr effect taking place in third-order nonlinear $\chi^{(3)}$ media leads to a non Gaussian operation, and has been suggested to realize quantum nondemolition measurements [99, 100], and to generate quantum superpositions [101, 102] as well as squeezing [103] and entanglement [104]. A well known example of Kerr media are optical fibers where, however, nonlinearities are very small and accompanied by other unwanted effects. Larger Kerr nonlinearities have been observed with electro- magnetically induced transparency [105] and with Bose Einstein condensates [106] and cold atoms [107]. Notice that the dynamics in a Kerr medium may be accuraterly described in terms of the Wigner function in the phase-space [108].

In the following we first consider the estimation of the displacement and squeezing parameters by evaluating the quantum Fisher information of a displaced squeezed vacuum state. Then we consider a displaced squeezed vacuum state undergoing self-Kerr interaction and investigate their use in estimation of displacement and squeezing parameters. Indeed, displacement and squeezing are basic Gaussian operations in continuous variable systems and represent building blocks to manipulate Gaussian states for quantum information processing. Besides, they represent the ultimate description of interferometric interaction. As a consequence, their characterization, i.e the optimal estimation of displacement and squeezing parameters has been widely investigated [32, 109, 110, 111, 112, 97] by using different tools from quantum estimation theory (QET) [113, 14, 30, 31, 114, 66, 25, 42]. Upon maximizing the quantum Fisher information we find that single-mode squeezed vacuum represents an optimal class of probe states.

Our main goal is to assess Kerr interaction and the resulting nonGaussianity as a resource for parameter estimation, and to this aim we consider two different situations with different physical constraints. On the one hand we study schemes where we fix the overall energy available to the probe, without posing any constraint on the available Gaussian squeezing; this will be referred to as the fixed energy case. On the other hand, we will analyze the more realistic case where the amount of Gaussian squeezing is fixed, or even absent, and refer to this case as the fixed squeezing case. As we will see, at fixed energy Gaussian squeezing still represents the optimal resource for parameter estimation. On the other hand, when the amount of Gaussian squeezing is fixed then Kerr interaction turns out to be useful to improve estimation, especially when the probe states have a large number of *non squeezing* photons, i.e large amplitude. In this case precision obtained by Gaussian states is achieved or enhanced.

The section is structured as follows: we first analyze the use of Kerr interaction to improve estimation of the displacement by considering different Gaussian probes and then we address the estimation of squeezing. The results reviewed in this section are reported in [115].

2.5.1 Estimation of displacement

Let us first consider the estimation of displacement, i.e. of the real parameter $\lambda \in \mathbb{R}$ imposed by the unitary $U_\lambda = \exp\{-i\lambda A_d\}$, $A_d = a^\dagger + a$ being the corresponding generator. Given a generic pure Gaussian probe, i.e. a displaced squeezed state of the form

$$|\alpha, r\rangle = D(\alpha)S(r)|0\rangle$$

(with $\alpha = |\alpha|e^{i\phi}$ and $r > 0$) where $D(\alpha) = \exp\{\alpha a^\dagger - \bar{\alpha}a)\}$ and $S(r) = \exp\{\frac{r}{2}(a^{\dagger 2} - a^2)\}$, the quantum Fisher information of λ for the state $|\alpha, r\rangle$, that corresponds to the fluctuations of the generator, may be evaluated from Eq. (1.75)

$$\begin{aligned} G^{(d)} =& 4\left(\langle\alpha, r|A_d^2|\alpha, r\rangle - \langle\alpha, r|A_d|\alpha, r\rangle^2\right) \\ =& 4\left(\langle\alpha, r|(a^2 + a^{\dagger 2} + 2a^\dagger a + 1)|\alpha, r\rangle - \langle\alpha, r|(a + a^\dagger)|\alpha, r\rangle^2\right) \end{aligned} \tag{2.116}$$

By normal ordering for creation and annihilation operators [116, 117] we have

$$\langle\alpha, r|A_d^2|\alpha, r\rangle = 4|\alpha|^2\cos^2\phi + \cosh(2r) + \sinh(2r) \tag{2.117}$$

$$\langle\alpha, r|A_d|\alpha, r\rangle = 2|\alpha|\cos\phi \tag{2.118}$$

Then one obtains

$$G^{(d)} = 4 + 8N\beta + 8\sqrt{N\beta(1 + N\beta)}, \tag{2.119}$$

where $N = \sinh^2 r + |\alpha|^2$ is the number of photons of the probe state and where $\beta = \sinh^2 r/N$ is the corresponding squeezing fraction ($0 \leq \beta \leq 1$). As expected for a unitary family the QFI does not depend on the value of the parameter. Besides, the QFI depends only on the squeezing energy $N_{sq} = \beta N$, and thus increasing the amplitude energy $N_\alpha = |\alpha|^2$, does not lead to any enhancement of precision. Therefore, at fixed energy, the maximum QFI

$$G_S^{(d)} = 4 + 8N + 8\sqrt{N(1+N)} \tag{2.120}$$

is achieved for $\beta = 1$, *i.e.* for squeezed vacuum. In the opposite limit ($\beta = 0$), *i.e.* for coherent states, the QFI is constant:

$$G_C^{(d)} = 4 \tag{2.121}$$

therefore it does not depend on the energy N and also on the phase.

Let us consider now a generic Gaussian state that undergoes Kerr interaction

$$|\alpha, r, \gamma\rangle = U_\gamma D(\alpha) S(r)|0\rangle$$

where $U_\gamma = \exp(-i\gamma(a^\dagger a)^2)$. The QFI for this class of states can be evaluated numerically upon varying the parameters γ, $|\alpha|$, ϕ, and r. We found that at fixed energy, the optimal probe state is still the squeezed vacuum state. The optimal QFI is a monotonous decreasing function of γ and the Kerr dynamics does not improve estimation precision. In other words, at fixed energy, squeezed vacuum state is the best probe not only among the class of Gaussian states, but also maximizing the QFI over the wider class of states Kerr perturbed Gaussian states.

Let us now address estimation of displacement in the more realistic configuration, where the amount of Gaussian squeezing is fixed or absent. For Kerr modified coherent states $|\alpha, \gamma\rangle$, QFI can be evaluated analytically at fixed energy $N = |\alpha|^2$ and γ, arriving at

$$\begin{aligned} G_\gamma^{(d)} = 4 + 8Ne^{-4N\sin^2\gamma}\Big\{ & e^{4N\sin^2\gamma} - 1 + \cos[2(\gamma - \phi + N\sin 2\gamma)] \\ & - e^{-4N\cos 2\gamma \sin^2\gamma}\cos[4\gamma - 2\phi + N\sin 4\gamma]\Big\} \end{aligned} \tag{2.122}$$

and then optimized numerically over the coherent phase ϕ. The results are reported in Fig. 2.1 (left panel) as a function of the number of photons $|\alpha|^2$ and for different values of γ. The QFI increases with $N_\alpha = |\alpha|^2$ and γ and the precision achievable with current technology squeezing, say $N_{sq} \lesssim 2$, may be attained and surpassed for realistic values of the Kerr coupling γ and large enough signal amplitude, say $\gamma|\alpha|^2 \lesssim 1$. Better performances may be

obtained by considering Kerr modified squeezed states $|\alpha, r, \gamma\rangle$ with fixed squeezing r and large amplitude $|\alpha| \gg 1$. The QFI for this case, as evaluated numerically and optimized over the amplitude phase ϕ is reported in Fig. 2.1 (right plot). We observe that, after a regime where QFI oscillates around the value obtained for vanishing γ, then it increases monotonically with $|\alpha|^2$ and exceed the corresponding Gaussian QFI for large enough values of $|\alpha|^2$ and/or γ. Due to numerical limitations, we have considered $|\alpha|^2 \leq 100$, and thus we have seen enhancement of precision only for the largest values of γ. We expect analogue performances by considering smaller values of γ and larger numbers of photons.

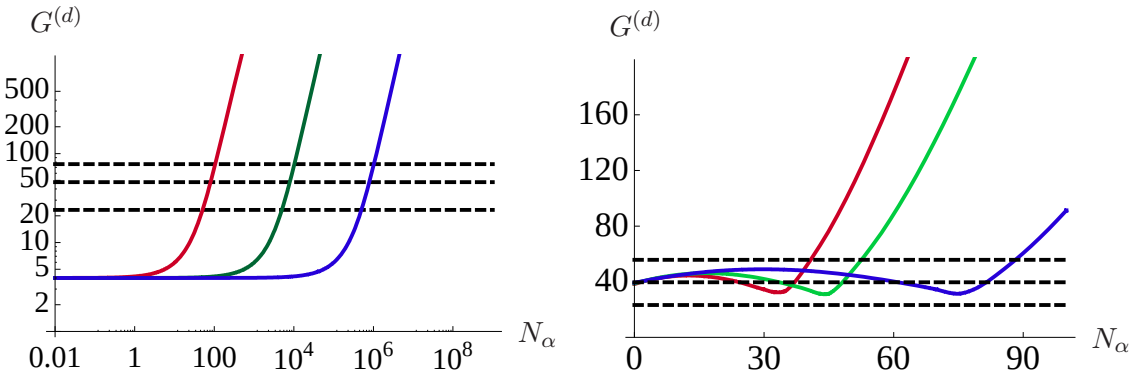

Figure 2.1: (Color online) Left: QFI $G_\gamma^{(d)}$ for displacement estimation by Kerr modified coherent states (solid lines) as a function of the number of photons N_α and for different values of γ. From top to bottom: (red) $\gamma = 10^{-2}$; (green) $\gamma = 10^{-4}$; (blue) $\gamma = 10^{-6}$. Dashed lines refer to QFI $G_S^{(d)}$ of squeezed vacuum states for different values of squeezing photons. From bottom to top: $N_{sq} = 1, 2, 3$. Right: QFI $G_\gamma^{(d)}$ for Kerr modified displaced squeezed states, $N_{sq} = 2$, for different values of γ: (red) $\gamma = 0.01$; (green) $\gamma = 0.008$; (blue) $\gamma = 0.005$. Dashed lines denote QFI $G_S^{(d)}$ of squeezed vacuum states for different values of squeezing photons. From bottom to top: $N_{sq} = 1, 2, 3$.

2.5.2 Estimation of squeezing

Let us now consider estimation of squeezing, that is the estimation of the real parameter $z \in \mathbb{R}$ imposed by the unitary evolution $U_z = \exp\{-izA_s\}$ with generator $A_s = \frac{1}{2}(a^{\dagger 2} + a^2)$. Given a generic single-mode Gaussian state $|\alpha, r\rangle = D(\alpha)S(r)|0\rangle$, the QFI for squeezing estimation has been evaluated by using the normal ordering for creation and annihilation operators [116]. As in the previous case of displacement estimation with pure states, the quantum Fisher information is equal to the fluctuations of the generator A_s, Eq. (1.75)

which are given by

$$\begin{aligned}\langle\alpha, r|A_s^2|\alpha, r\rangle =&\langle a^{\dagger 4} + 2a^{\dagger 2}a^2 + a^4 + 4a^\dagger a + 2\rangle \\ =&\frac{1}{2}[1 + 4\alpha^4(1 + \cos(4\phi)) + 3\cosh(4r) + 8\alpha^2(\cosh(2r) \\ &+ 2\cos(2\phi)\sinh(2r))] \qquad (2.123)\\ \langle\alpha, r|A_s|\alpha, r\rangle^2 =&\langle a^{\dagger 2} + a^2\rangle = (2\alpha^2\cos(2\phi) + \sinh(2r))^2 \qquad (2.124)\end{aligned}$$

The quantum Fisher information becomes

$$G^{(s)} = 1 + \cosh(4r) + 4\alpha^2(\cosh(2r) + \cos(2\phi)\sinh(2r)). \qquad (2.125)$$

Introducing the total energy N and the fraction of squeezing β, the Eq. (2.125) becomes

$$G^{(s)} = 1 - 4N(\beta - 1)(1 + 2N\beta + 2\sqrt{n\beta(1 + N\beta)}\cos(2\phi)) + 1 + 8N\beta(1 + N\beta) \qquad (2.126)$$

The maximum is obtained for $\beta = 1$ (squeezed vacuum) and we have

$$G_S^{(s)} = 8N^2 + 8N + 2 \qquad (2.127)$$

and is again achieved using squeezed vacuum probe [97]. In order to investigate the effect of Kerr interaction we consider Kerr modified Gaussian states $|\alpha, r, \gamma\rangle$. At fixed energy QFI has been evaluated and optimized numerically against the squeezing fraction β and phase ϕ. In this case, the optimal squeezing fraction decreases monotonically with both γ and the total number of photons N and the maximized QFI is a decreasing function of γ, that is Kerr interaction does not improve, actually degrades, the estimation precision achievable with squeezed vacuum probe.

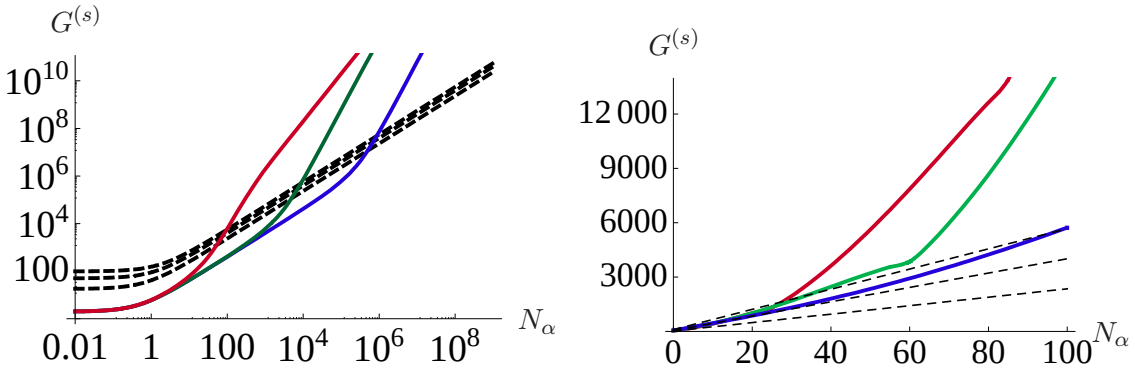

Figure 2.2: (Color online) Left: QFI $G_\gamma^{(s)}$ for squeezing estimation by Kerr modified coherent probes (solid lines) as a function of the number of photons N_α and for different values of γ. From top to bottom: (red) $\gamma = 10^{-2}$; (green) $\gamma = 10^{-4}$; (blue) $\gamma = 10^{-6}$. Dashed lines refer to the QFI $G_S^{(s)}$ for displaced squeezed probes and different values of squeezing photons. From bottom to top: $N_{sq} = 1, 2, 3$. Right: QFI $G_\gamma^{(s)}$ for Kerr modified displaced squeezed states (solid lines) with $N_{sq} = 2$ squeezing photons, as a function of field amplitude photons $N_\alpha = |\alpha|^2$ and for different values of γ: (red) $\gamma = 0.01$; (green) $\gamma = 0.005$; (blue) $\gamma = 0.001$. Dashed lines refer to the QFI $G_S^{(s)}$ for displaced squeezed vacuum states and different values of squeezing photons. From bottom to top: $N_{sq} = 1, 2, 3$.

Let us now consider situations where squeezing is not available, or its amount is fixed, and where the field amplitude may be increased at will. The QFI for probe states of the form $|\alpha, \gamma\rangle = U_\gamma D(\alpha)|0\rangle$ can be evaluated analytically as

$$G_\gamma^{(s)} = 2 + 2N\Big\{2 + N - Ne^{-4N\sin^2\gamma}(1 + \cos[2(4\gamma - 2\phi + N\sin 42\gamma)]) + Ne^{-N(1-\cos 8\gamma)}\cos[16\gamma - 4\phi + N\sin 8\gamma]\Big\}, \tag{2.128}$$

and then maximized numerically over the amplitude phase ϕ. In Fig. 2.2 we report the optimized QFI together with the QFI of displaced squeezed vacuum states with $N_{sq} \leq 3$ and the same value of $|\alpha|^2$. Results indicate that upon using coherent states with large amplitude we may achieve and improve the precision of squeezed vacuum states already for small, realistic, values of the Kerr coupling γ. When the amount of Gaussian squeezing is nonzero but fixed we can combine the effects of squeezing and Kerr interaction by considering Kerr modified displaced squeezed states with a large number of amplitude photons ($|\alpha|^2 \gg 1$). As it is apparent from Fig. 2.2 the QFI increases with $|\alpha|^2$ and overtake quite rapidly the values of QFI of the corresponding Gaussian state.

2.6 Quantum discrimination of lossy channels

In this section we address the discrimination of lossy channels for continuous variable systems using Gaussian states as probing signals, and focus to the case when one of the values for the loss parameter is zero, i.e. we address the detection of a possible loss against the alternative hypothesis of an ideal lossless channel. Indeed, one of the main obstacles to the development of quantum technologies is the decoherence associated to losses and absorption processes occurring during the propagation of a quantum signal. The description of the dynamics of systems subject to noisy environments [118], as well the detection, quantification and estimation of losses and, more generally, the characterization of lossy channels at the quantum level, received much attention in the recent years [118, 119, 120, 121]. An efficient characterization of decoherence is relevant for quantum repeaters [122], quantum memories [123], cavity QED systems [124], or superconducting quantum circuits [125]. Here, we consider a situation where the loss (damping) rate of a channel may assume only two possible values and we want to discriminate between them by probing the channel with a given class of signals. In particular, we use Gaussian states as probing signals, and focus attention to the case when one of the values for the loss parameter is zero, i.e. we address the detection of a possible loss against the alternative hypothesis of an ideal lossless channel.

This is a problem of quantum state discrimination and basically consists in looking for the minimum error probability in identifying one of two possible output states from the channel. Upon assuming that repeated probing is possible, i.e. that N identical copies of the output states are given [14, 56, 126, 127], the quantity which gives the minimal error probability when discriminating two states is the quantum Chernoff bound (QCB).

For continuous variables systems the quantum discrimination of Gaussian states is a central point in view of their experimental accessibility and their relatively simple mathematical description [67, 128]. Upper bounds for the error probability of discrimination of Gaussian states of n bosonic modes have been investigated [51] and closed formula for the QCB of Gaussian states have been derived [48, 50, 51].

In the following, we deal with the detection of loss in continuous variable systems. In particular, our results apply to quantum optical implementations, where single- and two-mode Gaussian states may be reliably realized in a controlled way with current technology [129]. We address the problem of detecting lossy channels, i.e. we consider that the damping constant of a bosonic channel may be zero or assume a nonzero value, and we want to determine which one on the basis of repeated measurements on the signal exiting the channel. Besides, in order to stay close to schemes feasible with current technology, we

analyze in details the effect of the mixedness of probe states. An analogue problem, namely the estimation of the damping constant of a bosonic channel among a continuous set of possible values that it can assume, has already been addressed in literature [35, 130, 131], and recently [132] it was proved that two-mode squeezed vacuum probe states are optimal, i.e. they give the best estimate with respect to coherent, thermal or single-mode squeezed states. Moreover, recent analysis of transmission process in Gaussian continuous variable channels [133] has revealed the importance of assessing the deviation from ideal conditions, i.e the identity channel, in implementing large-scale quantum communication.

The results we report here aim basically at characterizing the kind of states that give the optimal discrimination and whether the improvements obtained in the discrimination using two-mode probes may be ascribed to the correlations between the two modes. We thus focus on single- and two-mode squeezed thermal states, which are feasible signals allowing a fair comparison between single- and two-mode probes at fixed energy. In order to quantify correlations, besides entanglement and mutual information, we exploit the recent results [64, 77, 134, 135, 136, 137] about quantum discord, which has been defined with the aim of capturing quantum correlations in mixed separable states that are not quantified by entanglement.

In 2.6.1 we specialize the calculation of the QCB to single- and two-mode Gaussian states, and we introduce the discrimination scheme for single-mode and two-mode Gaussian states and calculate the QCB in presence of a lossy channel or an absorber. Section 2.6.1 reports the main results about the QCB of the single and two-mode states as a function of the total energy for squeezed vacuum probe states or squeezed thermal states. Finally, in Section 2.6.2 we analyze the role of correlations in the enhancement of the discrimination by two-mode states.

2.6.1 Quantum Chernoff bound for Gaussian states

In the following we will focus on single mode and two-mode squeezed thermal states (STS), namely

$$\varrho_1 = S(r)\nu S(r)^\dagger$$
$$\varrho_2 = S_2(r)\nu_1 \otimes \nu_2\, S_2(r)^\dagger$$

As we will see, single- and two-mode STS evolving in a lossy channel lead to a state in the same class and thus the problem of channel discrimination may be reduced to the evaluation of the Chernoff bound for this classes of states. In order to perform this calculation one has to compute the positive power ϱ^s. For single mode it can be written

as a Gaussian state with a rescaled mean photon number $f(n,s)$, i.e. [51]

$$\varrho_1^s = S(r)\nu^s S(r)^\dagger = \mathcal{N}_{(n,s)} S(r)\nu_{(n,s)} S(r)^\dagger \tag{2.129}$$

where

$$\begin{aligned}\nu^s &= \left(\frac{1}{n+1}\right)^s \sum_{m=0}^{\infty} \left(\frac{n}{n+1}\right)^{ms} |m\rangle\langle m| \\ &= \mathcal{N}_{(n,s)} \frac{1}{f(n,s)+1} \sum_{m=0}^{\infty} \left(\frac{f(n,s)}{f(n,s)+1}\right)^m |m\rangle\langle m| \\ &= \mathcal{N}_{(n,s)}\, \nu_{(n,s)},\end{aligned} \tag{2.130}$$

and

$$\begin{aligned}\mathcal{N}(n,s) &= \mathrm{Tr}[\nu^s] = \frac{1}{(n+1)^s - n^s} \\ f(n,s) &= \frac{n^s}{(n+1)^s - n^s}\,.\end{aligned} \tag{2.131}$$

The two mode case follows straightforwardly

$$\begin{aligned}\varrho_2^s =& S_2(r)\,\nu_1^s \otimes \nu_2^s\, S_2(r)^\dagger \\ =& \mathcal{N}_{(n_1,s)}\mathcal{N}_{(n_2,s)} S_2(r)\,\nu_{(n_1,s)} \otimes \nu_{(n_2,s)}\, S_2(r)^\dagger.\end{aligned} \tag{2.132}$$

We then recall that for any given two squeezed thermal Gaussian states ϱ and ϱ', the overlap $\mathrm{Tr}[\varrho\,\varrho']$ may be written in terms of their covariance matrices

$$\mathrm{Tr}[\varrho\varrho'] = [\det(\boldsymbol{\sigma} + \boldsymbol{\sigma'})]^{-1/2} \tag{2.133}$$

where σ, σ' are the covariance matrices of the two states. Overall, we may write the QCB (1.111) in the single mode case $Q_1 = \min Q_{1s}$, where

$$\begin{aligned}Q_{1s} &= \mathrm{Tr}\left[\varrho^s \varrho'^{(1-s)}\right] \\ &= \mathcal{N}_{(n,s)}\mathcal{N}_{(n',1-s)} \mathrm{Tr}\left[S(r)\nu_{(n,s)} S(r)^\dagger S(r')\nu'_{(n',1-s)} S(r')^\dagger\right] \\ &= \frac{\mathcal{N}_{(n,s)}\,\mathcal{N}_{(n',1-s)}}{\sqrt{\det(\boldsymbol{\sigma}_{(n,s)} + \boldsymbol{\sigma'}_{(n',1-s)})}}\,.\end{aligned} \tag{2.134}$$

For the two-mode case we have $Q_2 = \min Q_{2s}$, where

$$\begin{aligned}Q_{2s} =& \mathrm{Tr}\left[\varrho^s \varrho'^{(1-s)}\right] \\ =& \frac{\mathcal{N}_{(n_1,s)}\,\mathcal{N}_{(n_2,s)}\,\mathcal{N}_{(n'_1,1-s)}\,\mathcal{N}_{(n'_2,1-s)}}{\sqrt{\det(\boldsymbol{\sigma}_{(n_1,n_2,s)} + \boldsymbol{\sigma'}_{(n'_1,n'_2,1-s)})}}\,.\end{aligned} \tag{2.135}$$

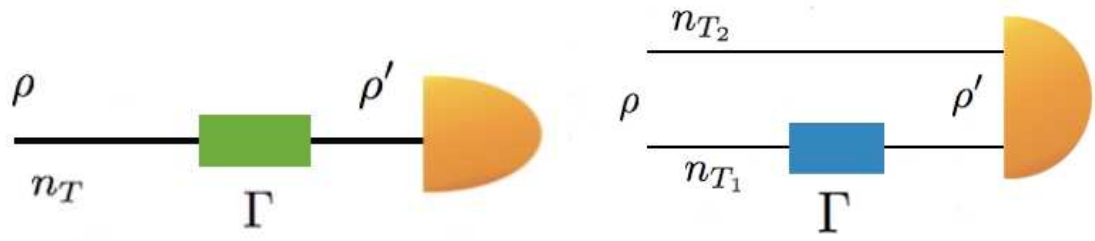

Figure 2.3: Single- and two-mode schemes for the discrimination of lossy channels. Top: a single mode Gaussian state enters in a lossy channel with damping rate Γ and then a measurement apparatus detect the output signal ρ'. Bottom: the lossy channel acts on a mode of a bipartite two-mode squeezed thermal state ρ and then the final state ρ' is measured.

Gaussian states in a lossy channel

In what follows, we study the evolution of a Gaussian state in a dissipative channel $\mathcal{E}_\Gamma$ characterized by a damping rate Γ, which may result from the interaction of the system with an external environment, as for example a bath of oscillators, or from an absorption process. We address the problem of detecting whether or not the dissipation dynamics occurred, i.e. the problem of discriminating between an input state ϱ and the final state $\varrho' = \mathcal{E}_\Gamma(\varrho)$. We focus to Gaussian states in view of their experimental accessibility and their relatively simple mathematical description. Besides, lossy channels are Gaussian channels, i.e. transform Gaussian states into Gaussian states as we already seen in section 2.4.

We assume to have many copies at disposal and thus use the quantum Chernoff bound Q defined in Eq. (1.111) as a distinguishability measure. A schematic diagram of the measurement schemes we have in mind is shown in Fig.2.3: we have either a single mode STS evolving in a lossy channel with parameter Γ followed by a measurement at the output, or a two-mode STS with the damping process occurring on one of the two modes, followed by a measurement on both of the modes.

The propagation of a mode of radiation in a lossy channel corresponds to the coupling of the mode a with a zero temperature reservoir made of large number of external modes. By assuming a Markovian reservoir and weak coupling between the system and the reservoir the dynamics of the system is described by the Lindblad Master equation given in (2.99) by setting $N = 0$,

$$\dot{\varrho} = \frac{\Gamma}{2}\mathcal{L}[a]\varrho \tag{2.136}$$

where $\mathcal{L}[a]\varrho = 2a\varrho a^\dagger - a^\dagger a\varrho - \varrho a^\dagger a$.

Single-mode case

Let us now start with single-mode states. The solution of Eq. (2.136) is given by (2.103) which describes the evolution of an initial Gaussian state with CM $\boldsymbol{\sigma}_0$ towards the stationary state given by the Gaussian state of the environment with covariance matrix $\boldsymbol{\sigma}_\infty$. The input state we considered in the scheme of Fig. 2.3 is a squeezed thermal state with an average number of thermal photons given by n_T and, without loss of generality, a real squeezing parameter r. The covariance matrix is described in Eq. (2.62). The evolved covariance matrix of the single mode case, Eq. (2.103) is given in Eq. (2.105) where from now on we omit the index of $\boldsymbol{\sigma}_0$, replace $\boldsymbol{\sigma}(t) = \boldsymbol{\sigma}'$ and, since the loss parameter always appears as Γt, consider that the time t has been absorbed in Γ. At the output the number of thermal photons n_Γ and the squeezing parameter r_Γ are those given in Eq. (2.106). The quantum Chernoff bound is then obtained from Eq. (2.134) with the substitutions $n \to n_T$ and $n' \to n_\Gamma$.

Two-mode case

According to the scheme of Fig. 2.3, the map describing the evolution of a two-mode state is $\mathcal{E}_\Gamma \otimes \mathbb{I}_2$. At the level of the CM it corresponds to the transformation of Eq. (2.108) where we have used the same notation introduced for the single-mode case. If the input state is a two-mode squeezed thermal state of the form $\varrho_2 = S_2(r)\nu_1 \otimes \nu_2 S_2(r)^\dagger$ and covariance matrix given in Eq. (2.71), then also the output state belongs to the same class, with the replacements $r \to r_\Gamma$, $n_{T1} \to n_{\Gamma 1}$, $n_{T2} \to n_{\Gamma 2}$. The covariance matrix in Eq. (2.108) may be recast in the standard form as

$$\boldsymbol{\sigma}_\Gamma = \frac{1}{2}\begin{pmatrix} A_\Gamma \mathbb{I}_2 & C_\Gamma \sigma_z \\ C_\Gamma \sigma_z & B_\Gamma \mathbb{I}_2 \end{pmatrix} \tag{2.137}$$

where

$$\begin{aligned} A_\Gamma &= \cosh(2r_\Gamma) + 2n_{\Gamma_1}\cosh^2 r_\Gamma + 2n_{\Gamma_2}\sinh^2 r_\Gamma \\ B_\Gamma &= \cosh(2r_\Gamma) + 2n_{\Gamma_1}\sinh^2 r_\Gamma + 2n_{\Gamma_2}\cosh^2 r_\Gamma \\ C_\Gamma &= (1 + n_{\Gamma_1} + n_{\Gamma_2})\sinh 2r_\Gamma\,, \end{aligned} \tag{2.138}$$

and the explicit form of the parameters of the evolved state may be obtained from the very definition of the symplectic invariants. For two-mode squeezed thermal states we have

$$\begin{aligned} A' - B' &= n_{\Gamma_1} - n_{\Gamma_2} \\ \sqrt{\det \boldsymbol{\sigma}'} &= \frac{1}{4}(2n_{\Gamma_1} + 1)(2n_{\Gamma_2} + 1) \\ C' &= (n_{\Gamma_1} + n_{\Gamma_2} + 1)\,\sinh 2r_\Gamma \end{aligned} \tag{2.139}$$

The QCB is then obtained using Eq. (2.135) and the replacements $n_1 \to n_{T_1}$, $n_2 \to n_{T_2}$, $n_1' \to n_{\Gamma_1}$, $n_2' \to n_{\Gamma_2}$.

Detection of lossy channels

In this section we address the discrimination of lossy channels probed by single- and two-mode STS and evaluate the QCB as a function of the most important parameter of the input state i.e. its total energy and squeezing. In particular, we optimize the discrimination of lossless ($\Gamma = 0$) from a lossy ($\Gamma > 0$) channel by maximizing over thermal probes, i.e. single- and two-modes squeezed thermal states. In our first analysis, we show that for fixed total energy, single- and two-mode squeezed vacuum states are optimal. In particular, we show the conditions where the two-mode state outperforms the single-mode counterpart. Then, by fixing both the total energy and squeezing, we will find the optimal STS. We recall that the minimization of the QCB over single-copy states implies the minimization over multy-copy states. This implies that finding the optimal input state ϱ automatically assures that $\varrho \otimes \varrho \otimes \dots$ is the optimal multi-copy state to be used as input when we consider a multiple access to the unknown channel.

In order to perform our investigation we introduce a suitable parametrization of the input energy. Let us denote by N_1 and N_2 the total energy (average total number of photons) of a single- and two-mode state respectively. They are given by Eqs. (2.66) and (2.83)

$$N_1 = n_T + n_S + 2n_S n_T, \tag{2.140}$$

$$N_2 = n_{T_1} + n_{T_2} + 2n_S + 2n_S(n_{T_1} + n_{T_2}), \tag{2.141}$$

where n_T accounts for the mean number of thermal photons for the single mode, n_{T_1} and n_{T_2} the corresponding quantity for the two-mode state, and $n_S = \sinh^2 r$ denote the energy due to squeezing, i.e. the energy of a single-mode squeezed vacuum. In order to analyze the effect of squeezing and to compare the performances of single- and two-mode states we introduce a different parametrization of the states, based on the total energy and the squeezing fraction β, which is defined as the fraction of total energy employed in squeezing. Using Eq. (2.143) we have, for single-mode states

$$n_S = \beta_1 N_1 \tag{2.142}$$

$$n_T = \frac{(1-\beta_1)N_1}{1+2\beta_1 N_1}\,. \tag{2.143}$$

Thus the single-mode STS can be parametrized as $\varrho = \varrho(N_1, \beta_1)$. Note that for $\beta_1 = 0$ the state is completely thermal with energy $N_1 = n_T$, while for $\beta_1 = 1$ the state is a squeezed

vacuum with energy $N_1 = n_S$. We denote $Q_1(N_1, \beta_1)$ the output QCB which is computed by using the output state $\varrho(N_1, \beta_1)$.
For two-mode states we also introduce an asymmetry parameter $\gamma \in [0, 1]$, denoting the fraction of the total thermal energy used for the first mode, thus arriving at

$$n_S = \frac{\beta_2}{2} N_2 \tag{2.144}$$

$$n_{T_1} = \gamma \, \frac{(1-\beta_2)N_2}{1+\beta_2 N_2} \tag{2.145}$$

$$n_{T_2} = (1-\gamma)\frac{(1-\beta_2)N_2}{1+\beta_2 N_2}. \tag{2.146}$$

Thus the two-mode squeezed thermal state can be parametrized as $\varrho = \varrho(N_2, \beta_2, \gamma)$. Note that for $\beta_2 = 0$ we have two thermal states with thermal energy $n_{T_1} = \gamma \, N_2$ and $n_{T_2} = (1-\gamma) \, N_2$. For $\beta_2 = 1$ we have instead a squeezed vacuum state with total energy $N_2 = 2 \, n_S$. We denote by $Q_2(N_2, \beta_2, \gamma)$ the output QCB which is computed by using the input state $\varrho(N_2, \beta_2, \gamma)$.

In order to make a fair comparison between the performances of single- and two-mode probes in discriminating the channels, we fix the mean number of photons in the input state. In other words we set

$$N_1 = N_2 = N \tag{2.147}$$

and minimize the output QCB among single-mode and two-mode squeezed thermal states. As a first step we compute the optimal quantities

$$Q_1(N) = \inf_{\beta_1} Q_1(N, \beta_1) \tag{2.148}$$

$$Q_2(N) = \inf_{\beta_2, \gamma} Q_2(N, \beta_2, \gamma). \tag{2.149}$$

Then we compare $Q_1(N)$ with $Q_2(N)$. According to our findings, in the Eqs. (2.148) and (2.149), the infima are achieved for $\beta_1 = \beta_2 = 1$. This is numerically shown in Fig. 2.4 for the single-mode case and in Fig. 2.5 for the two-mode case. Thus, we have found that, at fixed input energy N, the optimal thermal probes are given by single- and two-mode squeezed vacuum states. In this case, the input state is pure and the QCB corresponds to the fidelity (which is the case when the s-overlap in Eq. (1.111) is minimized for s approching the border). Let us adopt the transmissivity $\eta = e^{-\Gamma}$ to quantify the damping of the channel, so that $\Gamma = 0$ (ideal channel) corresponds to $\eta = 1$, and $\Gamma > 0$ (lossy channel) corresponds to $0 \leq \eta < 1$. Then, for single-mode we can write

$$Q_1(N) = \frac{1}{\sqrt{1 + N(1-\eta^2)}} \, , \tag{2.150}$$

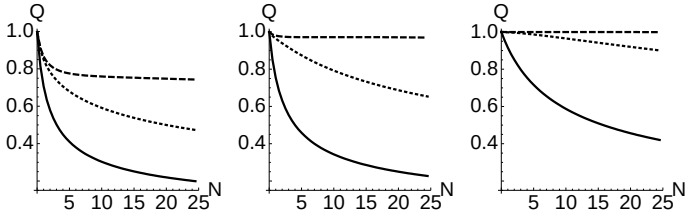

Figure 2.4: Output QCB $Q_1(N,\beta_1)$ optimized over input single-mode squeezed thermal states $\rho=\rho(N,\beta_1)$. From left to right we consider different values of the transmissivity: $\eta=0.1$ (left panel), $\eta=0.5$ (middle panel) and $\eta=0.9$ (right panel). In each panel, we plot $Q_1(N,\beta_1)$ as function of the energy N for different values of β_1. From top to bottom: $\beta_1=0.1$ (dashed line), $\beta_1=0.5$ (dotted line) and $\beta_1=1$ (solid line). The minimum curve is always achieved for $\beta_1=1$, i.e., for an input single-mode squeezed vacuum state.

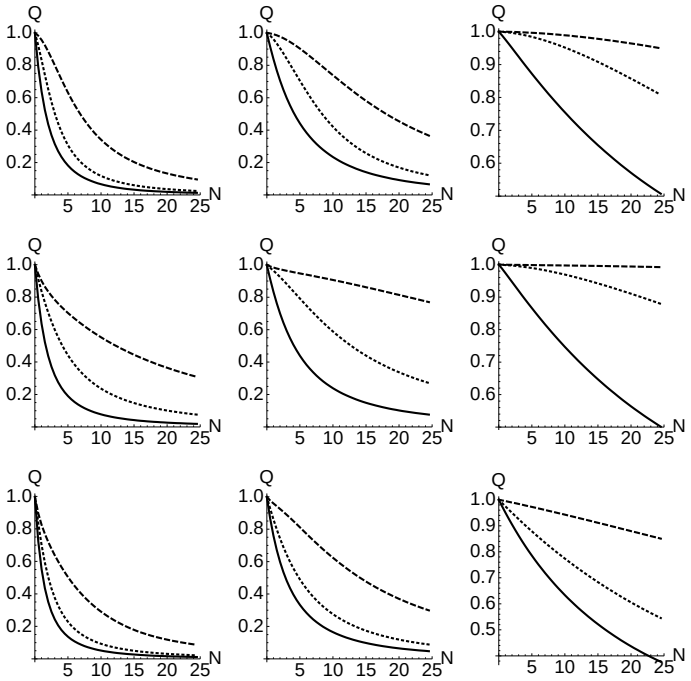

Figure 2.5: Output QCB $Q_2(N,\beta_2,\gamma)$ optimized over input two-mode squeezed thermal states $\rho=\rho(N,\beta_2,\gamma)$. From left to right we consider different values of the transmissivity: $\eta=0.1$, 0.5 and 0.9. From top to bottom, we consider different values of the asymmetry parameter $\gamma=0$, 0.5 and 1. In each panel, we then plot Q_2 as function of the energy N for different values of β_2. From top to bottom: $\beta_2=0.1$ (dashed line), $\beta_2=0.5$ (dotted line) and $\beta_2=1$ (solid line). The minimum curve is always achieved for $\beta_2=1$ corresponding to an input two-mode squeezed vacuum state.

and for two-modes we derive

$$Q_2(N) = \frac{4}{\left[2 + N(1 - \sqrt{\eta})\right]^2} \ . \tag{2.151}$$

In Fig. 2.6, we show the behaviors of the single-mode QCB $Q_1(N)$ and two-mode QCB $Q_2(N)$ as function of the input energy N for several values of transmissivity η (or, equivalently, the damping rate Γ). As expected the discrimination improves by increasing the input energy N and decreasing the transmissivity η.

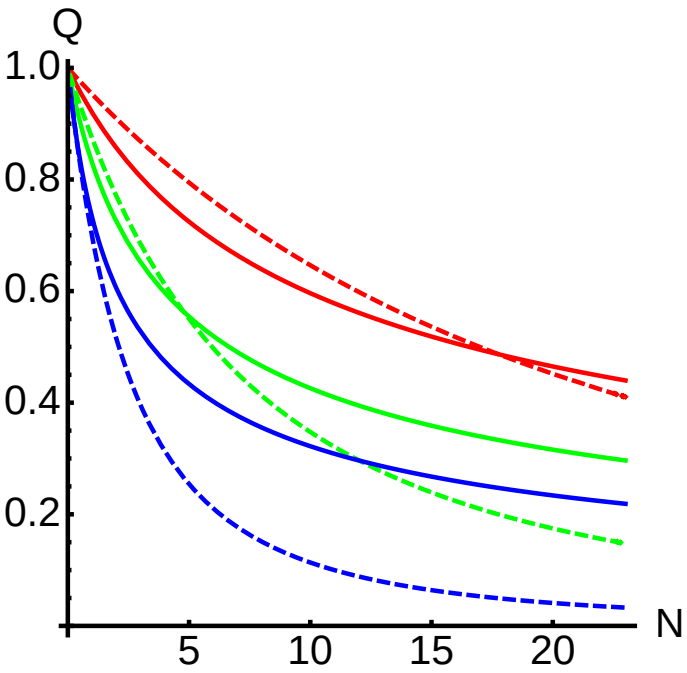

Figure 2.6: (Color online). Single-mode QCB $Q_1(N)$ (solid lines) and two-mode QCB $Q_2(N)$ (dashed lines) as a function of the input energy N for different damping rates. From top to bottom $\Gamma = 0.1, 0.3, 1$ (red, green and blue, respectively). By comparing curves with the same color (fixed damping Γ), we can see that $Q_2(N)$ outperforms $Q_1(N)$ only after a certain value of the input energy N.

As we can see from Fig. 2.6, for a given value of the transmissivity η, the two-mode QCB $Q_2(N)$ outperforms the single-mode QCB $Q_1(N)$ only after a threshold energy. In fact, for any value of the transmissivity η larger than a critical value η_c there is a threshold energy $N_{th} = N_{th}(\eta)$ that makes the two-mode squeezed vacuum state more convenient than the single-mode counterpart. This threshold energy decreases for decreasing values of η. In particular, for transmissivities less than the critical value η_c, the threshold energy becomes zero, i.e., the two-mode state is always better than single-mode state. We have numerically evaluated the critical value $\eta_c \simeq 0.296$ (corresponding to $\Gamma_c \simeq 1.22$). This

phenomenon is fully illustrated in Fig. 2.7, where we have plotted the threshold energy as function of the transmissivity $N_{th} = N_{th}(\eta)$. For $N > N_{th}$ (dark area), the optimal state is the two-mode squeezed vacuum state, while for $N < N_{th}$ (white area) it is the single-mode squeezed vacuum state. In particular, note that $N_{th} = 0$ at $\eta = \eta_c$. Close to the critical transmissivity we have $N_{th} \simeq -\eta_c + \sinh^2(2.14\eta)$ [1].

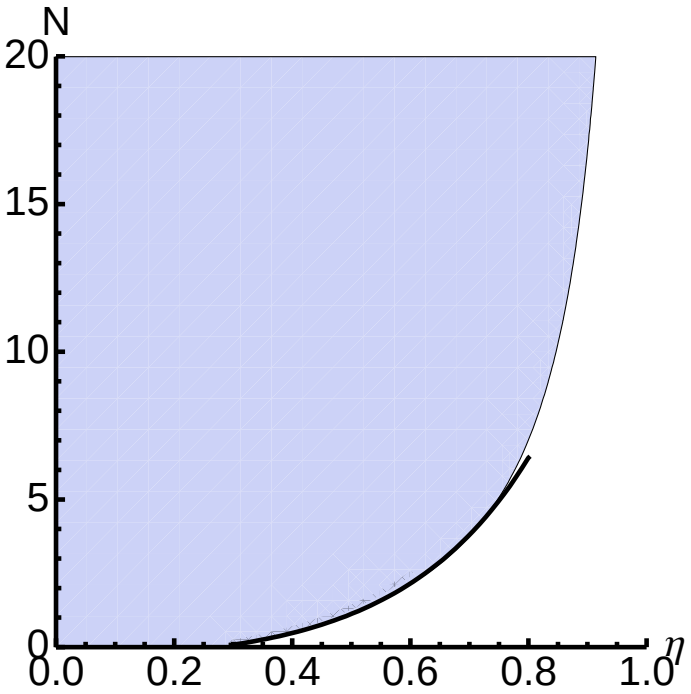

Figure 2.7: Threshold energy as a function of the transmissivity $N_{th} = N_{th}(\eta)$. The dark area indicates the values of the energy N for which the two-mode squeezed vacuum state is optimal. The other region indicates where the single-mode squeezed vacuum state is optimal. The dashed line denotes the behavior of the threshold energy N_{th} close to the critical transmissivity η_c.

It should be said that, in realistic conditions, it is unlikely to have pure squeezing. For this reason, it is important to investigate the performances of the squeezed thermal states by fixing this physical parameter together with the total energy. Thus, in this section, we fix both the input energy and squeezing, i.e., we set

$$\begin{aligned} &N_1 = N_2 = N, \\ &\beta_1 = \beta_2 = \beta \quad (0 \leq \beta \leq 1) \ . \end{aligned} \tag{2.152}$$

[1] Clearly we can invert the curve and introduce a threshold transmissivity as function of the energy $\eta_{th} = \eta_{th}(N)$. For values $\eta < \eta_{th}$ the two-mode state is better than the single-mode state, while the opposite happens for $\eta > \eta_{th}$. In this case, we have $\eta_{th} \simeq \eta_c + 0.18\, N^{0.7}$ for small N and $\eta_{th} \simeq 1 - 2/N$ for large N.

Then, we compare the single-mode squeezed thermal state $\varrho = \varrho(N, \beta)$ with the two-mode squeezed thermal states $\varrho = \varrho(N, \beta, \gamma)$ for various values of γ. In other words, we compare $Q_1(N, \beta)$ and $Q_2(N, \beta, \gamma)$.

For fixed N and β, we find that the minimum of $Q_2(N, \beta, \gamma)$ is achieved for $\gamma = 1$ (easy to check numerically). This means that two-mode discrimination is easier when all the thermal photons are sent through the lossy channel. In this case we find numerically that $Q_2(N, \beta, 1) < Q_1(N, \beta)$ for every values of the input parameters N and β, and every value of damping rate Γ in the channel. In other words, at fixed energy and squeezing, there is a two-mode squeezed thermal state (the asymmetric one with $\gamma = 1$) able to outperform the single-mode squeezed thermal state in the detection of any loss. In order to quantify the improvement we introduce the QCB reduction

$$\Delta Q = Q_1(N, \beta) - Q_2(N, \beta, 1). \tag{2.153}$$

The more positive this quantity is, the more convenient is the use of the two-mode state instead of the single-mode one. In Fig. 2.8 we show the behavior of ΔQ as function of the input energy and squeezing for two different values of the damping. As one can see from the plot, the QCB reduction is always positive. Its value increases with the energy while reaching a maximum for intermediate values of the squeezing. By comparing the two insets of Fig. 2.8, we can also note that the QCB reduction increases for increasing damping Γ (i.e., decreasing transmissivity). Thus, we have just shown that, for fixed values of N

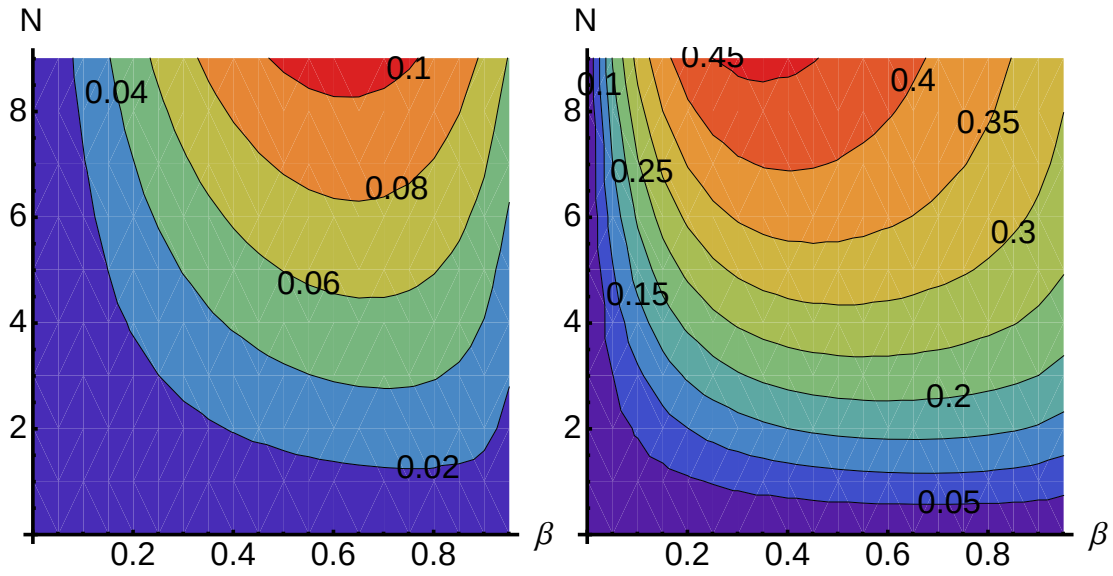

Figure 2.8: (Color online) Density plot of the QCB reduction ΔQ as function of the input energy N and the squeezing β. The left plot is for $\Gamma = 0.1$ and the right one for $\Gamma = 0.9$.

and β, the asymmetric two-mode squeezed thermal state ($\gamma = 1$) is the optimal thermal

probe in the detection of any loss Γ. Here we also show that this is approximately true for $\gamma \lesssim 1$. In other words, we show that the inequality $Q_2(N,\beta,\gamma) < Q_1(N,\beta)$ is robust against fluctuations of γ below the optimal value $\gamma = 1$. This property is clearly important for practical implementations. To study this situation, let us consider the γ-dependent QCB reduction

$$\Delta Q_\gamma = Q_1(N,\beta) - Q_2(N,\beta,\gamma) \ . \tag{2.154}$$

In Fig. 2.9 we have specified this quantity for different values of the asymmetry parameter γ (each inset refers to a different value of γ). Then, for every chosen γ, we have computed ΔQ_γ over a sample of 10^3 random values of N, β, and Γ (in each inset). As one can see from the figure, the quantity ΔQ_γ is approximately positive also when γ is quite different from the unity.

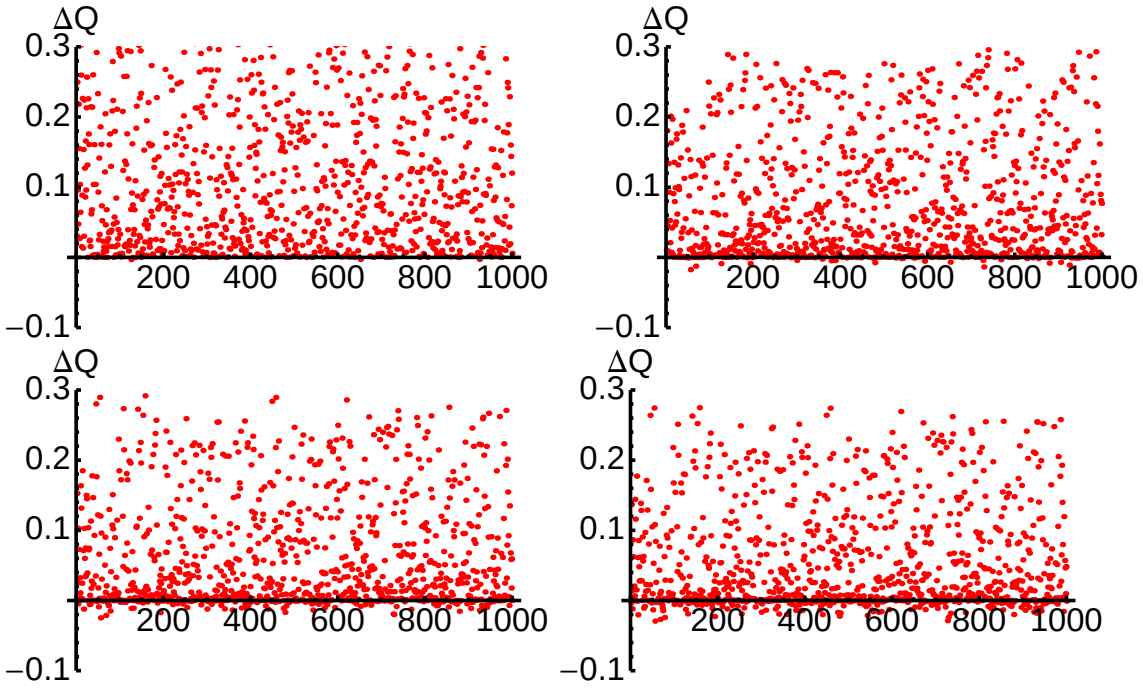

Figure 2.9: (Color online) QCB reduction ΔQ_γ for different values of γ (top left $\gamma = 0.99$, top right $\gamma = 0.9$, bottom left $\gamma = 0.8$, bottom right $\gamma = 0.7$). In each inset, ΔQ_γ is computed over a sample of 10^3 random values of N, β, and Γ.

2.6.2 Quantum Chernoff bound and correlations

Since two-mode probes are always convenient for $\beta \neq 1$ and $\gamma = 1$, a natural question arises on whether this improvement should be ascribed to some kind of correlations, either classical or quantum, as, for example, those quantified by entanglement, quantum discord or quantum mutual information.

In order to quantify the degree of entanglement of a two-mode Gaussian state, it is suitable to use the logarithmic negativity given in Eq. (2.90) $E = \max\{0, -\log 2\tilde{d}_-\}$ where $\tilde{d}_-$ is the smallest symplectic eigenvalue of the partially transposed state (2.87), $\tilde{d}_-^2 = \frac{1}{2}[\tilde{\Delta} - \sqrt{\tilde{\Delta}^2 - 4I_4}]$ where $\tilde{\Delta} = I_1 + I_2 - 2I_3$. The quantum discord for a bipartite STS with CM as in Eq. (2.71) is given in (2.91) $D = h(\sqrt{I_2}) - h(d_-) - h(d_+) + h(\frac{\sqrt{I_1}+2\sqrt{I_1 I_2}+2I_3}{1+2\sqrt{I_2}})$ where $h(x) = (x + \frac{1}{2})\log(x + \frac{1}{2}) - (x - \frac{1}{2})\log(x - \frac{1}{2})$. Finally, the quantum mutual information, for a Gaussian bipartite state in the canonical form (2.71) reads (2.92) $I = \frac{1}{2}\left[h(\sqrt{I_1}) + h(\sqrt{I_2}) - h(d_+) - h(d_-)\right]$ where the symplectic eigenvalues $d_\pm$ are given in Eq. (2.76). A bipartite Gaussian state is entangled iff $\tilde{d}_- < 1/2$, so that the logarithmic negativity gives positive values for all the entangled states and 0 otherwise. For what concerns the discord, we have that for $0 \leq D \leq 1$ the state may be either entangled or separable, whereas all the states with $D > 1$ are entangled. For pure states the previous three measures are equivalent, whereas for mixed states, as in the case under investigation in this section, they generally quantify different kind of correlations.

Here we consider the QCB reduction $\Delta Q_{\bar{\gamma}} = Q_1(N, \beta) - Q_2(N, \beta, \bar{\gamma})$ between a single-mode squeezed thermal state $\rho = \rho(N, \beta)$ and a two-mode squeezed thermal state $\rho = \rho(N, \beta, \bar{\gamma})$ with $\bar{\gamma} = 0.999$. By fixing the input squeezing β and varying the input energy N, we study the behaviour of $\Delta Q_{\bar{\gamma}}$ as function of the three correlation quantifiers, i.e., quantum mutual information, quantum discord and entanglement (computed over the input two-mode state). As shown in the upper panels of Fig. 2.10, the QCB reduction $\Delta Q_{\bar{\gamma}}$ is an increasing function of all the three correlation quantifiers for fixed input squeezing ($\beta = 0.1$ for the left panel and $\beta = 0.9$ for the right one). Note that, in each panel and for each quantifier, we plot three different curves corresponding to different values of the damping $\Gamma = 0.9$, 0.5 and 0.1. The monotonicity of the QCB reduction in all the correlation quantifiers suggests that the presence of correlations should definitely be considered as a resource for loss detection, whether these correlations are classical or genuinely quantum, i.e., those quantified by entanglement. In other words, employing the input squeezing in the form of correlations is always beneficial for loss detection when we consider squeezed thermal states as input sources. The importance of correlations is confirmed by the plots in the middle panels. Here we consider again the QCB reduction $\Delta Q_{\bar{\gamma}} = Q_1(N, \beta) - Q_2(N, \beta, \bar{\gamma})$ for $\bar{\gamma} = 0.999$. Then, by varying input squeezing β and energy N, we study $\Delta Q_{\bar{\gamma}}$ as function of both discord and entanglement (damping is $\Gamma = 0.2$ in the left panel, and $\Gamma = 0.8$ in the right one). These plots show how the QCB reduction is approximately an increasing function of both discord and entanglement. Finally, in the lower panels of Fig. 2.10, we also show how entanglement (left) and discord (right) are increasing functions of the quantum mutual information with good approximation (these

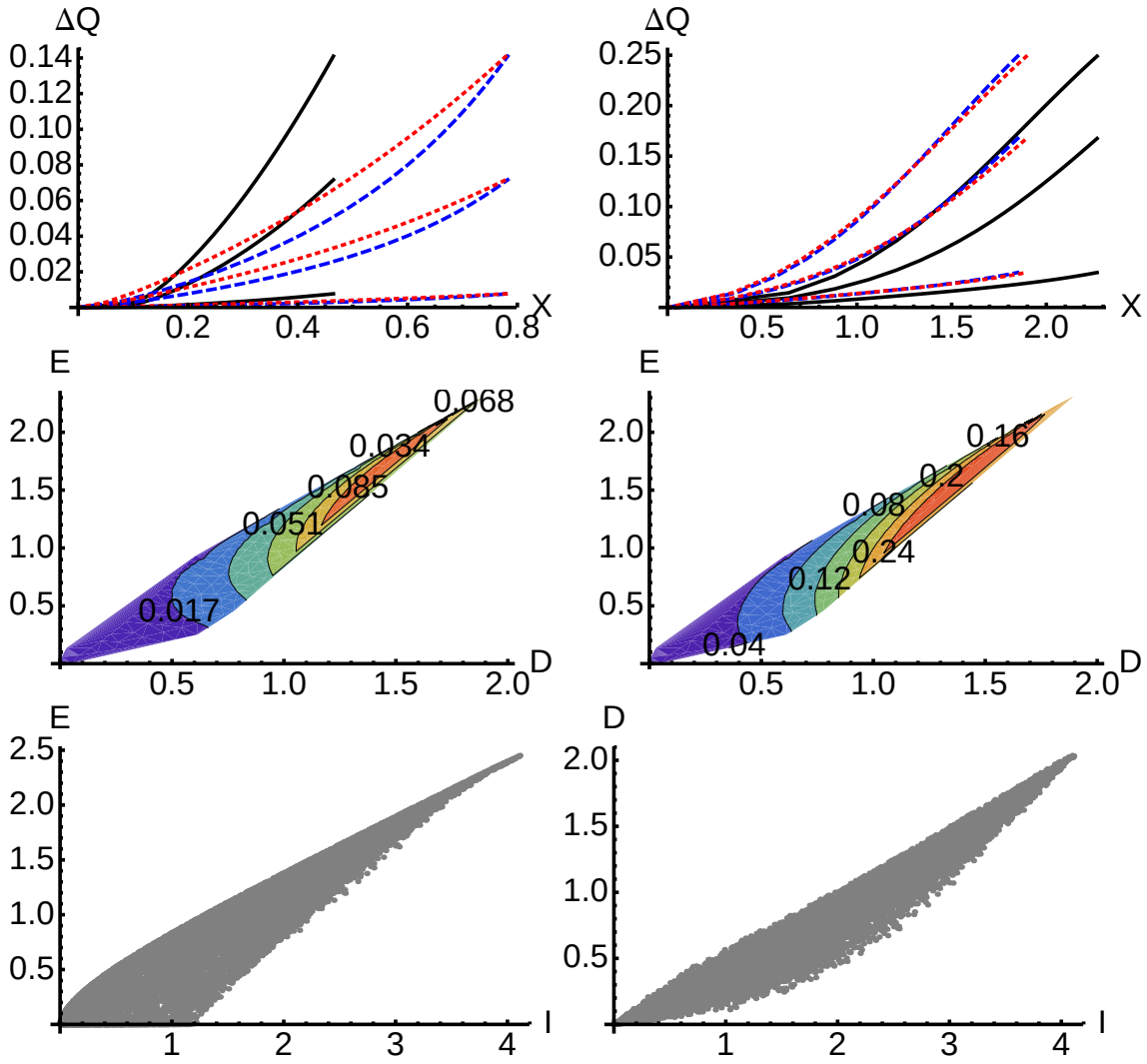

Figure 2.10: (Color online) *Upper panels*. QCB reduction $\Delta Q_{\bar{\gamma}}$ (with $\bar{\gamma} = 0.999$) as a function of the three correlation quantifiers X=I,D,E where I is the quantum mutual information (dotted red), D is the quantum discord (dashed blue) and E is the entanglement (solid black). The plots are for fixed squeezing: $\beta = 0.1$ for the left panel and $\beta = 0.9$ for the right one. For each quantifier we plot three different curves corresponding to different values of the damping (from top to bottom $\Gamma = 0.9, 0.5$ and 0.1). Each curve is generated by varying the input energy N between 0 and 5 photons. *Middle panels*. Density plots of the QCB reduction $\Delta Q_{\bar{\gamma}}$ as a function of the input discord and entanglement. The plots are for fixed damping: $\Gamma = 0.2$ in the left panel and $\Gamma = 0.8$ in the right one. In each panel, the density plot is generated by varying the squeezing $0 \leq \beta \leq 1$ and the energy $0 \leq N \leq 5$. *Lower panels*. Entanglement (left) and discord (right) as a function of the quantum mutual information. Plots are generated by taking a random sample of 10^4 two-mode squeezed thermal states, i.e., random values of N and β with $\gamma = \bar{\gamma}$.

plots are generated by choosing a random sample of 10^4 two-mode squeezed thermal states).

2.7 Quantum discrimination of Gaussian noisy channels

In this section we address discrimination of Gaussian noise channels using both minimum error probality (Bayes) and maximum detection probability (Neyman-Pearson) strategies. We focus on the asymptotic regime of many measurements and evaluate the quantum Chernoff bound and the quantum relative entropy, which provide the decreasing rate of the probabilities of discrimination errors and type-II errors in the two strategies respectively. We also consider the discrimination of channels with infinitesimally close values of the noise parameter and evaluate the metrics associated with the two different notions of distinguishability.

Quantum Chernoff bound for Gaussian noise channels

The input states that we consider are single-mode DSTS's as given in Eq. (2.61). The Gaussian noise map described in Eq. (2.111), acts on a single-mode DSTS by adding Δ thermal photons to the initial n_0 photons of the input state. In terms of the covariance matrix we have that the initial state is described by σ_0 of Eq. (2.62) and the output state after the evolution in the channel is given by σ_Δ of Eq. (2.113). In order to calculate the Chernoff bound for this class of states it is sufficient to realize that the powers $\varrho_1^s, \varrho_2^{1-s}$ are also Gaussian states with a rescaled mean photon number N_1, N_2, i.e.

$$\begin{aligned}\varrho_1^s =& D(\alpha_1)S(r_1)\nu(n_1)^s S^\dagger(r_1)D^\dagger(\alpha_1)\\ =& g(n_1,s)D(\alpha_1)S(r_1)\nu(N_1)S^\dagger(r_1)D^\dagger(\alpha_1) \qquad (2.155)\\ \varrho_2^{1-s} =& g(n_2,1-s)D(\alpha_2)S(r_2)\nu(N_2)S^\dagger(r_2)D^\dagger(\alpha_2) \qquad (2.156)\end{aligned}$$

where

$$\nu(n_1)^s = g(n_1,s)\nu(N_1) \qquad (2.157)$$

$$\nu(n_2)^{1-s} = g(n_2,1-s)\nu(N_2) \qquad (2.158)$$

and $N_i = \frac{n_i^x}{(n_i+1)^x - n_i^x}$, $g(n_i,x) = \frac{1}{(n_i+1)^x - n_i^x}$ with $i = 1,2$ and $x = s, 1-s$. Then the QCB of Eq. (2.134) becomes

$$Q_s(\varrho_1,\varrho_2) = g(n_1,s)g(n_2,1-s)\mathrm{Tr}[S(r_1)\nu(N_1)S^\dagger(r_1)S(r_2)\nu(N_2)S^\dagger(r_2)] \qquad (2.159)$$

where we used that $\alpha_1 = \alpha_2 = \alpha_0$ to simplify displacement operators and omitted the index 1 in the notation of Q_s. Note that Q_s does not depend on displacement. We recall that the inner product $\mathrm{Tr}(\varrho_1\varrho_2)$ is given by (2.133) and using this last equation, the quantum Chernoff bound (1.111) becomes $Q = \min Q_s$

$$Q_s = g(n_1,s)g(n_2,1-s)[\det(\sigma_1' + \sigma_2']^{-1/2} \qquad (2.160)$$

where σ_i', $i = 1, 2$ are the covariance matrices of the states ϱ_1^s and ϱ_2^{1-s} as given in Eq. (2.62) with mean number of thermal photons N_i, squeezing r_i and phase ϕ_i.

The fidelity defined in Eq. (1.20) for two single-mode STS's is given by [51, 138, 139]

$$\mathcal{F} = \frac{1}{\sqrt{\Sigma + \delta} - \sqrt{\delta}} \tag{2.161}$$

where $\Sigma = \det[\sigma_1 + \sigma_2]$ and $\delta = 4(\det[\sigma_1] - 1/4)(\det[\sigma_2] - 1/4)$.

Since the initial amplitude is not changed by Gaussian noise, it is useless to employ displaced states as probe signals. From now on we consider $\alpha_0 = 0$ and introduce a parametrization based on the total energy E_i and the fraction of squeezing β_i (that is the fraction of the total energy employed in squeezing) by defining the number of thermal and squeezed photons n_T and n_S as in Eqs. (2.142) and (2.143). We have

$$n_{T,i} = \frac{(1 - \beta_i)E_i}{1 + 2\beta_i E_i} \tag{2.162}$$

$$n_{S,i} = \sinh^2 r_i = \beta_i E_i \tag{2.163}$$

where $0 \leq \beta_i \leq 1$, $i = 1, 2$ is a rather involved function of E_0, β_0 and Δ_i and

$$\begin{aligned} E_i &= n_{T,i} + n_{S,i} + 2n_{S,i}n_{T,i} \\ &= E_0 + \Delta_i \end{aligned} \tag{2.164}$$

Thus the single-mode squeezed thermal state can be parametrized as $\varrho_i = \varrho_i(E_0, \beta_0, \Delta_i)$, $i = 1, 2$. In our problem of discrimination between two Gaussian noises Δ_1 and Δ_2 we denote $Q(E_0, \beta_0, \Delta_1, \Delta_2)$ the QCB which is calculated by using the states $\varrho_1(E_0, \beta_0, \Delta_1)$ and $\varrho_2(E_0, \beta_0, \Delta_2)$. We note that $\det[\sigma_1 + \sigma_2]^{-1/2}$ is independent on ϕ_i, therefore the QCB does not depend on the squeeze angle. From numerics we have that $Q(E_0, \beta_0, \Delta_1, \Delta_2) = Q(E_0, \beta_0, \Delta_2, \Delta_1)$, i.e. the QCB is symmetric for change of the parameters. Moreover, denoting with s^* the optimal value of s which minimizes the QCB, we have that $Q(E_0, \beta_0, \Delta_1, \Delta_2)$ is minimized by s^*, and that $Q(E_0, \beta_0, \Delta_2, \Delta_1)$ by $1 - s^*$. The minimum value of Q corresponds to the optimal condition of discriminability and it is given by $\beta_0 = 1$ i.e. for initial squeezed vacuum states.

In the following we consider two different cases, first we address the discrimination between an initial single-mode STS ϱ_0 and the evolved state $\varrho_\Delta = \mathcal{G}_\Delta(\varrho_0)$ i.e. we address the discrimination of the identity channel ($\Delta_1 = 0$) from a channel with Gaussian noise ($\Delta_1 = \Delta > 0$) by evaluating the QCB $Q(E_0, \beta_0, \Delta_1, \Delta_2) = Q(E_0, \beta_0, 0, \Delta)$. Then we will consider the discrimination between two different STS's ϱ_{Δ_1} and ϱ_{Δ_2} evolved in different channels from the same initial probe state through the maps $\mathcal{G}_{\Delta_1}(\varrho_0)$ and $\mathcal{G}_{\Delta_2}(\varrho_0)$ i.e. we address the discrimination between two channels with different gaussian noises (Δ_1 and Δ_2) by evaluating the QCB $Q(E_0, \beta_0, \Delta_1, \Delta_2)$.

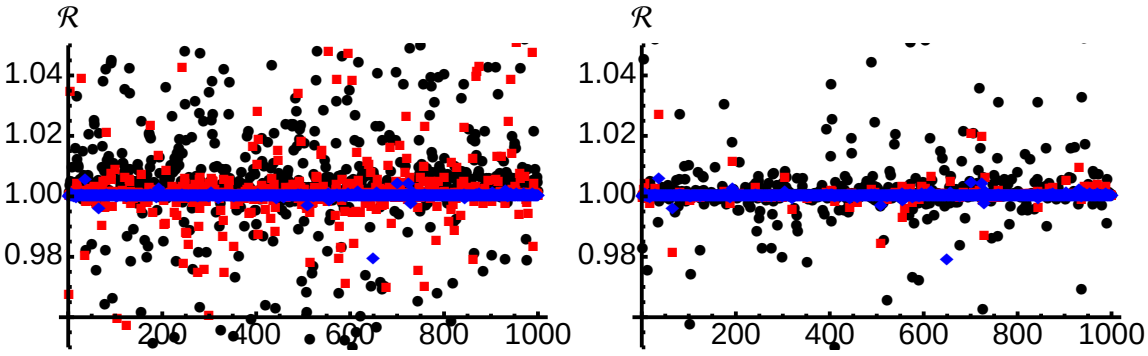

Figure 2.11: (Color online) QCB ratio $\mathcal{R}$ for a sample of STS with random values of Δ_1 and Δ_2 and left: $\beta = 1$, $E_0 = 1, 10, 1000$ (black,red and blue points); right: $E = 1000$ and $\beta = 0.1, 0.5, 0.99$ (black, red and blue points).

In the first case ($\Delta_1 = 0$ and $\Delta_2 = \Delta$), the QCB $Q(E_0, \beta_0, 0, \Delta)$ is a monotonic decreasing function of β_0, E_0 and Δ and therefore the optimal Q is obtained for $\beta_0 = 1$ and $E_0, \Delta \gg 1$. In the latter case, $\Delta_1 \neq 0$, the minimum Q is obtained for $\beta_0 = 1$ and high energies $E_0 \gg$. The QCB has a maximum for $\Delta_1 = \Delta_2$ in $Q = 1$ and then it decreases with β_0, E_0 and Δ_i. At high energies $E_0 \gg 1$, we have the scaling:

$$\begin{aligned} Q(E_0, \beta_0, \Delta_1, \Delta_2) =& Q\left(E_0, \beta_0, \frac{\Delta_1}{\Delta_2}, 1\right) \\ =& Q\left(E_0, \beta_0, 1, \frac{\Delta_2}{\Delta_1}\right). \end{aligned} \tag{2.165}$$

The closer is $\beta \simeq 1$, the more accurate is the scaling. We study the behavior of the QCB in the regime of $E_0 \gg 1$, where the scaling holds, by analyzing the ratio

$$\mathcal{R} = \frac{Q(E_0, \beta_0, \Delta_1/\Delta_2, 1)}{Q(E_0, \beta_0, \Delta_1, \Delta_2)}.$$

In Fig. 2.11 left, we report $\mathcal{R}$ for 10^3 random values of Δ_1 and Δ_2 and fixed $\beta_0 = 1$ at different energies: $E_0 = 1, 10, 1000$ (black, red and blue points respectively). As it is apparent from the plot, the scaling is valid, i.e. the ratio $\mathcal{R} = 1$ for $E_0 = 10^3$ (blue points), whereas in the case of small E_0 this is no more valid. The right hand of Fig. 2.11 shows that for fixed energy $E = 1000$ and different values of $\beta_0 = 0.1, 0.5, 1$ (black, red and blue points respectively) the scaling is almost valid, due to the fact that for high energy values the QCB has a low dependence on β_0. Note also that almost all the points of both the figures are included in the small range $(0.96 - 1.05)$ and therefore for practical scopes one could consider this scaling valid for all the β_0's.

In Fig. 2.12, we plot the QCB for $\Delta_1 = 0$, $\Delta_2 = \Delta$ and $\Delta_1 = 1$, $\Delta_2 = \Delta$ as a function of Δ at different E_0 and β_0. Both the panels show that the case $\Delta_1 = 0$ (dashed

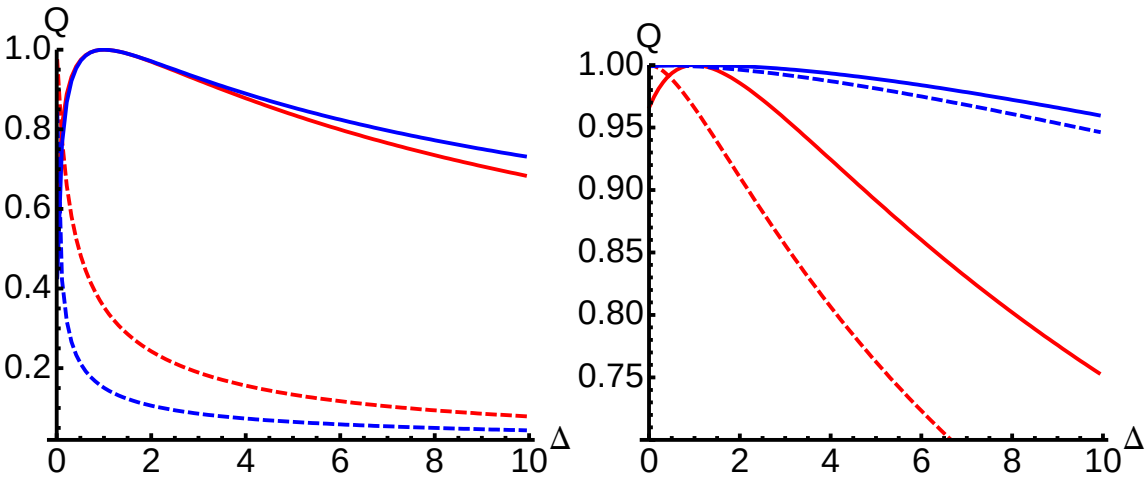

Figure 2.12: (Color online) Left: Plot of the QCB $Q(E_0, 1, 0, \Delta)$ (dashed line) and $Q(E_0, 1, 1, \Delta)$ (solid line) at different energies $E_0 = 1, 10$ (red and blue respectively). Right: plot of $Q(E_0, 0, 0, \Delta)$ (dashed line) and $Q(E_0, 0, 1, \Delta)$ (solid line) at different energies $E_0 = 1, 10$ (red and blue respectively).

lines) corresponds to the condition of optimal discriminability i.e. it gives the minimum value of the QCB. In particular, the left panel shows that for $\beta_0 = 1$, i.e. for an initial squeezed vacuum probe state, the increasing of the energy makes the discrimination easier in the case $\Delta = 0$, whereas in the case $\Delta = 1$ it gets worse. The right panel depicts the QCB of an initial thermal state with $\beta_0 = 0$ in the two cases $\Delta_1 = 0$ and $\Delta_1 = 1$. The discrimination is worse than the case $\beta_1 = 1$ but it improves by decreasing the energy.

Since we are discriminating Gaussian states, it is of interest to compare the QCB with two bounds that are easy to compute because they depend only on the symplectic spectra. These bounds are called the Young bound Y and the Minkowski bound M and are derived in [51] for n-mode STS's. Here we report their expression specialized to the single-mode case. Let us introduce the two functions

$$\Phi_p^{\pm}(x) = (x + 1/2)^p \pm (x - 1/2)^p \tag{2.166}$$

$$\Gamma_p(x) = 2[(2x + 1)^{2p} - (2x - 1)^{2p}]^{-1/2} \tag{2.167}$$

The so called Minkowski bound is then $M = \inf_s M_s$, where

$$M_s = 2\left[\Phi_s^+(d_1)\Phi_{1-s}^-(d_2) + \Phi_{1-s}^+(d_2)\Phi_s^-(d_1)\right]^{-1} \tag{2.168}$$

and $d_j = n_{T,j} + 1/2$, $j = 1, 2$ is the symplectic spectrum of ϱ_j. The Young bound is defined as $Y = \inf_s Y_s$ where

$$Y_s = \Gamma_s(d_1)\Gamma_{1-s}(d_2). \tag{2.169}$$

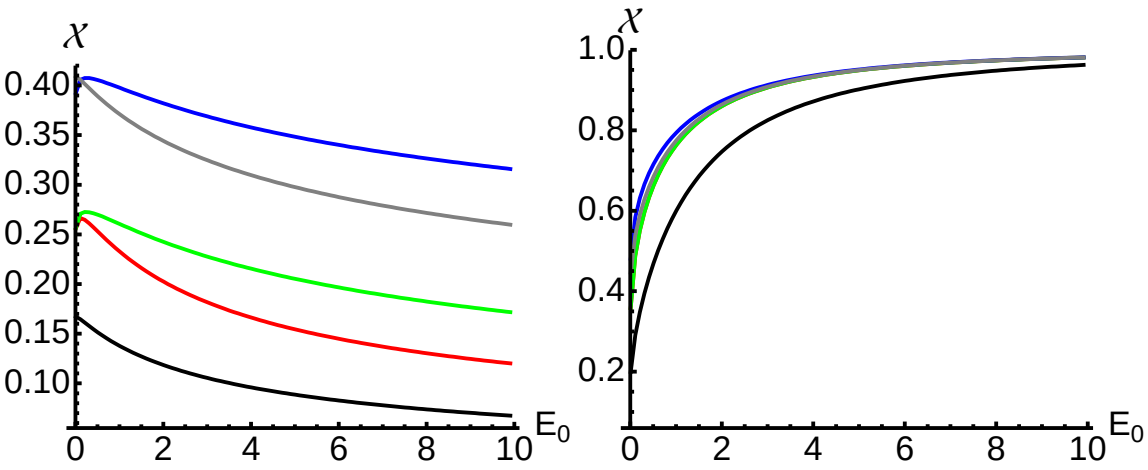

Figure 2.13: (Color online) Plot of Q (red), $\mathcal{F}_-$ (black), $\mathcal{F}_+$ (gray), M (green) and Y (blue) for $\Delta_1 = 0$ and $\Delta_2 = \Delta = 5$ as a function of the energy E_0 and $\beta_0 = 0.999$ (left), $\beta_0 = 0$ (right).

In Figs. 2.13 and 2.14 we plot the bounds to Q given by $\mathcal{F}$, $\mathcal{F}_+$, Y and M, reported in Eqs. (2.161), (2.168), (2.169) and signed with $\mathcal{X}$ in the figure. In the left panel of Fig. 2.13 we illustrate the case of an initial nearly pure squeezed vacuum with $\beta = 0.999$ that evolves into a state ϱ_Δ with $\Delta = 5$. Note that for a pure squeezed vacuum $\beta = 1$, $Q = \mathcal{F}$ whereas just for a slightly different value of $\beta = 0.999$ the quantum fidelity becomes a lower bound. M (green line) is a tighter bound to Q than Y (blue) and F_+ (gray). For $\beta_0 = 0$, i.e. an initial thermal state without squeezing, we have that $Q = M = \sqrt{\mathcal{F}}$, $\forall E_0$ and that the Young bound becomes a lower bound to Q: $Y < \mathcal{F} \leq Q$.

The discrimination between two STS ϱ_{Δ_1} and ϱ_{Δ_2} evolved in different channels from ϱ_0 is analyzed in Fig. 2.14. We have that for $\beta_0 = 1$, $M, \mathcal{F}_+ \geq Q$ and $M = \mathcal{F}_+ = Q$ at $\beta_0 = 0$, whereas $\mathcal{F} < Q$ $\forall E_0$ and $\forall \beta_0$.

Quantum Chernoff metric

Let us consider two infinitesimally close STS's ϱ_Δ and $\varrho_\Delta + d\varrho_\Delta$ which result from the interaction with a channel characterized by a Gaussian noise Δ and $\Delta + d\Delta$ respectively. For STS's, the quantum Chernoff metric ds^2_{QCB} of Eq. (1.132) is given by [50]

$$ds^2_{QCB} = g_{QCB}(\Delta) d\Delta^2 = \frac{(\beta'_\Delta)^2}{32 \sinh^2 \frac{\beta}{2}} + \frac{(r'_\Delta)^2}{2}, \tag{2.170}$$

where $x'_\Delta = \frac{d}{d\Delta} x_\Delta$, $\beta_\Delta = \log\left(\frac{n_T+1}{n_T}\right)$, being $n_T = \frac{(1-\beta)E}{1+2\beta E}$ the number of thermal photons as given in Eq. (2.162) and $r_\Delta = \sinh^{-1}\sqrt{\beta E}$, with $E = E_0 + \Delta$ the total energy and $0 \leq \beta \leq 1$.

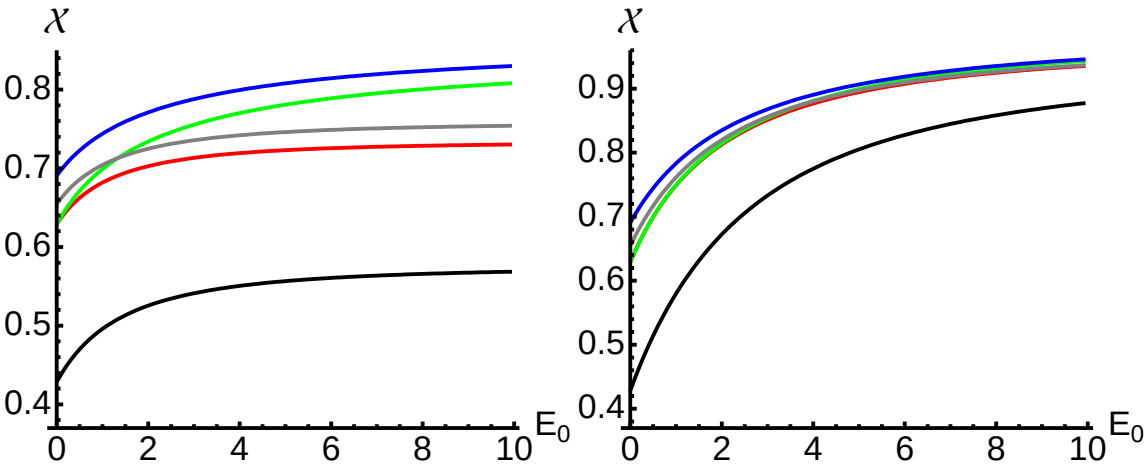

Figure 2.14: (Color online) Plot of Q (red), $\mathcal{F}_-$ (black), $\mathcal{F}_+$ (gray), M (green) and Y (blue) for $\Delta_1 = 1$ and $\Delta_2 = \Delta = 10$ as a function of the energy E_0 and $\beta_0 = 1$ (left), $\beta_0 = 0.01$ (right).

For two thermal states ν_Δ and $\nu_\Delta + d\nu_\Delta$ with mean number of photons given by $n_T = E_0 + \Delta$, where E_0 is the mean energy before the interaction with the Gaussian noisy channel, the quantum Chernoff metric reads

$$ds^2_{QCB} = \frac{1}{8(E_0+\Delta)(1+E_0+\Delta)} d\Delta^2 \tag{2.171}$$

Since for thermal states $ds^2_B/2 = ds^2_{QCB}$ and, from (1.78), $g_\Delta = \frac{1}{4}G_\Delta$, we obtain the expression of the quantum Fisher information

$$G_\Delta = \frac{1}{n_T(1+n_T)}. \tag{2.172}$$

For a pure squeezed vacuum state ϱ_0, with $\beta = 1$, the quantum Chernoff metric diverges for $\Delta = 0$ and its behavior is

$$g_{QCB}(\Delta) \simeq \frac{1}{4\Delta}\left(\frac{1}{2} + E_0\right) + \mathcal{O}(\Delta^0) \tag{2.173}$$

where we expanded around $\Delta = 0$. From Eq. (2.173) we see that the statistical distance between a pure state ($\Delta = 0$) and a neighboring impure state ($\Delta > 0$) diverges as $\Delta \to 0$. This feature has been found in a similar calculation of the Bures metric by Twamley [22]. For $\beta = 1$, $\Delta \neq 0$ and $E_0 = 0$ we have a thermal state again as in (2.171) $g_{QCB}(\Delta) = \frac{1}{8\Delta(\Delta+1)}$. Moreover, the metric tensor g_{QCB} for $\beta = 1$ and $\Delta \neq 0$ scales at high energies as

$$g_{QCB}(\Delta) = \frac{1}{16\Delta^2} + \mathcal{O}(1/E). \tag{2.174}$$

Quantum relative entropy

As we have already seen in section 1.4.3, an alternative approach to the binary decision problem is provided by the Neyman-Pearson strategy. In this context, the quantum relative entropy (1.34) between two states ϱ_0 and ϱ_1 gives the asymptotic optimal exponent for the decay of the probability of errors in discriminating ϱ_0 and ϱ_1 after performing n measurements on ϱ_1, when $n \to \infty$. The QRE for two STS's ϱ_1 and ϱ_2 is [140]

$$\begin{aligned} S(\varrho_1||\varrho_2) =& -\left[(n_{T,2}+1)\log(n_{T,2}+1) - n_{T,2}\log(n_{T,2})\right] + \frac{1}{2}\log[n_{T,1}(n_{T,1}+1)] \\ &+ \frac{2}{2n_{T,1}+1}\Big\{(\tilde{A}_1+1/2)(\tilde{A}_2+1/2) - \Re[\tilde{B}_1\tilde{B}_2^*]\Big\}\log\left(\frac{n_{T,1}+1}{n_{T,1}}\right) \end{aligned} \tag{2.175}$$

where $\tilde{A}_i = (n_{T,i}+\frac{1}{2})\cosh(2r_i) - 1/2$, $\tilde{B}_i = -(n_{T,i}+1/2)\sinh(2r_i)$, $i = 1,2$ are the coefficients of the characteristic functions corresponding to ϱ_i. As in the case of the quantum Chernoff bound, the condition of maximal discriminability is achieved for $\beta_0 = 1$, i.e. the optimal probes states are squeezed vacua, and $\Delta_1 = 0$. We set $E_0 = 0$ and consider that the total energy of the two states is given by $E_1 = \Delta_1$ and $E_2 = \Delta_2$. Then the quantum relative entropy is given by

$$S = \Delta_2\log\left(\frac{\Delta_1+1}{\Delta_1}\right) + \log(\Delta_1+1) + \Delta_2\log\Delta_2 - (1+\Delta_2)\log(1+\Delta_2), \tag{2.176}$$

and, around $\Delta_1 = 0$ it diverges as

$$S = \Delta_2(\log\Delta_2 - \log\Delta_1) - (1+\Delta_2)\log(1+\Delta_2) + (1+\Delta_2)\Delta_1 + \mathcal{O}(\Delta_1^2) \tag{2.177}$$

where we expanded up to first order in Δ_1.

Let us consider the problem of discriminating two thermal states $\varrho_1 = \nu_1$ with mean number of photons $n_{T,1} = E_0 + \Delta_1$ ($\beta_0 = 0$) and $\varrho_2 = \nu_2$ with $n_{T,2} = E_0 + \Delta_2$. The behavior of the QRE is given by

$$S(\nu_1||\nu_2) = \log(1+n_{T,1}) + n_{T,2}\log\left(n_{T,2}(1+\frac{1}{n_{T,1}})\right) - (1+n_{T,2})\log(1+n_{T,2}). \tag{2.178}$$

Kubo-Mori-Bogoljubov metric

We now consider a thermal state ν_Δ with mean photon number given by $n_T = E_0 + \Delta$. By expressing $\nu_\Delta = e^{-\beta_\Delta a^\dagger a}/Z$, $Z_\Delta = \mathrm{Tr}[e^{-\beta_\Delta a^\dagger a}]$, the logarithmic derivative of Eq. (1.142) is

$$\tilde{L}_\Delta = -\frac{Z'_\Delta}{Z_\Delta} - \beta'_\Delta a^\dagger a \tag{2.179}$$

where $x' = \frac{d}{d\Delta}x$. Then the KMB Fisher information is given by

$$\tilde{G}(\Delta) = \left(\frac{Z'_\Delta}{Z_\Delta}\right)^2 + (\beta'_\Delta)^2 \mathrm{Tr}[\nu_\Delta (a^\dagger a)^2] + 2\frac{Z'_\Delta \beta'_\Delta}{Z_\Delta}\mathrm{Tr}[\nu_\Delta (a^\dagger a)^2] = \frac{1}{n_T(n_T+1)} \qquad (2.180)$$

where $\mathrm{Tr}[\nu_\Delta (a^\dagger a)^2] = 2n_T(n_T+1)$ and $\mathrm{Tr}[\nu_\Delta a^\dagger a] = n_T$. According to the definition (1.140), by expanding the r.h.s. of Eq. (2.178) to the second order in ϵ with $\Delta_1 = \Delta + \epsilon$ and $\Delta_2 = \Delta$ we obtain the same result. By comparing Eq. (2.180) with (2.172), we conclude that for thermal states the KMB Fisher information is equal to the quantum Fisher information thus saturating the bound (1.143).

2.8 Conclusions and Outlooks

In this chapter we considered the estimation of parameters and the discrimination problem for Gaussian states. We have addressed the use of Kerr interaction to improve estimation of displacement and squeezing parameters and analyzed in details the behaviour of the quantum Fisher information as a function of probe and interaction parameters. We found that at fixed energy, with no constraint on the available Gaussian squeezing, Kerr dynamics is not useful and performances of Gaussian states are superior. On the other hand, in the more realistic case where the amount of Gaussian squeezing is fixed, or absent, then Kerr interaction improves estimation, especially for probe states with large amplitude. It should be noticed that Gaussian squeezing in $\chi^{(2)}$ media is obtained by parametric processes and the amount of squeezing linearly increases with the pump intensity. On the other hand, in $\chi^{(3)}$ media, the energy needed to obtain significant nonlinear effects is provided by the signal itsels. Overall, our results indicate that precision achievable with current technology Gaussian squeezing may be attained and surpassed for realistic values of the Kerr coupling and large enough signal amplitude.

For what concerns the discrimination problem, we have focused to the case when one of the two channels is the identity, i.e., the problem of discriminating the presence of a damping process from its absence (loss detection). For this kind of discrimininination we have considered thermal probes as input, i.e., single- and two-mode squeezed thermal states. The performance of the channel discrimination has been quantified using the QCB, computed over the two possible states at the output of the unknown channel for a given input state. Finding the optimal input state ρ which minimizes this bound gives automatically the optimal multi-copy state $\rho\otimes\rho\otimes\cdots$ when we consider many accesses to the unknown channel. In this scenario, we have fixed the mean total energy of the input state and optimized the discrimination (detection of loss) over the class of single- and two-mode squeezed thermal states. We have found numerically that the optimal states are pure, thus corresponding to single- and two-mode squeezed vacuum states. Furthermore, we have determined the conditions where the two-mode state outperforms the single-mode counterpart. This happens when the input energy exceeds a certain threshold, which becomes zero for suitably low values of the transmissivity (i.e., high values of damping).

In our investigation we have then considered the problem of loss detection in more realistic conditions, where it is unlikely to have pure squeezing. In this case, we have studied the optimal state for fixed total energy and squeezing, i.e., by fixing all the relevant resources needed to create the input state. Under these constraints, we have shown that a two-mode squeezed thermal state which conveys all the thermal photons in the dissipative

channel is the optimal thermal probe. In addition, this result is robust against fluctuations, i.e., it holds approximately also when the thermal photons are distributed in a more balanced way between the probe mode (sent through the dissipative channel) and the reference mode (bypassing the channel).

Finally we have closely investigated the role of correlations in our problem of loss detection. We have found that, for fixed input squeezing, the reduction of the QCB is an increasing function of several correlation quantifiers, such as the quantum entanglement, the quantum discord and the quantum mutual information. We then verify that employing the input squeezing in the form of correlations (quantum or classical) is always beneficial for the detection of loss by means of thermal probes.

We finally addressed the problem of discriminating Gaussian noise channels using both minimum error probability and maximum detection probability strategy. For what concerns discriminability with the quantum Chernoff bound, we studied two cases: the discrimination between an initial single-mode STS and the evolved state through the Gaussian noise map and the discrimination between two different STS's evolved with in two different channels. We have found that the condition of maximal discriminability is obtained for initial squeezed vacuum states in both the situations and that in the second case the quantum Chernoff bound has a scaling behavior at high energies. We also found that discrimination in the first case is better than in the second one. We have considered the discrimination of channels with infinitesimally close values of the noise parameter and evaluated the metrics associated to the two distinguishability notions. We found that the quantum Chernoff metric diverges for $\Delta = 0$ and analyzed the scaling behavior for pure squeezed states and for thermal states. Moreover, for what concerns the KMB metric, we found that in the case of thermal states the KMB Fisher information is equal to the quantum Fisher information thus saturating the upper bound

3

Estimation and discrimination in fermionic systems

This chapter is devoted to the problem of estimating the parameters of many-body Hamiltonians which undergo a second-order quantum phase transition and discriminating between two ground states or two thermal states of those systems. In particular, we will consider the Ising model in a transverse magnetic field as a paradigmatic example of such a system both at zero and finite temperature. In Section 3.1, we introduce the XY model that reduces to the Ising model for a particular value of the anisotropy coefficient, explain the phase diagram and the properties of magnetization. We then introduce in Sec. **??** the basic concepts of the geometric approach to quantum phase transitions and provide the Bures metric tensor for the quantum Ising model. By exploiting the results about the relation between quantum Fisher information and Bures metric tensor, in Section 3.3 we derive the optimal estimator of the coupling constant of the quantum Ising model at zero temperature both for the case of few spins and in the thermodynamical limit and also analyze the effects of temperature and derive the scaling properties of the QFI. We also address the measurement of total magnetization as an estimator of the Hamiltonian parameter and show its optimality. Finally, in Section 3.4, we study the distinguishability of two quantum states of the quantum Ising model at zero and finite temperature.

3.1 The XY model

We consider the XY model describing a one-dimensional chain of spins with nearest-neighbor coupling, in a constant and uniform magnetic field. The XY model is a class of Hamiltonians distinguished by a different value of the anisotropy coefficient γ, which

introduces a different coupling between the x and y components of the spins. In particular, the case $\gamma = 1$ is known as Ising model, the case $\gamma = 0$ is the so called XX model. The Hamiltonian is

$$H = -\sum_{i=1}^{L}\left[J\Big(\frac{1+\gamma}{2}\Big)\hat{\sigma}_i^x\hat{\sigma}_{i+1}^x + J\Big(\frac{1-\gamma}{2}\Big)\hat{\sigma}_i^y\hat{\sigma}_{i+1}^y + h\hat{\sigma}_i^z\right] \tag{3.1}$$

where $\hat{\sigma}_i^x$, $\hat{\sigma}_i^y$ and $\hat{\sigma}_i^z$ may be represented by the usual Pauli spin matrices

$$\sigma^x = \begin{pmatrix} 0 & 1 \\ 1 & 0 \end{pmatrix} \qquad \sigma^y = \begin{pmatrix} 0 & -i \\ i & 0 \end{pmatrix} \qquad \sigma^z = \begin{pmatrix} 1 & 0 \\ 0 & -1 \end{pmatrix} \tag{3.2}$$

acting on spin i, with

$$[\sigma_i^\mu, \sigma_j^\nu] = 2i\delta_{ij}\sum_{\tau=x,y,z}\epsilon_{\mu\nu\tau}\sigma_i^\tau. \tag{3.3}$$

In the following we treat the ends of the chain as a cyclic chain, in which case $1 \leq i \leq L$ and $\sigma_{L+1}^\mu = \sigma_1^\mu$, $\mu = x, y, z$ (periodic boundary conditions). To solve the model, we first introduce the raising and lowering operators

$$\sigma_i^+ = \frac{\hat{\sigma}_i^x + i\hat{\sigma}_i^y}{2}, \tag{3.4}$$

$$\sigma_i^- = \frac{\hat{\sigma}_i^x - i\hat{\sigma}_i^y}{2} \tag{3.5}$$

which satisfy the commutation rules for $i \neq j$

$$[\sigma_i^z, \sigma_j^\pm] = \pm 2\delta_{ij}\sigma_i^\pm \qquad [\sigma_i^+, \sigma_j^-] = \delta_{ij}\sigma_i^z, \tag{3.6}$$

and anticomutation rules on the same site

$$\{\sigma_i^+, \sigma_i^-\} = 1 \qquad (\sigma_i^+)^2 = \sigma_i^2 = 0. \tag{3.7}$$

In terms of which the Pauli spin operators they are

$$\hat{\sigma}_i^x = \sigma_i^+ + \sigma_i^-, \quad \hat{\sigma}_i^y = (\sigma_i^+ - \sigma_i^-)/i, \quad \hat{\sigma}_i^z = \sigma_i^+\sigma_i^- - 1/2 \tag{3.8}$$

and substituting into (3.1) we obtain

$$H = -\sum_{i=1}^{L}[J(\gamma\sigma_i^+\sigma_{i+1}^+ + \sigma_i^+\sigma_{i+1}^- + \text{h.c.}) + h\hat{\sigma}_i^z]. \tag{3.9}$$

Note that

$$J = \gamma_x + \gamma_y, \qquad \gamma J = \gamma_x - \gamma_y \tag{3.10}$$

where $\gamma_x = J\left(\frac{1+\gamma}{2}\right)$, $\gamma_y = J\left(\frac{1-\gamma}{2}\right)$. In the thermodynamic limit, the diagonalization of the XY model is achieved by means of three transformations: the Jordan-Wigner (JW), Fourier and Bogoliubov (BGV) transformations. The JW transformation is based on the observation that there exists a unitary mapping between the Hilbert space of a system of N spins and the fermion Fock space of spinless fermions on L sites. By virtue of this identification, we can consider the canonical annihilation JW fermion operators c_i [141]

$$\sigma_i^+ = c_i^\dagger e^{i\pi \sum_{j=1}^{i-1} c_j^\dagger c_j}, \tag{3.11}$$

$$\sigma_i^- = e^{-i\pi \sum_{j=1}^{i-1} c_j^\dagger c_j} c_i, \tag{3.12}$$

$$\hat{\sigma}_i^z = 2c_i^\dagger c_i - \mathbb{I}. \tag{3.13}$$

Observe that the JW operators satisfy anticommutation relations $\forall i, j$

$$\{c_i, c_j^\dagger\} = \delta_{ij}, \qquad c_i^2 = (c_i^\dagger)^2 = 0, \tag{3.14}$$

whereas the $\sigma_i^\pm$ anticommute only on a site. Note also that the boundary term depends on the number of spin of the chain,

$$\sigma_j^+ \sigma_j^- = c_j^\dagger c_j, \qquad \forall j \tag{3.15}$$

$$\sigma_i^+ \sigma_{i+1}^+ = c_i^\dagger c_{i+1}^\dagger \qquad \text{for } i = 1, \dots L-1, \qquad \sigma_L^+ \sigma_1^+ = -c_L^\dagger c_1^\dagger e^{i\pi\mathcal{N}}, \tag{3.16}$$

$$\sigma_i^+ \sigma_{i+1}^- = c_i^\dagger c_{i+1} \qquad \text{for } i = 1, \dots L-1, \qquad \sigma_L^+ \sigma_1^- = -c_L^\dagger c_1 e^{i\pi\mathcal{N}}. \tag{3.17}$$

where $\mathcal{N} = \sum_{i=1}^L c_i^\dagger c_i = \sum_{i=1}^L (\sigma_i^z + 1/2)$. We have also that $e^{i\pi n_j} c_j = c_j$ and $e^{i\pi n_j} c_j^\dagger = -c_j^\dagger$. The Hamiltonian H becomes

$$H = -J \sum_{i=1}^{L-1} [(\gamma c_i^\dagger c_{i+1}^\dagger + c_i^\dagger c_{i+1}) + \text{h.c.}] + J e^{i\pi\mathcal{N}} [(\gamma c_L^\dagger c_1^\dagger + c_L^\dagger c_1) + \text{h.c.}] - 2h \sum_{i=1}^{L} c_i^\dagger c_i + Lh. \tag{3.18}$$

The Hamiltonian (3.1) with L spins and periodic boundary conditions can be mapped into a fermionic model with

- anti-periodic boundary conditions (ABC) on the fermionic operators c_i, in the sector with an even number of fermions: $e^{i\pi\mathcal{N}} = 1$,
- periodic boundary conditions (PBC) for the c_i in the sector with an odd number of fermions: $e^{i\pi\mathcal{N}} = -1$.

Note that the number of fermionic operators is not invariant

$$[\mathcal{N}, H] \neq 0, \tag{3.19}$$

while the parity operator $\mathcal{P} = e^{i\pi\mathcal{N}}$ satisfies

$$[e^{i\pi\mathcal{N}}, H] = 0. \tag{3.20}$$

The operator $\mathcal{P}$ can be written as

$$\mathcal{P} = P_+ - P_- \tag{3.21}$$

where P_+ and P_- are the projection operators associated to the eigenvalues ± 1 of $\mathcal{P}$ and satisfy the following properties:

$$\begin{aligned} P_+ + P_- &= 1 \\ P_+ P_- &= 0. \end{aligned} \tag{3.22}$$

Then the Hamiltonian (3.1) preserves the parity sectors and can be decomposed as

$$H = P_+ H P_+ + P_- H P_- = H^{(+)} + H^{(-)}. \tag{3.23}$$

One can study separately the two parity sectors where $\mathcal{P}$ acts as a c-number. In the thermodynamic limit the boundary terms $\propto c_L c_1, c_L^\dagger c_1 + \text{h.c.}$ can be neglected since they introduce corrections of order $1/L$ which go to zero for $L \to \infty$. For the diagonalization of the model with the boundary term see [142]. The problem is then reduced to the diagonalization of the so-called c-cyclic Hamiltonian [143] and can be achieved by means of a discrete Fourier transform. We set in the parity sector $P^z = e^{i\pi\mathcal{N}} = 1$ which implies anti-periodic conditions for the c_i and define the Fourier transform

$$c_j = \frac{1}{\sqrt{L}} \sum_{k=0}^{L-1} e^{i\phi_k j} c_k. \tag{3.24}$$

In this case (ABC) we have that $\phi_k = \frac{(2k+1)\pi}{L}$ with $k = 0, \dots L-1$, whereas for PBC the parameter ϕ_k is $\phi_k = \frac{2k\pi}{L}$ with $k = 0, \dots L-1$. Notice that

$$\begin{aligned} \sum_{i=1}^{L} (c_i^\dagger c_{i+1}^\dagger + \text{h.c.}) &= \sum_k (e^{i\phi_k} c_k^\dagger c_{-k}^\dagger + \text{h.c.}), \\ \sum_k (e^{i\phi_k} c_k^\dagger c_{-k}^\dagger) &= \left(\sum_{k^+} + \sum_{k^-} \right) (\cos(\phi_k) + i \sin(\phi_k)) c_k^\dagger c_{-k}^\dagger \\ &= \sum_k (i \sin(\phi_k)) c_k^\dagger c_{-k}^\dagger. \end{aligned} \tag{3.25}$$

The index $k = 0, \dots L-1$ labels the sites of the chain in the momentum space. Then, due to the translational symmetry of the system, one can choose $k = -M, \dots, M$ and $L = 2M+1$. Then we have

$$H = \sum_{k=-M}^{M} \left[(-J\cos(\phi_k) - h)(c_k^\dagger c_k + c_{-k}^\dagger c_{-k}) - iJ\gamma \sin(\phi_k)(c_k^\dagger c_{-k}^\dagger + c_k c_{-k}) + h \right], \tag{3.26}$$

and we can write

$$H = \sum_{k=1}^{M} \tilde{H}_k = \sum_{k=1}^{M} \left(\tilde{H}_k^{(+)} + \tilde{H}_k^{(-)} \right), \tag{3.27}$$

where

$$\begin{aligned} \tilde{H}_k^{(\pm)} &= \left\{ \alpha_k (c_k^\dagger c_k + c_{-k}^\dagger c_{-k}) + i\delta_k (c_k^\dagger c_{-k}^\dagger + c_k c_{-k}) + 2h \right\} \\ \alpha_k &= 2(-J\cos\phi_k^{(\pm)} - h), \qquad \delta_k = -2J\gamma \sin\phi_k^{(\pm)} \\ \phi_k^{(+)} &= \frac{(2k+1)\pi}{L}, \qquad \phi_k^{(-)} = \frac{2k\pi}{L} \end{aligned} \tag{3.28}$$

where we cancelled the boundary terms whose contribution is of order $\mathcal{O}(1/L)$. By exploiting the following relation

$$\sum_k \begin{pmatrix} c_k^\dagger & c_{-k} \end{pmatrix} \begin{pmatrix} \epsilon_k & W_k \\ W_k^* & \epsilon_{-k} \end{pmatrix} \begin{pmatrix} c_k \\ c_{-k}^\dagger \end{pmatrix} = \sum_k \left[(\epsilon_k + \epsilon_{-k}) c_k^\dagger c_k + W_k c_k^\dagger c_{-k} + W_k^* c_{-k} c_k - \epsilon_k \right], \tag{3.29}$$

and setting

$$\epsilon_k = -(J\cos\phi_k + h), \qquad W_k = -iJ\gamma \sin\phi_k, \tag{3.30}$$

we obtain the following quasi-particle spectrum

$$\tilde{\Lambda}_k = \sqrt{\epsilon_k^2 + |W_k|^2} = \sqrt{J^2\gamma^2 + h^2 + J^2(1-\gamma^2)\cos^2\phi_k + 2Jh\cos\phi_k}. \tag{3.31}$$

A final unitary matrix U_k such that

$$U_k \begin{pmatrix} \epsilon_k & W_k \\ W_k^* & \epsilon_{-k} \end{pmatrix} U_k^\dagger = \begin{pmatrix} \tilde{\Lambda}_k & 0 \\ 0 & -\tilde{\Lambda}_k \end{pmatrix}, \qquad \begin{pmatrix} \eta_k \\ \eta_{-k}^\dagger \end{pmatrix} = U_k \begin{pmatrix} c_k \\ c_{-k}^\dagger \end{pmatrix} \tag{3.32}$$

is needed to cast the Hamiltonian (3.26) into a free particle theory. This is the so-called Bogoliubov transformation that maps the c_k's into a new set of fermionic operators whose number is conserved. We then obtain

$$H = \sum_k \tilde{\Lambda}_k \left(\eta_k^\dagger \eta_k - \eta_{-k}\eta_{-k}^\dagger \right) = \sum_k \Lambda_k (\eta_k^\dagger \eta_k - \frac{1}{2}), \qquad \tilde{\Lambda}_k = 2\Lambda_k. \tag{3.33}$$

The U_k which diagonalized the XY Hamiltonian has the following form

$$U_k = \begin{pmatrix} u_k & v_k \\ -v_k^* & u_k^* \end{pmatrix}, \tag{3.34}$$

and the new fermionic operators become

$$\eta_k = u_k c_k + v_k c_{-k}^\dagger. \tag{3.35}$$

One possible choice for u_k and v_k may be

$$u_k = \cos(\theta_k/2), \qquad v_k = i\sin(\theta_k/2) \tag{3.36}$$

where $\theta_k = \tan^{-1}\epsilon_k/W_k$. The equation (3.33) holds in the sector with an even number of fermions. In this case periodic boundary conditions on the spins induce antiperiodic BC on the fermions and the momenta satisfy $\phi_k = \frac{(2n+1)\pi}{L}$. In the sector with an odd number of particles, instead, one has $\phi_k = \frac{2n\pi}{L}$ and the Hamiltonian becomes

$$H = (-2J-2h)c_0^\dagger c_0 + (2J-2h)c_\pi^\dagger c_\pi + 2h + \sum_{k\neq 0,\pi}\Lambda_k(\eta_k^\dagger\eta_k - \frac{1}{2}) \tag{3.37}$$

therefore one must carefully treat the excitations at $\phi_k = 0$ and $\phi_k = \pi$.

In any case, we are interested into the ground state of the system that belongs to the even sector so that, at zero temperature, we can use Eq. (3.33) for any finite L. At positive temperature, we are primarily interested in large system sizes and therefore we can neglect boundary terms in the Hamiltonian and use Eq. (3.33) in the whole Fock space. The ground state energy is then (in the sector with even $\mathcal{N}$)

$$\begin{aligned} E = -\sum_k \tilde{\Lambda}_k =& \sqrt{J^2\gamma^2 + h^2 + J^2(1-\gamma^2)\cos^2(k) + 2Jh\cos\phi_k} \\ =& \sqrt{(\gamma_x-\gamma_y)^2 + h^2 + 4\gamma_x\gamma_y\cos^2\phi_k + 2(\gamma_x+\gamma_y)h\cos\phi_k}. \end{aligned} \tag{3.38}$$

With this expression the correlators $\langle\hat{\sigma}_i^x\hat{\sigma}_{i+1}^x\rangle$ and $\langle\hat{\sigma}_i^y\hat{\sigma}_{i+1}^y\rangle$ can be obtained by differentiating with respect to γ_x and γ_y, i.e

$$\langle\sigma_i^\alpha\sigma_{i+1}^\alpha\rangle = -\frac{1}{L}\frac{\partial E}{\partial\gamma_\alpha}, \quad \alpha = x,y; \qquad \langle\hat{\sigma}_i^z\rangle = -\frac{1}{L}\frac{\partial E}{\partial h} \tag{3.39}$$

and we obtain

$$\langle\hat{\sigma}_i^x\hat{\sigma}_{i+1}^x\rangle = \frac{1}{L}\sum_k \frac{J\gamma + J(1-\gamma)\cos^2\phi_k + h\cos\phi_k}{\tilde{\Lambda}_k} \tag{3.40}$$

$$\langle\hat{\sigma}_i^y\hat{\sigma}_{i+1}^y\rangle = \frac{1}{L}\sum_k \frac{-J\gamma + J(1+\gamma)\cos^2\phi_k + h\cos\phi_k}{\tilde{\Lambda}_k} \tag{3.41}$$

$$\langle\hat{\sigma}_i^z\rangle = \frac{1}{L}\sum_k \frac{h + J\cos\phi_k}{\tilde{\Lambda}_k} \tag{3.42}$$

Phase diagram of the quantum Ising model

Let us consider the case $\gamma = 1$, that is the so-called Ising model. As the temperature and the field are varied, one may identify different physical regions. At zero temperature, the system undergoes a QPT for $h = J$. For $h < J$ the system is in a magnetically

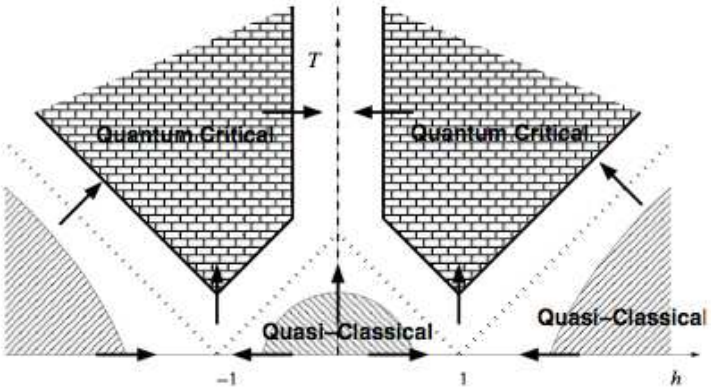

Figure 3.1: Phase diagram of the Ising model with $J = 1$ in a transverse field taking into account both critical points at $h = \pm 1$ and the purely classical Ising line $h = 0$. The arrows define the direction along which the fidelity decreases most rapidly: the latter represents the direction of highest distinguishability between two nearby Gibb's states (see the next section 3.2 for details).

ordered phase i.e. the spins are either all up or down (in eigenstates of $\hat{\sigma}^x$), instead for $h > 1$ the magnetic field dominates, and excitations are given by spin flip over a paramagnetic ground state. A signature of the ground state quantum phase diagram remains also at finite temperature [144] where for $T \ll \Delta = |J - h|$ the system behaves quasi-classically whereas for $T \gg \Delta$ quantum critical effects dominate. In each of the above described regions of the (h, T) plane the system displays very different dynamical as well thermodynamical properties. For example, in the quantum critical region the specific heat approaches zero linearly with temperature, whereas in the quasi-classical regions the approach is exponentially fast. We report in Fig. 3.1 an interesting phase diagram of the Ising model in transverse field in the (h, T) plane taken from [145]. The coupling constant is fixed to $J = 1$ and there has been taken into account both the quantum critical points $h = \pm 1$. The arrows define the direction along which the fidelity decreases most rapidly, that represents the points of maximal distinguishability between two states, i.e. the overlap decreases when the distance between two quantum states increases.

It is possible to show [146] that the transverse magnetization $m^z = \langle \hat{\sigma}_i^z \rangle$ in (3.42), obtained differentiating the energy with respect to the parameter h, for $J = 1$ has the following expression near the transition point $h = 1$

$$m^z \simeq \frac{2}{\pi} - \frac{h-1}{\pi}(\ln|h-1| + 1 + \ln 8). \tag{3.43}$$

As expected, m^z is a continuous function at the transition point whereas the next h-derivative exhibits a logarithmic divergence, as it is related to the specific heat in the

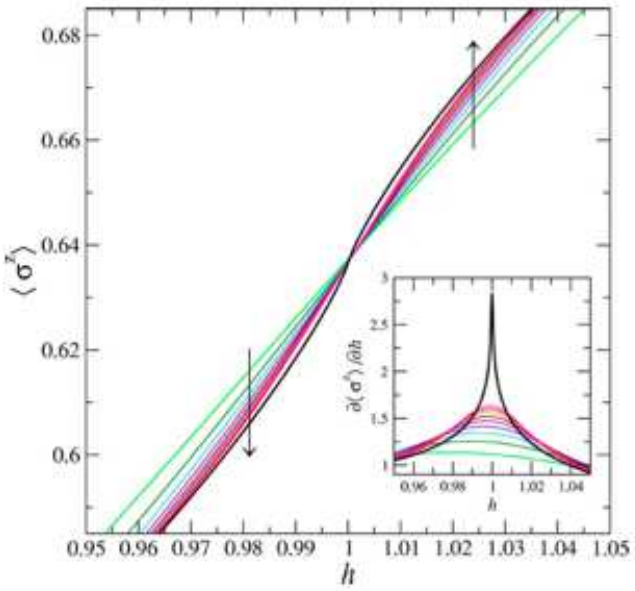

Figure 3.2: The transverse magnetization $\langle\hat{\sigma}_i^z\rangle$, is plotted for different sizes L ranging from 20 to 100 in steps of 10. The black thick line corresponds to the thermodynamic limit and the arrows indicate the direction of increasing L. The inset shows the derivative with respect to h which has a cusp at the pseudo quantum critical point $h = 1$.

corresponding $2D$ classical model. In the critical regime $L \ll \xi$, where ξ is the correlation length given by the formula $\sinh(1/2\xi) = |1-h|\,|h|^{-1/2}/2$ which can be obtained from the dispersion relation [146], the finite-size expression for the transverse magnetization is [146]

$$m_h^z(L) \simeq \frac{2}{\pi} + \frac{\ln(L) + \ln(8/\pi) + \gamma_C - 1}{\pi}(h-1) + \frac{\pi}{12}\frac{1}{L^2} \tag{3.44}$$

where $\gamma_C = 0.5772\ldots$ is the Euler-Mascheroni constant. In Fig. 3.2 [146], we report the plot of m^z for different sizes L of the Ising model. The inset shows the susceptibility which is given by $\partial\langle\hat{\sigma}_i^z\rangle/\partial h$ plotted for different sizes of L. The black thick line corresponds to the thermodynamic limit and the function has a cusp at $h = 1$. The finite-size expression of the susceptibility at $h = 1$ is then obtained from (3.44)

$$\frac{\partial\langle\hat{\sigma}_i^z\rangle}{\partial h}\Big|_{J=h=1} = \frac{-1+\gamma_C+\ln(8/\pi)}{\pi} + \frac{1}{\pi}\ln L + \mathcal{O}(L^{-1}). \tag{3.45}$$

3.2 Geometry of quantum phase transitions

In this Section we consider the so-called metric (or fidelity) approach to critical phenomena which basically consists into approaching quantum phase transitions from a geometrical point of view through the definition of distance functions between infinitesimally close quantum states. In the following we provide the general theoretical framework of this strategy according to [147] and then provide an example of characterization of the quantum phase transitions in terms of the metric tensor by considering the example of the quantum Ising model.

The analysis of quantum phase transitions has benefited from tools of quantum information theory. The von Neumann entropy and fidelity applied to many-body systems can identify phase transitions and reveal different scaling behaviors at different regions of the phase diagram [148, 149, 150, 151, 152]. More recently, it has been shown that quantum fidelity between quantum states, *i.e.* the overlap between ground state wave functions, can identify the quantum phase transition by comparing two ground states corresponding to slightly different values of the coupling constants $\{\lambda\}$ [39, 153, 154, 155, 156, 147, 145, 157, 158]. The intuition behind this is simple: the quantum critical points mark the separation between regions of the parameter space which correspond to ground states having deeply different structural properties, i.e. order parameters. This difference is then quantified by the simplest Hilbert-space geometrical quantity that is the overlap between the corresponding ground states. This new approach provides an alternative to the study of quantum phase transitions using order parameters and symmetry breaking patterns, which depends on *a priori* knowledge of the physics of the problem [159]. On the other hand, some systems fail to fall into this conceptual framework. This can be due to the difficulty of identifying the proper order parameter for systems whose symmetry breaking pattern is unknown or to the absence of a local order parameter , i.e. in the case of quantum phase transitions involving some kind of topological order [160]. Moreover, the fidelity approach to QPTs differently from bipartite entanglement measure approach [148, 149], considers the system as a whole, without resorting to bipartitions.

Let us consider a family of Hamiltonians $\{H(\lambda)\}$, $\lambda \in \mathcal{M}$ (where $\mathcal{M}$ is the parameter manifold) in the Hilbert space $\mathcal{H}$ of the system. If $|\Psi_0(\lambda)\rangle \in \mathcal{H}$ denotes the ground state (unique for simplicity) of $H(\lambda)$, one has defined the map $\Psi_0 \rightarrow \mathcal{M} \rightarrow |\Psi_0(\lambda)\rangle$ associating to each set of parameters the ground state of the corresponding Hamiltonian. This map can be seen also as a map between $\mathcal{M}$ and the projective space $P\mathcal{H}$ (the manifold of rays of $\mathcal{H}$). This space is a metric space equipped with the Fubini-Study distance $\mathcal{D}_{FS}(|\psi\rangle, |\phi\rangle) = \arccos\sqrt{|\langle\psi|\phi\rangle|^2}$ as defined in Eq. (1.22). In Ref. [13], Wootters showed

that this metric has a deep operational meaning: it quantifies the maximum amount of statistical distinguishability between the pure quantum states $|\psi\rangle$ and $|\phi\rangle$. More precisely, $\mathcal{D}_{FS}(|\psi\rangle, |\phi\rangle)$ is the maximum over all the possible projective measurements of the Fisher-Rao statistical distance between the probability distributions obtained from $|\psi\rangle$ and $|\phi\rangle$. Moreover the result extends to mixed states by replacing the pure state fidelity (1.21) with the Uhlmann fidelity (1.20) and the projective measurements with generalized ones [25], thus defining the Bures distance (1.23):

$$\mathcal{D}_A(\varrho, \sigma) = \cos^{-1} \sqrt{\mathcal{F}(\varrho, \sigma)}. \tag{3.46}$$

where ϱ and σ are two mixed quantum states. There results allow the identification of Hilbert-space geometry with a geometry in the information space: the bigger the Hilbert space distance between ϱ and σ, the higher the degree of statistical distinguishability of these two states. From this perspective we have that a single real number, i.e. the distance, virtually encodes information about all the observables one may think to measure. This remark contains the main intuition of the metric approach to quantum phase transitions: at the critical points, a small difference between the control parameters results in a greatly enhanced distinguishability in the corresponding ground states, which should be revealed by the behavior of their distance.

The projective manifold $P\mathcal{H}$, besides the structure of metric space, has the structure of a Riemannian manifold, i.e. it is equipped with a metric tensor. An elementary way of getting the form of the Riemannian metric over $P\mathcal{H}$ is by means of Eq. (1.22). For $\mathcal{F}$ very close to unity we have $\mathcal{D}^2_{FS}(\psi, \psi + d\psi) \simeq 2(1 - \langle\psi|\psi + d\psi\rangle)$. Since $\langle\psi|\psi + d\psi\rangle \simeq |1 + \langle\psi|d\psi\rangle + 1/2\langle\psi|d^2\psi\rangle|^2$, using this expression and the normalization of $|\psi\rangle$ one finds

$$ds^2 = \mathcal{D}^2_{FS}(\psi, \psi + d\psi) = \langle d\psi|d\psi\rangle - |\langle\psi|d\psi\rangle|^2. \tag{3.47}$$

By considering the ground state mapping Ψ_0 introduced above, we have $d|\Psi_0(\lambda)\rangle = \sum_\mu |\partial_\mu \Psi_0\rangle d\lambda^\mu$, with $\partial_\mu = \partial/\partial\lambda^\mu$, $\mu = 1, \ldots, \dim\mathcal{M}$. Using Eq. (3.47), one obtains

$$ds^2 = \sum_{\mu\nu} g_{\mu\nu} d\lambda^\mu d\lambda^\nu \tag{3.48}$$

where

$$g_{\mu\nu} = \mathrm{Re}\left[\langle\partial_\mu\Psi_0|\partial_\nu\Psi_0\rangle - (\langle\partial_\mu\Psi_0|\Psi_0\rangle)^2\right]. \tag{3.49}$$

The same derivation of the metric tensor for the case of two mixed states ϱ and $\sigma = \varrho + d\varrho$

leads to the Bures metric of Eq. (3.96):

$$\begin{aligned} ds_B^2 =& \mathcal{D}_B(\varrho, \varrho + d\varrho))^2 = \frac{1}{2}\sum_{m,n}\frac{|\langle\psi_n|d\varrho|\psi_m\rangle|^2}{\varrho_m + \varrho_n} \\ =& \frac{1}{4}\sum_n \frac{dp_n^2}{p_n} + \frac{1}{2}\sum_{n\neq m}\frac{(p_m - p_n)^2}{p_n + p_m}|\langle\psi_n|d\psi_m\rangle|^2 \end{aligned} \tag{3.50}$$

where $\varrho = \sum_n p_n|\psi_n\rangle\langle\psi_n|$.

We now provide a simple perturbative argument for which one should expect a divergent behavior of the metric tensor (3.49) at quantum phase transitions. By using the first order perturbative expansion

$$|\Psi_0(\lambda + d\lambda)\rangle \sim |\Psi_0(\lambda)\rangle + \sum_{n\neq 0}(E_0 - E_n)^{-1}|\Psi_n(\lambda)\rangle\langle\Psi_n(\lambda)|dH|\Psi_0(\lambda)\rangle, \tag{3.51}$$

where $dH = H(\lambda+d\lambda) - H(\lambda)$, one obtains for the entries of (3.49) the following expression

$$g_{\mu\nu} = \mathrm{Re}\sum_{n\neq 0}\frac{(\langle\Psi_0(\lambda)|\partial_\mu H|\Psi_n(\lambda)\rangle)^2}{[E_n(\lambda) - E_0(\lambda)]^2}. \tag{3.52}$$

Continuous QPTs are known to occur when, for some specific values of the parameters and in the thermodynamical limit, the energy gap above the GS closes. This amounts to a vanishing denominator in Eq. (3.52) which may break down the analyticity of the metric tensor entries.

In order to show explicitly the divergences in $g_{\mu\nu}$, we consider the example of the XY model and in particular the quantum Ising model reviewing the derivation of the Bures metric given in [145]. We start by considering the Bures metric for a quantum statistical model defined by the set of thermal states $\varrho_\lambda = e^{-\beta H(\lambda)}/Z$, $Z = \mathrm{Tr}[e^{-\beta H(\lambda)}]$ associated to a family of Hamiltonians $\{H(\lambda)\}$ depending on a set of parameters λ living in some manifold $\mathcal{M}$. First notice that $\varrho_\lambda = Z^{-1}\sum_n e^{-\beta E_n}|\psi_n\rangle\langle\psi_n|$ where E_n and $|n\rangle$ are the eigenvalues and eigenvectors of the Hamiltonian H. By differentiating the Hamiltonian eigenvalue equation one has $\langle\psi_i|d\psi_j\rangle = \langle\psi_i|dH|\psi_j\rangle(E_i - E_j)$. Moreover, $dp_i = d(e^{-\beta E_i}/Z) = -Zp_i[dE_i - (\sum_i dE_i p_i)]$, therefore the first term in Eq. (3.96) can be written as $\beta^2/4\sum_i p_i(dE_i^2 - \langle dE\rangle^2)$ where $\langle dE\rangle_\beta = \sum_j dE_j p_j$. This means that the first term of (3.96), i.e. the Fisher Rao distance is expressed as the variance of the diagonal observable $\langle dH_d\rangle = \sum_j dE_j|j\rangle\langle j|$. Summarizing we have

$$ds_B^2 = \frac{\beta^2}{4}(\langle dH_d^2\rangle_\beta - \langle dH_d\rangle_\beta^2) + \frac{1}{2}\sum_{n\neq m}\left|\frac{\langle\psi_n|dH|\psi_m\rangle}{E_n - E_m}\right|^2\frac{(e^{-\beta E_n} - e^{-\beta E_m})^2}{Z(e^{-\beta E_n + e^{-\beta E_m}})}. \tag{3.53}$$

We recall that the quasifree Hamiltonian we consider is given in (3.33) by $H = \sum_k \Lambda_k(\eta_k^\dagger\eta_k - 1/2)$. One has that k is a suitable quasiparticle label, that for translationally invariant

systems amounts to a linear momentum. The ground state is the vacuum of η_k operators i.e. $\eta_k|GS\rangle = 0$, $\forall k$. The dependence on the parameters h and J is both through Λ_k and the η_k's. To derive the Bures metric, we first observe that the first and second terms in Eq. (3.96) depend on β, h and J. For simplicity, we will consider only a single parameter in the derivation of $g_\mu\nu$, in particular $\mu = \nu = h$. The Bures metric then can be expressed in terms of the classical and non classical part

$$g_{hh} = g^c_{hh}(\beta, J, h) + g^{nc}_{hh}(\beta, J, h) \tag{3.54}$$

such that $ds^2_B = g_{hh}dh^2$. The Hamiltonian eigenvalues are given by $E_j = \sum_k n_k\Lambda_k$, where the n_k's are fermion occupation numbers, i.e. $n_k = 0, 1$. Then we have that $dE_j = \sum_k n_k d\Lambda_k$ and $\langle E_j\rangle_\beta = \sum_k \langle n_k\rangle_\beta d\Lambda_k$. Furthermore, $\langle n_\mu n_\nu\rangle_\beta - \langle n_\mu\rangle_\beta\langle n_\nu\rangle_\beta = \delta_{\mu\nu}\langle n_\nu\rangle_\beta(1-\langle n_\nu\rangle_\beta)$ where $\langle n_\nu\rangle_\beta = [\exp(\beta\Lambda_\nu)+1]^{-1}$. The final result for the classical part is [145]

$$\frac{1}{4}\sum_k \frac{(dp_n)^2}{p_n} = \frac{\beta^2}{16}\sum_k \frac{(\partial_J\Lambda_k)^2}{\cosh(\beta\Lambda_k/2)}dh^2 \tag{3.55}$$

In order to compute the nonclassical part of Eq. (3.96), one has to explicitly consider the eigenvectors of Eq. (3.33). Following the notation of Ref. [161] one has $|m = \{\alpha_k, \alpha_{-k}\}_{k>0}\rangle = \otimes_{k>0}|\alpha_k, \alpha_{-k}\rangle$, where,

$$\begin{aligned} |0_k0_k\rangle &= \cos(\theta_k/2)|00\rangle_{k,-k} - \sin(\theta_k/2)|11\rangle_{k-k}, \\ |0_k1_{-k}\rangle &= |01\rangle_{k,-k}, \qquad |1_k0_{-k}\rangle = |10\rangle_{k,-k}, \\ |1_k1_k\rangle &= \cos(\theta_k/2)|11\rangle_{k,-k} + \sin(\theta_k/2)|00\rangle_{k,-k}. \end{aligned} \tag{3.56}$$

We assume that the parameter dependence is only in the angles θ_k's which is true for all the translationally invariant systems and we find that the nonvanishing matrix elements $\langle\psi_n|d\psi_m\rangle$ are given by $\langle 0_k0_{-k}|d|1_k1_{-k}\rangle = d\theta_k/2$ and that the thermal factor $(p_n-p_m)^2/(p_n+p_m)$ has the form $\sinh^2(\beta\Lambda_k)/\{[\cosh(\beta\Lambda_k)+1][\cosh(\beta\Lambda_k)]\} = [\cosh(\beta\Lambda_k)-1]/\cosh(\beta\Lambda_k)$. Putting all together

$$\frac{1}{2}\sum_{n\neq m}\frac{(p_m-p_n)^2}{p_n+p_m}|\langle\psi_n|d\psi_m\rangle|^2 = \frac{1}{4}\sum_{k>0}\frac{\cosh(\beta\Lambda_k)-1}{\cosh(\beta\Lambda_k)}(d\theta_k)^2dh^2. \tag{3.57}$$

The two elements (3.55) and (3.57) define the metric element (3.54). This result can be applied to any quasifree fermionic model $H \propto \sum_k \Lambda_k\eta^\dagger_k\eta_k$. The analysis of the behavior of the metric tensor g for the Ising model allows one to conclude that, for the specific model studied, the quantum critical and quasiclassical regions can be clearly identified in terms of the markedly different temperature behavior of the geometric tensor g. Indeed

one has that for fixed $J = 1$, in the quantum-critical region $\beta\Delta \simeq 0$, $\Delta = |J - h|$ the low temperature expansion

$$g^c_{hh} = \frac{\pi}{96h^2} T + \mathcal{O}(T^2) \tag{3.58}$$

$$g^{nc}_{hh} = \frac{1}{\pi^2}\left[\frac{\mathcal{C}}{\pi^2} T^{-1} - \frac{1}{16} + \mathcal{O}(T)\right] \tag{3.59}$$

where $\mathcal{C}$ is the Catalan constant. Note that the in the limit $T \to 0$, the nonclassical part of the metric tensor matches the behavior of the metric tensor (3.49) in the ground state.

We reported this result of [145], to give an example of the metric (or fidelity) approach to quantum phase transitions whose main result is that the set of critical parameters can be identified and analyzed in terms of the scaling and finite-size scaling behavior of the metric. More precisely the metric has the following properties:

- In the thermodynamical limit and in neighborhood of the critical values λ_c, the zero temperature metric has the scaling behavior

  $$ds^2_B \sim L^d |\lambda - \lambda_c|^{-\nu\Delta_g}, \tag{3.60}$$

  where L is the system size, d the spatial dimensionality, ν is the correlation length exponent $\xi = |\lambda - \lambda_c|^{-\nu}$ and $\Delta_g = 2\zeta + d - 2\Delta_V$. Here ζ is the dynamical exponent and Δ_V the scaling dimension of the operator coupled to λ.

- At the critical points, or more generally in the critical region defined by $L \ll \xi$, the finite-size scaling is

  $$ds^2_B \sim L^{d+\Delta_g}. \tag{3.61}$$

  The main point is that for a wide class of QPTs, Δ_g can be greater than zero thus giving a superextensive behavior of the metric in the critical region whereas at regular points the scaling is always extensive:

  $$ds^2_B \sim L^d. \tag{3.62}$$

  The superextensive behavior gives rise for $L \to \infty$ to a peak of the metric (or a drop of the fidelity) that allows one to identify the boundaries between the different phases.

- Moreover, when the temperature is turned on, one can still see signatures of the criticality. This is true when the temperature is low but bigger than the system's energy gap and one has

  $$ds^2_B \sim T^{-\beta} \tag{3.63}$$

  with $\beta > 0$.

3.3 Estimation of parameters in the quantum Ising model

It is a general fact that the coupling constant of a many-body Hamiltonian does not correspond to any observable and one has to infer its value through indirect measurements. For many-body quantum systems, changing the coupling constant drives the system into different phases. In particular, close to critical points, quantum states belonging to different phases should be distinguished more effectively than states belonging to the same phase [145, 147, 153, 154, 155, 156, 162]. Distinguishability is usually quantified by fidelity.

In estimating the value of a parameter, one is led to define the Fisher information which represents an infinitesimal distance among probability distributions, and gives the ultimate precision attainable by an estimator via the Cramer-Rao theorem. Its quantum counterpart, the quantum Fisher information (QFI), is related to the degree of statistical distinguishability of a quantum state from its neighbours, and it turns out to be proportional to *Bures metric* between quantum states [13, 20, 25, 163, 164, 165, 166].

As noticed in [39] one can exploit the geometrical theory of quantum estimation to derive the ultimate quantum bounds to the precision of any estimation procedure, and the fidelity approach to QPTs to find working regimes achieving those bounds. Indeed, precision may be largely enhanced at the critical points in comparison to the regular ones. In this Section we show that the general idea advocated in [39] can be successfully implemented in systems of interest for quantum information processing. To this aim we address a paradigmatic example of a many-body system exhibiting a (zero temperature) QPT: the one-dimensional Ising model with a transverse magnetic field.

In most physical situations, some parameters of the Hamiltonian, *e.g.* the coupling constant, are unaccessible, whereas others may be tuned with reasonable control by the experimenter (*e.g.* external field). Therefore, the idea is to tune the controllable parameters in order to maximize the QFI and thus the distinguishability and the estimation precision. In doing this we consider the system both at zero and finite temperature, and fully exploit QET to derive the optimal quantum measurement for the unobservable coupling constant in terms of the symmetric logarithmic derivative. In the thermodynamic limit we find that optimal estimation is achieved tuning the field at the critical value, in accordance with [39], whereas at finite size L, the request of maximum QFI defines a pseudo-critical point which scales to the proper critical point as L goes to infinity. In turn, a precision improvement of order L may be achieved with respect to the non critical case.

The optimal measurement arising from the present QET approach may be not achievable with current technology. Therefore, having in mind a practical implementation, we consider estimators based on feasible detection schemes, and show, for systems of few

spins, that the measurement of the total magnetization allows for estimation of the coupling constant with precision at the ultimate quantum level.

The section is structured as follows: we first derive the ultimate quantum limits to the precision of coupling constant estimation at zero temperature, both for the case of few spins and then in the thermodynamical limit. In subsection 3.4.2 we analyze the effects of temperature and derive the scaling properties of QFI. Finally we address the measurement of total magnetization in 3.3.4 as estimator of the Hamiltonian parameter and show its optimality. The results reviewed in this section are reported in [3].

3.3.1 Criticality as a resource

To the aims of the following work, it is crucial to notice that the quantum Fisher information (QFI) is proportional to the Bures metric. Indeed, by evaluating the trace defining the QFI in the eigenbasis of ϱ_λ one readily finds [25]

$$g_{\mu\nu} = \frac{1}{4}\mathcal{G}_{\mu\nu} \tag{3.64}$$

as we have already seen in (1.78). This remark, along with the results of the metric approach to criticality summarized in the previous section, lead to the following conclusion: *the estimation of a physical quantity driving a quantum phase transition is dramatically enhanced at the quantum critical point.*

In order to accurately asses the improvement in the estimation accuracy, we focus on the single parameter case and in particular we consider the coupling constant of the quantum Ising model which is defined by the Hamiltonian

$$H = -J\sum_{i=1}^{L}\sigma_i^x\sigma_{i+1}^x - h\sum_{i=1}^{L}\sigma_i^z. \tag{3.65}$$

The quantum statistical model is then defined by $\varrho_\lambda = Z^{-1}e^{-\beta H(\lambda)}$ and the particular case we will consider is $\lambda = J$, i.e. we are going to calculate the quantum Fisher information of the coupling constant J of the Ising model in order to estimate J with the best precision.

The QFI for the parameter J may be evaluated starting from Eq. (3.50)

$$G_J = \sum_n \frac{(\partial_J p_n)^2}{p_n} + 2\sum_{n\neq m}|\langle\psi_n|\partial_J\psi_m\rangle|^2\,\frac{(p_n-p_m)^2}{p_n+p_m}, \tag{3.66}$$

from the Bures metric tensor

$$g_\lambda = \frac{1}{2}\sum_{nm}\frac{|\langle\psi_m|\partial_\lambda\varrho_\lambda|\psi_n\rangle|^2}{p_n+p_m}\,. \tag{3.67}$$

Then one has that the QFI at finite temperature (remind that we only need differentiation with respect to J) is given by [145]

$$G_J(J,h,\beta) = \frac{\beta^2}{4}\sum_k \frac{(\partial_J \Lambda_k)^2}{\cosh^2(\beta\Lambda_k/2)} + \sum_k \frac{\cosh(\beta\Lambda_k)-1}{\cosh(\beta\Lambda_k)}(\partial_J\theta_k)^2 . \quad (3.68)$$

where $\theta_k = \tan^{-1}\frac{\epsilon_k}{\Delta_k}$.

3.3.2 Quantum estimation at zero temperature

We begin to test the idea of estimating the coupling constant J of the Ising model by finding the maximum of QFI at zero temperature where the system is in the ground state. At first we consider few spins and then we turn to address the thermodynamic limit.

Small L

We start with the case of $L = 2, 3$ and 4 in Eq.(3.65). In the following we review in detail the calculations carried out for $L = 2$. The cases $L = 3, 4$ follow straightforwardly. The QFI is obtained from Eq. (3.66) by explicit diagonalization of the Ising Hamiltonian where $p_n = e^{-\beta E_n}/Z$, E_n and $|\psi_n\rangle$ are the eigenvalues and eigenvectors of H. For example, for $L = 2$ we have $E_n = \pm 2J, \pm\sqrt{J^2+h^2}$ and $Z = 2\cosh(2\beta J) + 2\cosh(2\beta\sqrt{J^2+h^2})$. Taking the $T \to 0$ limit of the QFI, one gets

$$G_J(J,h,0) = \frac{h^2}{(h^2+J^2)^2}, \quad L = 2 \quad (3.69)$$

$$G_J(J,h,0) = \frac{3h^2}{4(h^2-hJ+J^2)^2}, \quad L = 3 \quad (3.70)$$

$$G_J(J,h,0) = \frac{h^2(h^4+4h^2J^2+J^4)}{(h^4+J^4)^2}, \quad L = 4 . \quad (3.71)$$

Maxima of the QFI G_J are obtained for $h^* = J$ for $L = 2, 3, 4$. Actually, this is true for any L (see also the next section), and the pseudocritical point h^*, which maximizes $\mathcal{H}_J$, turns out to be independent of L and equal to the true critical point. *i.e.* $h_c = J$, $\forall L$. At its maximum G_J goes like $1/J^2$, as also required by dimensional analysis, and the ultimate lower bound to precision (variance) of any quantum estimator of J scales as J^2.

Large L

In the following we discuss the QFI for a system of size L. We analyze the behavior of G_J near the critical region at $T = 0$. Taking the limit $T \to 0$ in Eq. (3.68), the classical elements of the Bures metric, which depends only on thermal fluctuations, vanishes due

to the factor of $(\cosh(\beta\Lambda_k/2))^{-2}$. Therefore, at zero temperature, only the nonclassical part of Eq. (3.68) survives and one obtains

$$G_J = \sum_k (\partial_J \theta_k)^2, \tag{3.72}$$

where $\partial_J \theta_k = \frac{1}{1+(\Delta_k/\epsilon_k)^2}(\partial_J \frac{\Delta_k}{\epsilon_k}) = \frac{-h \sin k}{\Lambda_k^2}$. Since we are in the ground state, the allowed quasi-momenta are $k = \frac{(2n+1)\pi}{L}$ with $n = 0, \ldots, L/2-1$. Explicitly we have

$$G_J \;=\; \sum_k \frac{h^2 \sin(k)^2}{\Lambda_k^4}. \tag{3.73}$$

We are interested in the behavior of the QFI in the quasi-critical region $\xi \gg L$ where the correlation length ξ scales as $\xi \sim |h-J|^{-\nu}$. In the Ising model $\nu = 1$ so the critical region is described by small values of the scaling variable $z \equiv L(h-J) \simeq L/\xi$, that is $z \approx 0$. Conversely the off-critical region is given by $z \to \infty$. We substitute $h = J + z/L$ in Eq. (3.73) and expand around $z = 0$ to obtain the scaling of G_J in the quasi-critical regime

$$G_J = \sum_{k_n} \frac{(J+\frac{z}{L})^2 \sin^2(k_n)}{[\frac{z^2}{L^2} + 4J(J+\frac{z}{L})\sin^2(k_n/2)]^2} \equiv \sum_{k_n} f_{k_n}(z)\,. \tag{3.74}$$

Since $\partial_z f(0) = 0$, the maximum of G_J is always at $z = 0$ for all values of L, in turn, the pseudo-critical point is $h_L^* = J = h_c \;\forall L$. As already noticed previously, the statement $h_L^* = h_c$ is peculiar to this particular situation. For instance, introducing an anysotropy γ so as to turn the Ising model into the anysotropic XY model, the pseudo-critical point gets shifted and one recovers the general situation $h_L^* = h_c + O\left(L^{-\delta}\right)$. The exponent δ is universal, .i.e. independent on the anisotropy (and given by $\delta = 2$ in this case), while the prefactor explicitly depends on γ, vanishing for $\gamma = 0$ [39]. Going to second order one obtains

$$\sum_k (\partial_J \theta_k)^2 \;=\; \sum_{k_n} \frac{1}{4J^2} \cot^2(k_n/2)\Big(1 - \frac{z^2}{2J^2L^2}\frac{1}{\sin^2(k_n/2)}\Big) + O\left(z^3\right). \tag{3.75}$$

Using Euler-Maclaurin formula one can show that

$$\begin{aligned}
\sum_{n=0}^{L/2-1} \cot^2\Big((2n+1)\frac{\pi}{2L}\Big) &= \frac{L^2}{2} - \frac{L}{2} + O(L^0) \\
\sum_{n=0}^{L/2-1} \frac{\cos^2\left((2n+1)\frac{\pi}{2L}\right)}{\sin^4\left((2n+1)\frac{\pi}{2L}\right)} &= \frac{L^4}{48} - \frac{L^2}{12} + O(L^0)
\end{aligned} \tag{3.76}$$

and we get

$$G_J = L^2\left(\frac{1}{8J^2} - \frac{z^2}{384J^4}\right) - \frac{L}{8J^2} + O(L^0). \tag{3.77}$$

This shows explicitely that at $h = J$ the Fisher information has a maximum and there it behaves as

$$G_J(L, T = 0, h^* = J) \simeq \frac{L^2}{8J^2} + O(L). \tag{3.78}$$

We observe that superextensive behavior of the QFI in the quasi-critical region around the QPT, $G_J \sim L^2$, implies that the estimation accuracy scales like L^{-2} at the critical points, while it goes like L^{-1} at regular points. Notice that, in assessing the estimability of a parameter λ, the quantity to be considered is the quantum signal-to-noise ratio (QSNR) given by $Q(\lambda) \equiv \lambda^2 G(\lambda)$ which takes into account of the scaling of the variance and the mean value of a parameter rather than its absolute value. We say that a parameter λ is effectively estimable when the corresponding $Q(\lambda)$ is large and that to a diverging QFI corresponds the optimal estimability. In both cases of few and many spins, at the critical point the QFI goes like $1/J^2$, this means that it is independent on $Q(J)$ and one can estimate small values of parameters without loss of precision.

3.3.3 Quantum estimation at finite temperature

We now consider the problem of estimating the coupling constant J of the Ising Hamiltonian at finite temperature. We first discuss in some detail the small size case where $L = 2, 3, 4$ and then we treat the case where $L \gg 1$.

Small L

As a warm-up let us first focus on the simplest, $L = 2$ case. A first step in the computation of the symmetric logarithmic derivative (SLD) from Eq. (1.54) for two qubit is to find the SLD in the single qubit case. Consider a system with "Hamiltonian" $H = \frac{1}{2}(\mathbb{I} + \mathbf{a} \cdot \boldsymbol{\sigma})$ where $\boldsymbol{\sigma} = (\sigma^x, \sigma^y, \sigma^z)^T$ is the vector of the Pauli matrices and $\mathbf{a} = (a_1, a_2, a_3)^T$, in the state $\varrho = e^{-H} Z^{-1} = \frac{1}{2}(\mathbb{I} - \hat{\mathbf{a}} \cdot \boldsymbol{\sigma} \tanh(a))$ where $Z = \mathrm{Tr} e^{-H} = 2\cosh(a)$, and the three-component vector $\mathbf{a}$ depends on parameter J. The SLD relative to this state turns out to be

$$\begin{aligned} \Lambda = &- \tanh(a) \, (\partial_J \hat{\mathbf{a}} \cdot \boldsymbol{\sigma}) \\ &- \left[1 + \tanh(a) - 2\tanh(a)^2\right] (\partial_J a) \, (\hat{\mathbf{a}} \cdot \boldsymbol{\sigma}) \, . \end{aligned} \tag{3.79}$$

where a is the modulus of $\mathbf{a}$ and $\hat{\mathbf{a}} = \mathbf{a}/a$. Now note that the Hamiltonian (3.65) for $L = 2$ (with PBC), has the following block-diagonal form in the basis $\{|++\rangle, |--\rangle, |+-\rangle, |-+\rangle\}$:

$$H = -2\beta \begin{pmatrix} J\sigma^x + h\sigma^z & 0 \\ 0 & J\sigma^x \end{pmatrix}. \tag{3.80}$$

We can then apply formula (3.79) in each subspace to obtain the full SLD. After some algebra one realizes that the SLD has the following form

$$\Lambda = c_1\sigma^x \otimes \sigma^x + c_2\sigma^y \otimes \sigma^y + c_3\left(\sigma^z \otimes \mathbb{1} + \mathbb{1} \otimes \sigma^z\right), \tag{3.81}$$

where $c_{1,2,3}$ are constants which depend on β, J, and h. When the temperature is sent to zero the above expression becomes

$$\begin{aligned}\Lambda_{T=0} =& \frac{h}{2\left(J^2+h^2\right)^{3/2}}\Big[h\left(\sigma^x \otimes \sigma^x - \sigma^y \otimes \sigma^y\right) \\ &- J\left(\sigma^z \otimes \mathbb{1} + \mathbb{1} \otimes \sigma^z\right)\Big].\end{aligned} \tag{3.82}$$

We see that, already in the simple two-qubit case, the SLD is a complicated operator both at positive and at zero temperature. More involved expressions are obtained $L = 3, 4$ and larger.

We do not report here the analytic expression of the corresponding QFIs G_J for $L = 2, 3, 4$ since they are a bit involved. Rather, in order to assess estimation precision at finite temperature compared to that at $T = 0$, we consider the ratio $\gamma_J = G_J(\beta, J, h)/G_J(\infty, J, h)$, for some fixed values of J and illustrate its behavior in Fig. 3.3. As it is apparent from Fig. 3.3 for small h the ratio is less than 1, i.e. estimation of J is more precise at zero temperature, whereas, for increasing h, a finite temperature may be preferable. In turn, for any value of J and β, there is a field value that makes finite temperature convenient: this is true also for low temperature as proved by the presence of a global maximum for small h, besides the local maximum at $h = J$. For $\beta \to \infty$ the maxima at small h disappear and we recover the zero temperature results. Notice that, in view of Eqs. (3.69), the ratio γ_J is proportional to the QSNR. Besides, since maxima of γ_J vary with β as described above, we conclude that the optimal field h^*, which maximizes $G_J(\beta)$, varies with temperature. For high temperature the maxima are located at a field value close to zero, whereas for decreasing temperature they switch towards values close to the critical one $h^* = J$. This may be explicitly seen for $L = 2$ by expanding the Fisher information at high and low temperatures respectively,

$$G_J(J, h, \beta) \simeq \beta^2[4 - (h^2 + 3J^2)\beta^2] + \mathcal{O}(\beta^6), \tag{3.83}$$

$$\begin{aligned}G_J(J, h, \beta) \simeq& G_J(J, h, \infty)(1 - e^{-\beta\Delta}) + 2e^{-\beta\Delta}\beta^2\left(1 - \frac{h}{\sqrt{h^2+J^2}}\right) \\ &\times\left[2 + e^{-\beta\Delta}\left(1 + \coth\frac{\beta\Delta}{2}\right)\right]\end{aligned} \tag{3.84}$$

with $\Delta = \Delta(J, h) = 2(\sqrt{J^2+h^2} - J)$. Upon looking for extremal points we have that $h^* \simeq 0$ for high temperature and $h^* = J + \mathcal{O}(e^{-\beta\Delta(J,J)})$ for low temperature.

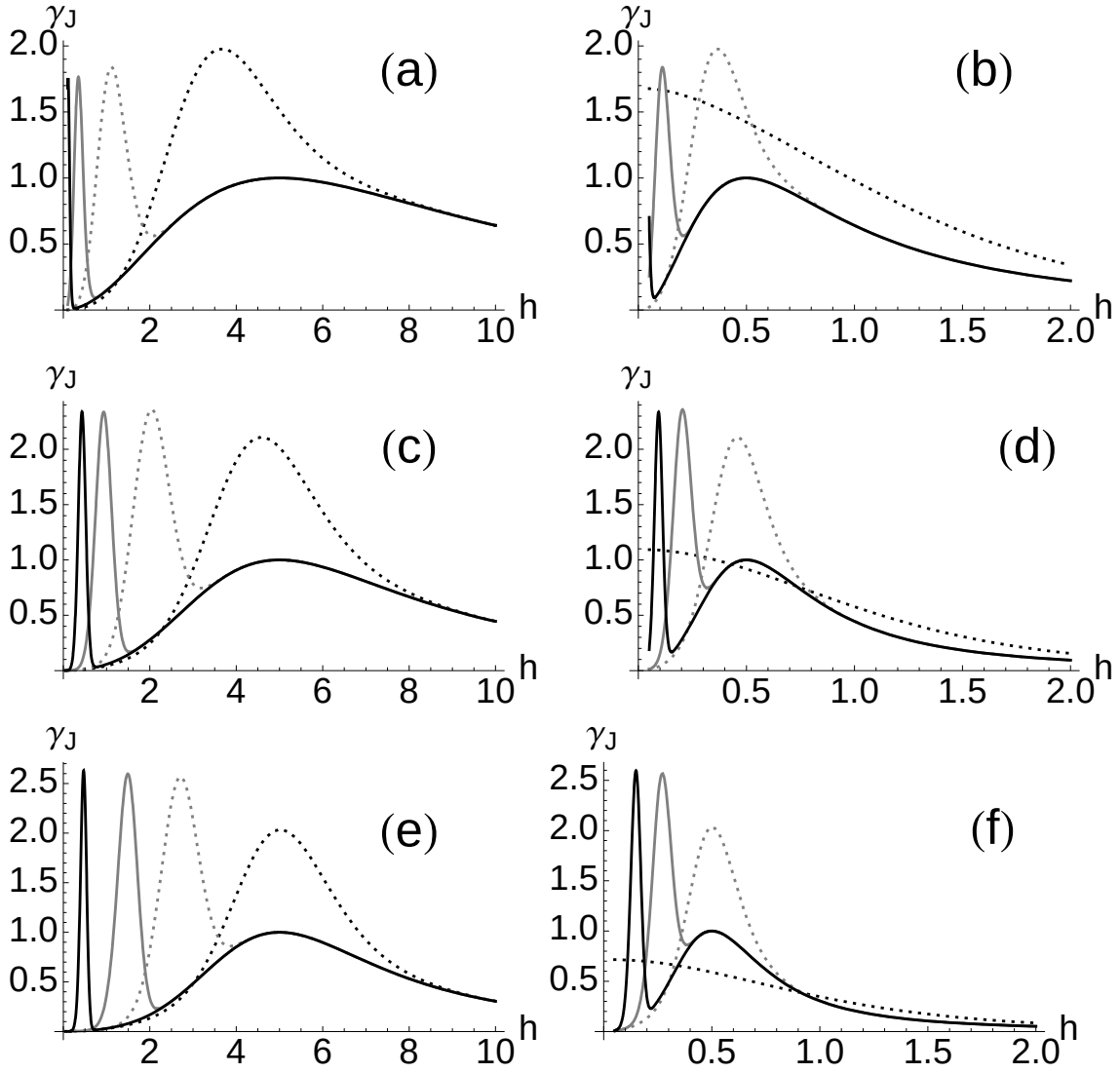

Figure 3.3: The ratio γ_J as a function of the externall field h for $L = 2$ [(a),(b)], $,3$ [(c), (d)], 4 [(e), (f)] and $J = 5$ [(a), (c), (e)], $J = 0.5$ [(b), (d), (f)]. The curves refer to different values of $\beta = 1$ (black dashed), $\beta = 10$ (gray dashed), $\beta = 100$ (solid gray) and $\beta = 1000$ (solid black).

Large L

At positive temperature and L large, the sums in equation (3.68) are replaced by $L\int dk$. The quantity $\tilde{G}_J \equiv G_J/L$ is always convergent, the convergent rate being exponentialy fast in L in the (renormalized classical) region $T \ll \Delta$ whereas is effectively only algebraic when $T \gg \Delta$ (the quantum-critical region). Thus, up to contribution vanishing with L, $\tilde{G}_J = \tilde{G}_J^1 + \tilde{G}_J^2$ is a bounded function of its arguments as long as $T > 0$, given by

$$\tilde{G}_J^1 = \frac{\beta^2}{8\pi}\int_0^\pi \frac{dk}{\cosh^2(\beta\Lambda_k/2)}\frac{(J+h\cos(k))^2}{\Lambda_k^2} \tag{3.85}$$

$$\tilde{G}_J^2 = \frac{1}{2\pi}\int_0^\pi dk\frac{\cosh(\beta\Lambda_k)-1}{\cosh(\beta\Lambda_k)}\frac{h^2\sin(k)^2}{\Lambda_k^4}\,. \tag{3.86}$$

For any $T > 0$ the function $\tilde{G}_J$ has a cusp in $h = J$ where it achievs its maximum value. Changing variable from momentum to energy, the integrals above can be approximatly evaluated in the quantum critical region $\beta|J-h| \ll 1$ (actually we also require low temperature, i.e. $\beta|J+h| \gg 1$). The result is

$$\tilde{G}_J^1 = \frac{9\zeta(3)}{8\pi}\frac{T}{J^2|J+h|} + O\left(T^0\right) \tag{3.87}$$

$$\tilde{G}_J^2 = \frac{\mathcal{C}}{\pi^2}\frac{|J+h|}{TJ^2} - \frac{1}{8J^2} + O(T)\,, \tag{3.88}$$

where $\mathcal{C}$ is Catalan's constant $\mathcal{C} = 0.915$ and the Riemann Zeta-function gives $\zeta(3) = 1.202$. Summarizing, for large sizes and at positive temperature, the maximum of the QFI as a function of h is always located at $h = J$ for all values of J, T. At the maximum, the QFI is approximately given by

$$G_J \simeq \frac{2\mathcal{C}}{\pi^2}\frac{L}{TJ}. \tag{3.89}$$

As a consequence, the QSNR scales as $Q_J \sim JL/T$, in other words, at finite temperature, the estimation of small values of the coupling constant is unavoidably less precise than the estimation of large values. As expected, large L and/or low temperature improve the precision of estimation.

3.3.4 Practical implementations

The SLD represents an optimal measurement, *i.e.* the corresponding Fisher information is equal to the QFI. However, as we have seen (see e.g. Eq. 3.82), generally the SLD does not correspond to an observable whose measurement can be easily implemented in practice. Therefore, in this section, we consider the total magnetization $M_z = \frac{1}{L}\sum_i \sigma_i^z$, as a feasible and natural measurement to be performed on the system in order to estimate the coupling J. We assume that the system is at thermal equilibrium, $\rho = Z^{-1}e^{-\beta H}$, and consider

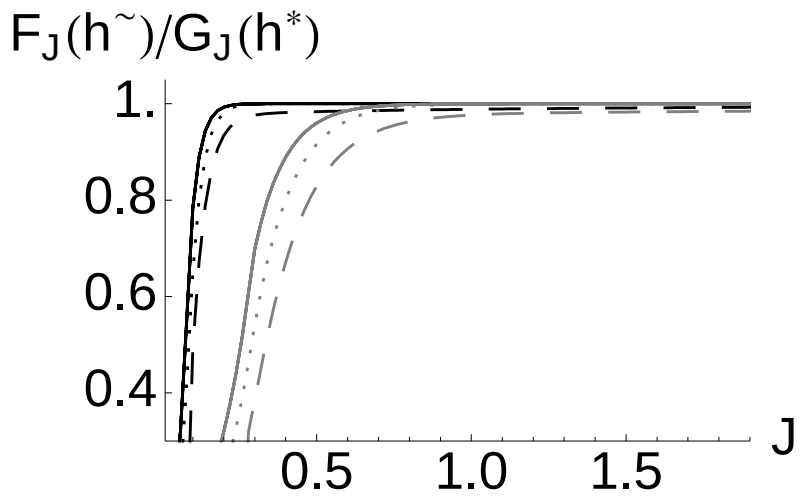

Figure 3.4: The ratio $F_J(\beta, J, \tilde{h})/G_J(\beta, J, h^*)$ as a function of J for $L = 2$ (solid lines), $L = 3$ (dotted lines) and $L = 4$ (dashed lines). The bottom group of lines (gray) is for $\beta = 3$, whereas the top group (black) is for $\beta = 10$.

short chains $L = 2, 3, 4$. We illustrate the procedure in detail for the simplest $L = 2$ case. Upon measuring M_z, the possible outcomes are $m = \{1, 0, -1\}$ with eigenprojectors P_m given by

$$\begin{aligned} P_1 &= |00\rangle\langle 00| \qquad P_{-1} = |11\rangle\langle 11| \\ P_0 &= |10\rangle\langle 10| + |01\rangle\langle 01|\,, \end{aligned} \tag{3.90}$$

and corresponding probabilities $p(m|J) = \mathrm{Tr}(\rho P_m)$,

$$\begin{aligned} p(\pm 1|J) =& \frac{\cosh(2\beta\sqrt{J^2+h^2})}{2\left[\cosh(2\beta J) + \cosh(2\beta\sqrt{J^2+h^2})\right]} \times \\ & \left(1 \pm h(J^2+h^2)^{-1/2}\tanh(2\beta\sqrt{J^2+h^2})\right) \end{aligned} \tag{3.91}$$

$$p(0|J) = \frac{\cosh(2\beta J)}{\cosh(2\beta J) + \cosh(2\beta\sqrt{J^2+h^2})}\,. \tag{3.92}$$

The FI is then obtained by substituting $p(m|J)$ into Eq. (1.37). The resulting expression provides a bound for the variance of any estimator of J based on M measurements of magnetization: $\mathrm{Var}(J) \geq 1/MF_J$. The Braunstein-Caves inequality says that the FI of any measurement F_J is upper bounded by the quantum Fisher information G_J. For the magnetization this is illustrated in Fig. 3.4 where we plot the ratio $F_J(\beta, J, \tilde{h})/G_J(\beta, J, h^*)$ for $L = 2, 3, 4$, $\tilde{h}$ being the field maximizing the FI. Notice that for increasing J the FI of the magnetization saturates to the QFI, i.e. magnetization measurements become optimal. The saturation is faster for lower temperatures (we report the ratio for $\beta = 3$ and $\beta = 10$).

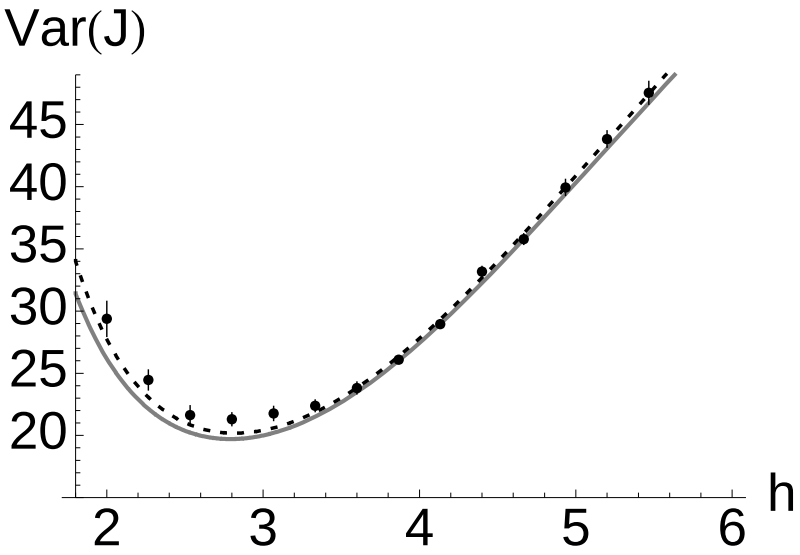

Figure 3.5: The ratio $F_J(\beta, J, \tilde{h})/G_J(\beta, J, h^*)$ as a function of J for $L = 2$ (solid lines), $L = 3$ (dotted lines) and $L = 4$ (dashed lines). The bottom group of lines (gray) is for $\beta = 3$, whereas the top group (black) is for $\beta = 10$.

Notice also that for low temperature the dependence of the ratio on the size L almost disappears. In summary, for any temperature, there is a threshold value for J, above which the measurement of the magnetization in optimal for the estimation of J itself. This threshold value decreases with temperature, and for zero temperature magnetization is optimal for any J. Indeed, after explicit calculation of the Fisher information of Eq. (1.37) for $L = 2, 3, 4$, we found that in the limit $T \to 0$, $F_J(h, T = 0) = G_J(h, T = 0)$, i.e. the FI of the magnetization is equal to the QFI. In other words, estimation based on magnetization measurements may achieve the ultimate bound to precision imposed by quantum mechanics. Besides, at finite temperature, despite the fact that the equality does not hold exactly, F_J is only slightly greater than G_J almost in the whole parameter range (J, T). This may be also seen in the behavior of F_J versus temperature: the ratio $\delta_J = F_J(\beta, J, h)/F_J(\infty, J, h)$ at fixed J may be greater than 1 for some values of the magnetic field, namely, magnetization measurements may be more precise at finite T, as it happens for the optimal measurement with precision bounded by the QFI. Of course, for $T \to 0$, $\delta_J \to 1$.

Overall, we conclude that the magnetization M_z is a good candidate for nearly optimal estimation. Of course we still need an efficient estimator, that is an estimator actually saturating the(classical) Cramer-Rao bound. To this aim we employ a Bayesian analysis, since Bayes estimators are known to be asymptotically efficient [167], i.e. $\mathrm{Var}(J) = 1/MF_J$ for $M \gg 1$. According to the Bayes rule, given a set of outcomes $\{m\}$ from

M independent measurements of the magnetization, the *a-posteriori* distribution of the parameter J is given by

$$p(J|\{m\}) = \frac{1}{N}\prod_m p(m|J)^{n_m} \ , \tag{3.93}$$

where N is a normalization constant and n_m is the number of measurements with outcome m. Bayes estimator is the mean $J_B = \int dJ p(J|\{m\})$of the a posteriori distribution and precision is quantified by the corresponding variance. In the asymptotic limit of many measurements $M \gg 1$, $n_m \to Mp(\{m\}|J^*)$, where J^* is the true value of the parameter to be estimated and the a posteriori distribution is rewritten as $p_a(J|\{m\}) = 1/N \sum_m \exp[Mp(m|J^*) \ln p(m|J)]$.

In order to check the actual meaning of "asymptotic" we have performed a set of Monte Carlo simulated experiments of the whole measurement process. In Fig. 3.5, we report the result of Monte Carlo simulated experiments of magnetization measurements for $J = 3$ and $\beta = 1$. The black dots represent the mean variance of the estimator in Eq. (3.93) averaged on 20 sets each of 500 measurements. The blue line is the plot of the mean variance of the Bayes estimator J_B averaged on 20 sets of 500 measurements. The dotted line is the corresponding variance evaluated using the asymptotic a posteriori distribution, whereas the solid gray line is the Cramer-Rao bound $(MF_J)^{-1}$. The plot shows that the Bayes estimator is indeed asymptotically efficient and that already with a few hundreds of measurements one may achieve the ultimate precision. Overall, putting this result togheter with the fact that $F_J \simeq G_J$ (see Fig. 3.4) we conclude that the measurement of the total magnetization of the system provides a nearly optimal and feasible measurement (at any β) to estimate the coupling of the small size one-dimensional quantum Ising model.

3.4 The discrimination problem for the quantum Ising model

In this section we study the discrimination problem for two ground states or two thermal states of the Ising model in a transverse magnetic field. We consider the system both at zero and finite temperature, and address discrimination of states corresponding to different values of the coupling parameter. In particular, we evaluate the error probability for single-copy discrimination, the Chernoff bound for n-copy discrimination in the asymptotic limit, and the Chernoff metric for the discrimination of infinitesimally close states. We are interested in the scaling properties of the above quantities with the coupling itself, the temperature and the size of the system. Moreover, we look for the optimal value of the field that minimizes the probability of error and maximizes both the Chernoff bound and the corresponding metric. It turns out that criticality is a resource for quantum discrimination of states. Indeed, at zero temperature the critical point signs a minimum in the probability of error and a divergence in the QCB metric. Remarkably, despite the fact that Chernoff metric is associated to quantum discrimination and the Bures metric is related to quantum estimation [39, 3], these different measures show the same critical behavior and carry the same information about the QPT of the system [54].

We first illustrate the notion of quantum Chernoff metric for the Ising model, then, in 3.4.1 we study the distinguishability of states at zero temperature, both for the case of few spins and then in the thermodynamic limit. Finally, in 3.4.2, we consider the effects of temperature and the scaling properties of the metric. The results reviewed in the section are reported in [168].

Upon considering two nearby states ϱ and $\varrho + d\varrho$, the QCB induces the following distance given in Eq. (3.95) over the manifold of quantum states

$$ds^2_{QCB} := 1 - \exp(-\xi_{QCB}) = \frac{1}{2}\sum_{m,n}\frac{|\langle\psi_n|d\varrho|\psi_m\rangle|^2}{(\sqrt{p_m}+\sqrt{p_n})^2} \tag{3.94}$$

where the $|\psi_n\rangle$'s are the eigenvectors of $\varrho = \sum_n p_n|\psi_n\rangle\langle\psi_n|$. In the following we will consider infinitesimally close states obtained upon varying a Hamiltonian parameter λ, and $d\varrho$ will correspond to $d\varrho = \partial\varrho/\partial\lambda\, d\lambda$. The above definition means that the bigger is the QCB distance, the smaller is the asymptotic error probability of discriminating a given state from its close neighbor.

In the following we will consider discrimination for ground and thermal states. In this case the eigenstates of ϱ are those of the Hamiltonian and the distance may be written as

the sum of two contributions

$$ds^2_{QCB} = \underbrace{\frac{1}{8}\sum_n \frac{(dp_n)^2}{p_n}}_{ds^2_c} + \underbrace{\frac{1}{2}\sum_{n\neq m} \frac{|\langle\psi_n|d\psi_m\rangle|^2(p_n-p_m)}{(\sqrt{p_n}+\sqrt{p_m})^2}}_{ds^2_{nc}} \tag{3.95}$$

where ds^2_c refers to the classical part since it only depends on the Boltzmann weights of the eigenstates in the density operator, whereas ds^2_{nc} to the nonclassical one because it explicitly depends on the dependence of the eigenstates from the parameter of interest. If we consider the Ising model of (3.65) and address discrimination of states labeled by different values of the coupling J, the QCB distance can be expressed by the metric g_J, $ds^2_{QCB} = g_J dJ^2$. We have [54]

$$g_J = \underbrace{\frac{\beta^2}{32}\sum_k \frac{(\partial_J\Lambda_k)^2}{\cosh^2(\beta\Lambda_k/2)}}_{g^c_J} + \underbrace{\frac{1}{4}\sum_k \tanh^2(\beta\Lambda_k/2)\,(\partial_J\theta_k)^2}_{g^{nc}_J} \tag{3.96}$$

Recent results about the Chernoff bound metric ds^2_{QCB} [54, 169] have shown that it may be used to investigate the phase diagram the Ising model, i.e. to identify, in terms of different scaling with temperature, quasiclassical and quantum-critical regions. These results extend recent ones obtained using the Bures metric ds^2_B (or the fidelity) [145, 162, 170] i.e

$$ds^2_B = \frac{1}{2}\sum_{nm} \frac{|\langle\psi_m|d\varrho|\psi_n\rangle|^2}{p_n+p_m}\,. \tag{3.97}$$

We recall the relation (**??**) $\frac{1}{2}ds^2_B \leq ds^2_{QCB} \leq ds^2_B$ which shows that the Bures and the QCB metric have the same divergent behavior i.e. one metric diverges iff the other does. Then one can exploit the results on the scaling behavior of the Bures metric derived in [145] to discriminate quantum states. Moreover, in the following we will see that when the system is in its ground state, $ds^2_{QCB} = ds^2_B$ whereas at increasing temperature T, $ds^2_{QCB} \to \frac{1}{2}ds^2_B$.

3.4.1 Quantum discrimination of ground states

At zero temperature the system is in the ground state and the problem is that of discriminating two pure states corresponding to two different values J_1 and J_2 of the coupling J. The probability of error is given in terms of the overlap $|\langle\psi_1|\psi_2\rangle|^2$, whereas the minimum of $\mathrm{Tr}\left[\varrho_1^s\,\varrho_2^{1-s}\right]$ reduces to the overlap itself since for pure states $\varrho^s = \varrho\ \forall s$. Thus the probability of error for the discrimination with n copies scales as $P_{e,n} \sim |\langle\psi_1|\psi_2\rangle|^{2n}$ and

the quantum Chernoff information may be expressed as $\xi_{QCB} = -\log[4\,P_e(1-P_e)]$. In this section we address the discrimination problem at zero temperature by evaluating the probability of error and the QCB metric, pointing out scaling properties, and minimizing (maximizing) them as a function of the external field. We first consider systems made of few spins and then address the thermodynamic limit.

Short Ising chains, $L = 2, 3, 4$

The probability of making a misidentification P_e may be minimized by varying the value of the external field. For the case $L = 2, 3$, and 4, P_e is obtained by explicit diagonalization of the Ising Hamiltonian. Minima of P_e correspond to the field value $\tilde{h} = \sqrt{J_1 J_2}$, *i.e* the geometrical mean of the two (pseudo) critical values, and follows the scaling behavior $P_{e,min}(J_1, J_2, \sqrt{J_1 J_2}) = P_{e,min}(1, J_2/J_1, \sqrt{J_2/J_1})$. More generally the probability of error is such that

$$P_e(kJ_1, kJ_2, kh) = P_e(J_1, J_2, h) \qquad \forall k > 0\,. \tag{3.98}$$

Upon exploiting this scaling and fixing $J_1 = 1$ we can study P_e at $\tilde{h}$ as a function of $J_2 \equiv J$. The behavior of the QCB $Q(J) \equiv P_{e,min}(1, J, \sqrt{J})$ is illustrated in the left panel of Fig. 3.6. The function has a cusp in $J = 1$, whereas the tails of the curve for $J \to 0$ and $J \to \infty$ go to zero faster with increasing size. This means that as the number of spins increases, the overlap between two different ground states approaches to zero. According to the scaling in Eq. (3.98) the relevant parameter is the ratio between the two couplings and not the absolute difference. In turn, this means that $Q(J)$ is symmetric around $J = 1$ in a log-linear plot. Expanding $Q(J)$ around $J = 1$ and $J = 0$ we obtain the following behavior

$$\begin{aligned} Q(J) &\overset{J\simeq 1}{=} \frac{1}{2} - \alpha_L\,|J-1| + O\,|J-1|^2 \\ Q(J) &\overset{J\to 0}{=} \frac{1}{2} - A_L + \beta_L\sqrt{J} + \gamma_L J + O(J^{3/2}) \end{aligned} \tag{3.99}$$

where $\alpha_L \in (0, 1/2)$ is an increasing function of L. According to the scaling (3.98) the behavior of $Q(J)$ for large J is obtained by the replacement $J \to 1/J$ in the second line of Eq. (3.99). The parameters A_L, α_L, β_L, and γ_L are reported in Table 3.4.1 for $L = 2, 3, 4$. The corresponding Chernoff information $\xi_J = -\log[4\,Q(J)(1-Q(J))]$ does not carry additional information about the discrimination problem, but exhibits a simpler behavior

$$\begin{aligned} \xi_J &\overset{J\simeq 1}{=} \frac{\delta_L}{16}\,|J-1|^2 + O\,|J-1|^3 \\ \xi_J &\overset{J\to 0}{=} L\log 2 - L\sqrt{J} + \frac{L}{2}J + O(J^{3/2})\,, \end{aligned} \tag{3.100}$$

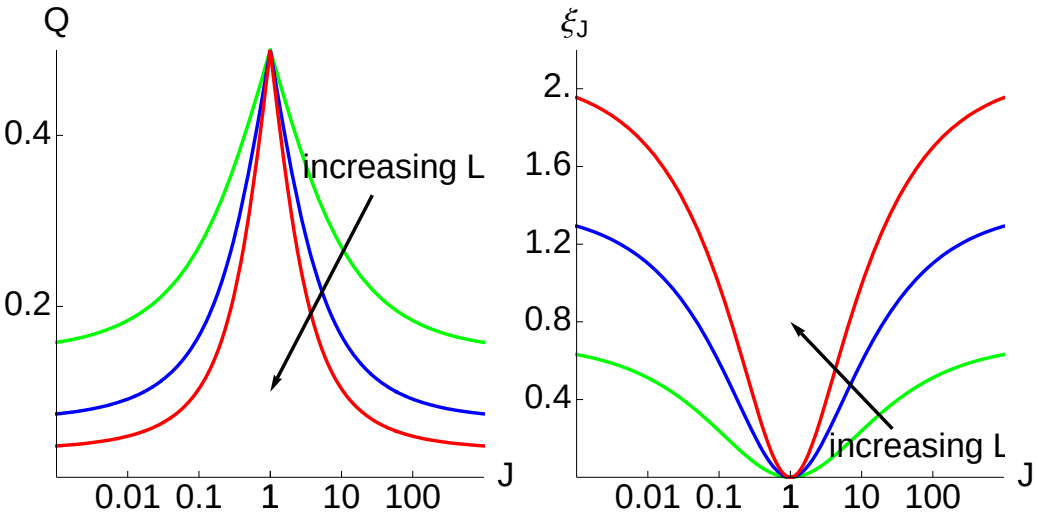

Figure 3.6: (Left):Log-linear plot of the zero temperature rescaled minimum probability of error $Q(J) \equiv P_{e,min}(1, J, \sqrt{J})$ as a function of J for $L = 2, 3, 4$ (green, blue and red lines, respectively). The function has a cusp in $J = 1$ and the two tails go to zero faster with increasing size. According to the scaling in Eq. (3.98) the relevant parameter is the ratio between the two couplings and not the absolute difference. In the log-linear plot, this means that $Q(J)$ is symmetric around $J = 1$. (Right): The Chernoff information in the same conditions.

where $\delta_L = L!/4L$ for $L = 3, 4$ and half of this value for $L = 2$. The behavior of ξ_J for large J is again obtained by replacing $J \to 1/J$ in the second line of Eq. (3.100). In the right panel of Fig. 3.6 we show ξ_J as a function of J for $L = 2, 3, 4$.

Table 3.1: Parameters A_L, α_L, β_L, and γ_L appearing in Eq. (3.99), *i.e* the expansion of the rescaled probability of error $Q(J)$ around $J = 0$ and $J = 1$.

L	α	β	γ	A
2	$\alpha_2 = 1/8 = 0.125$	$\beta_2 = 1/2\sqrt{2} \simeq 0.354$	$\gamma_2 = 1/4\sqrt{2} \simeq 0.177$	$A_2 = 1/2\sqrt{2} \simeq 0.354$
3	$\alpha_3 = \sqrt{3}/8 \simeq 0.217$	$\beta_3 = \sqrt{3}/8 \simeq 0.217$	$\gamma_3 = 5\sqrt{3}/32 \simeq 0.271$	$A_3 = \sqrt{3}/4 \simeq 0.433$
4	$\alpha_4 \simeq 0.306$	$\beta_4 = 1/2\sqrt{14} \simeq 0.134$	$\gamma_4 = 23/28\sqrt{14} \simeq 0.220$	$A_4 = \sqrt{14}/8 \simeq 0.468$

As mentioned previously, when we compare ground states of Hamiltonians with infinitesimally close values of the coupling J, the proper measure to be considered is the QCB metric, with the point of maximal discriminability of two states corresponding maxima of the QCB metric tensor. At zero temperature $ds^2_{QCB} = ds^2_B$ and thus [3] one recovers

the result of (3.69):

$$\begin{aligned} g_J &= \frac{h^2}{4(h^2+J^2)^2}, \quad L=2 \\ g_J &= \frac{3h^2}{16(h^2-hJ+J^2)^2}, \quad L=3 \\ g_J &= \frac{h^2(h^4+4h^2J^2+J^4)}{4(h^4+J^4)^2}, \quad L=4 \end{aligned}$$

Notice the simple scaling $g_J(kJ,kh) = g_J(J,h)$, which is valid $\forall L$. Maxima of g_J are thus obtained for $h^* = J$ for $L = 2,3,4$, and actually this is true for any L (see also the next Section). The pseudo-critical point h^* which maximizes the QCB metric, turns out to be independent of L and equal to the true critical point, $h_c = J$, $\forall L$. At its maximum g_J goes like $1/J^2$ which means that it is easier to discriminate two infinitesimally close ground states for small J rather than for large ones.

Large L

For large L, the overlap (fidelity $\mathcal{F}$) between two different ground states $|\psi_k\rangle \equiv |\psi_0(J_k)\rangle$, $k = 1,2$ is given by

$$\mathcal{F} = \langle\psi_1|\psi_2\rangle = \prod_k \cos\frac{\theta_{1k}-\theta_{2k}}{2} \tag{3.101}$$

where $k = (2n+1)\pi/L$ and n runs from 1 to $L/2$. Obviously, $\mathcal{F} = 1$ if $J_1 = J_2$. Otherwise, one has $\cos[(\theta_{1k}-\theta_{2k})/2] < 1$ and the fidelity $\mathcal{F}$ quickly decays as the ratio of the couplings is different from one. Solving $\partial_h \cos[(\theta_{1k}-\theta_{2k})/2] = 0$ one finds that the overlap has a cusp in $\tilde{h} = \pm\sqrt{J_1 J_2}$, where it achieves the minimum value, corresponding to the minimum of the probability of error P_e. In the thermodynamic limit $L \to \infty$, the overlap between two different ground states goes to zero no matter how small is the difference in the parameters J_1 and J_2. In other words, the different ground states become mutually orthogonal, a behavior known as orthogonality catastrophe [153]. In the critical region, corresponding to the vanishing of one of the single particle energies $\epsilon_k^2 + \Delta_k^2 = 0$ with $k = 2\pi/L$, this behavior is enhanced, occurs for smaller L, and corresponds to a drop in the fidelity even for small values of $|J_2 - J_1|$.

For what concerns the QCB metric, upon taking the limit $T \to 0$ in Eq. (3.96), we have that the classical part ds_c^2, which depends only on thermal fluctuations, vanishes due to the factor of $(\cosh(\beta\Lambda_k/2))^{-2}$. Therefore, at zero temperature, only the nonclassical part of Eq. (3.96) survives and one obtains $g_J = \frac{1}{4}\sum_k (\partial_J\theta_k)^2$, where

$$\partial_J\theta_k = \frac{1}{1+(\Delta_k/\epsilon_k)^2}(\partial_J\frac{\Delta_k}{\epsilon_k}) = \frac{-h\sin k}{\Lambda_k^2}\,.$$

Since we are in the ground state, the allowed quasi-momenta are $k = \frac{(2n+1)\pi}{L}$ with $n = 0, \ldots, L/2-1$. Explicitly we have

$$g_J = \frac{1}{4}\sum_k \frac{h^2 \sin(k)^2}{\Lambda_k^4}. \tag{3.102}$$

Then the scaling of g_J is given by

$$g_J = \frac{L^2}{4}\left(\frac{1}{8J^2} - \frac{z^2}{384J^4}\right) - \frac{L}{8J^2} + O(L^0)\,,$$

as we have already seen in (3.77). From Eq. (3.78) one concludes that the $1/J^2$ scaling of the metric may be compensated by using long chains, which thus appears as the natural setting to address the discrimination problem for large J.

3.4.2 Quantum discrimination of thermal states

We address the problem of discriminating two states at finite temperature, *i.e.* we consider two thermal states of the form $\varrho_J = Z^{-1}e^{-\beta H(J)}$, $Z = \mathrm{Tr}[e^{-\beta H(J)}]$, and analyze the behavior of the error probability, the Chernoff information and the Chernoff metric as a function of the temperature and the external field. We discuss short chains $L = 2, 3, 4$ and then the case of large L.

Short Ising chains $L = 2, 3, 4$

For short chains we have evaluated the probability of error by explicit diagonalization of $\varrho_2 - \varrho_1$, with $\varrho_k \equiv \varrho_{J_k}$. The probability of error follows the scaling

$$P_e(kJ_1, kJ_2, kh, \beta/k) = P_e(J_1, J_2, h, \beta)\,, \tag{3.103}$$

which may be exploited to analyze its behavior upon fixing $J_1 = 1$. The main difference with the zero temperature case is that the error probability does depend on the absolute difference between the two couplings, and not only on the ratio between them. The optimal field $\tilde{h}$, minimizing $Q_\beta(J) = P_e(1, J, \tilde{h}, \beta)$ is zero for small J, then we have a transient behavior and finally, for large J, $\tilde{h} = \sqrt{J}$. The range of J for which $\tilde{h} \simeq 0$ increases with temperature (small β). In the left panel of Fig. 3.7 we compare $Q_\beta(J)$ for $L = 2$ and different values of β to the analogous zero temperature quantity $Q_\infty(J)$. As it is apparent from the plot the main effect of temperature is the loss of symmetry around $J = 1$. Analogous behavior may be observed for larger L. Notice that discrimination at finite temperature is not necessarily degraded.

Upon diagonalization of the Hamiltonian we have also evaluated the quantum Chernoff bound by numerical minimization of $\min_s \mathrm{Tr}\left[\varrho_1^s\, \varrho_2^{1-s}\right]$ and obtained for ξ_{QCB} the same

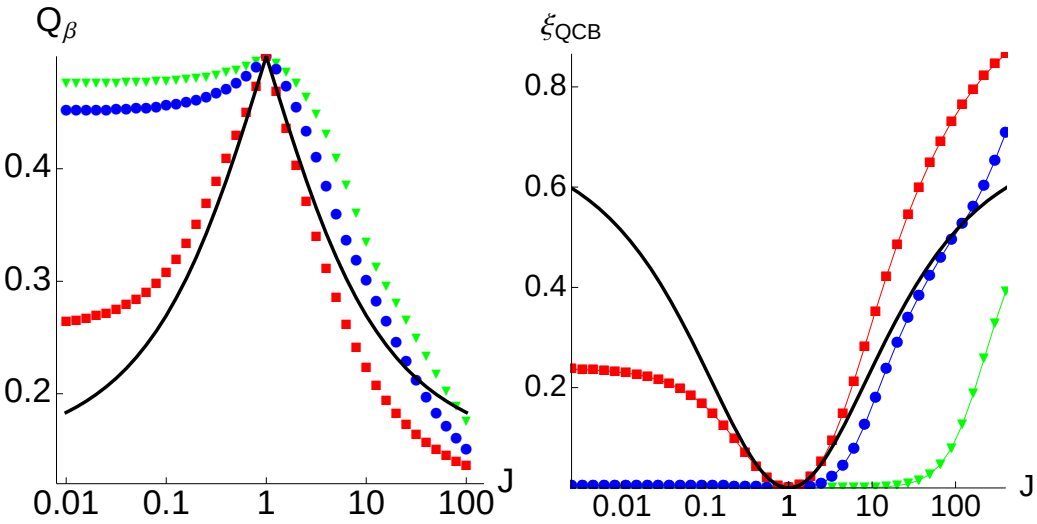

Figure 3.7: (Left): Log-linear plot of the rescaled minimum probability of error $Q_\beta(J) \equiv P_{e,min}(1, J, \sqrt{J}, \beta)$ for $L = 2$ as a function of J. Green triangles correspond to $\beta = 0.05$, blue circles to $\beta = 0.1$ and red squares to $\beta = 1$. The black solid curve is the probability of error in the zero temperature case. The main effect of temperature is the loss of symmetry around $J = 1$. (Right): Log-Linear plot of the quantum Chernoff information ξ_{QCB} for $L = 2$. Green triangles correspond to $\beta = 0.05$, blue circles to $\beta = 0.1$ and red squares to $\beta = 1$. We also report the zero temperature QCB for comparison (solid black curve).

scaling properties (3.103) observed for the error probability. In the right panel of Fig. 3.7 we compare the quantum Chernoff information for $L = 2$ and different values of β to the analogous zero temperature quantity. Again the main effect of temperature is the loss of symmetry around $J = 1$. Analogous behavior may be observed for larger L. For vanishing J the Chernoff information $\xi_{QCB}(1, J \to 0, \sqrt{J}, \beta) \equiv \xi_0$ saturates to a limiting value scaling with β as

$$\xi_0 \simeq \beta^2/2 \qquad \beta \to 0 \tag{3.104}$$

$$\xi_0 \simeq \frac{\sqrt{2}}{\pi} \arctan(\beta/2) \qquad \beta \to \infty\,. \tag{3.105}$$

On the other hand, for diverging J $\xi_{QCB}(1, J \to \infty, \sqrt{J}, \beta) \equiv \xi_\infty$ shows the non monotone behaviour illustrated in the right panel Fig. 3.8. In the left panel we report ξ_0 as a function of β together with the approximating functions of Eqs. (3.104) and (3.105). Overall, we notice that both for the single-copy and many-copy case, increasing the temperature may also results in an improvement of discrimination, at least in the region of large couplings and intermediate temperatures.

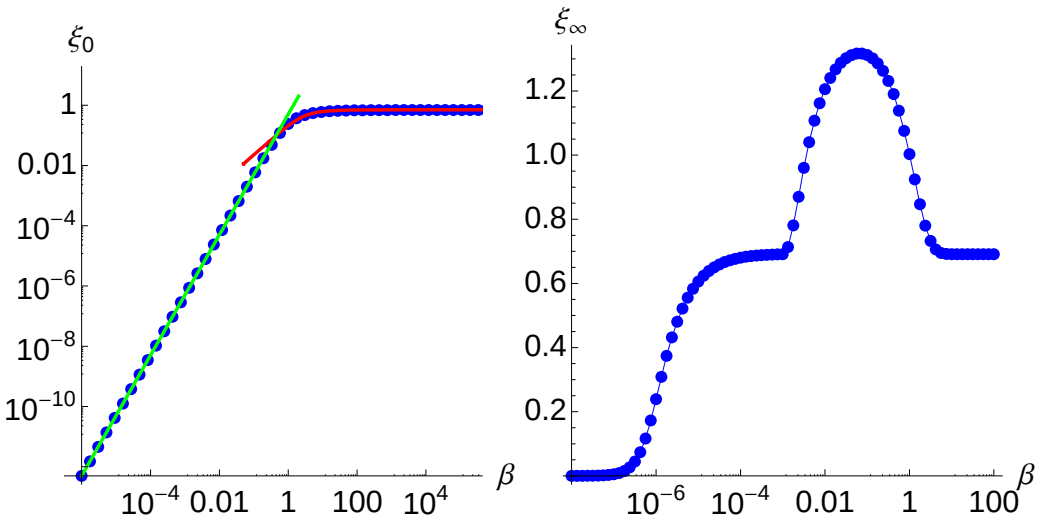

Figure 3.8: (Left): Log-log plot of the Chernoff information for vanishing J, $\xi_0 \equiv \xi_{QCB}(1, J \to 0, \sqrt{J}, \beta)$, as a function of inverse temperature β (blue points) together with the approximating functions of Eq. (3.104) (green line) and (3.105) (red line). (Right): Log-linear plot of the Chernoff information for diverging J, $\xi_\infty \equiv \xi_{QCB}(1, J \to \infty, \sqrt{J}, \beta)$, as a function of inverse temperature β

Finally, we have evaluated the QCB metric and found that it follows the scaling

$$g_J(J, h, \beta) = \beta^2 \Phi_L(\beta J, \beta h) \tag{3.106}$$

where the form of the function Φ_L depends on the size only. The same scaling is also true for the Bures metric with different functions Φ_L. Indeed, this behavior follows directly from the common structure of the two metrics and by the fact that g_J is obtained from the square of the derivative with respect to J. The scaling is actually true for any size L. The optimal value h^* of the external field, which maximizes the QCB metric at fixed J and β may be found numerically. Upon exploiting the scaling properties we consider $\beta = 1$ and found that h^* is zero for small J, then we have a transient behavior and finally, for large J, $h^* = J$. According to the scaling above, the range of J for which $h^* \simeq 0$ increases with temperature (small β) and viceversa. In turn, for $\beta \to \infty$ we recover the results of the previous Section, *i.e.* the critical point is always the optimal one for discrimination. This behavior is illustrated in the left panel Fig. 3.9, where we report the optimal field h^* as a function of J for $\beta = 1$. The inset shows the small J region. As we have noticed in the previous section the two metrics are equal in the zero temperature limit. For finite temperature this is no longer true and a question arises on whether the whole range of values allowed by the inequality $\frac{ds_B^2}{2} \leq ds_{QCB}^2 \leq ds_B^2$ is actually spanned by the QCB metric. This is indeed the case, as it may be seen by analyzing the behavior of the ratio

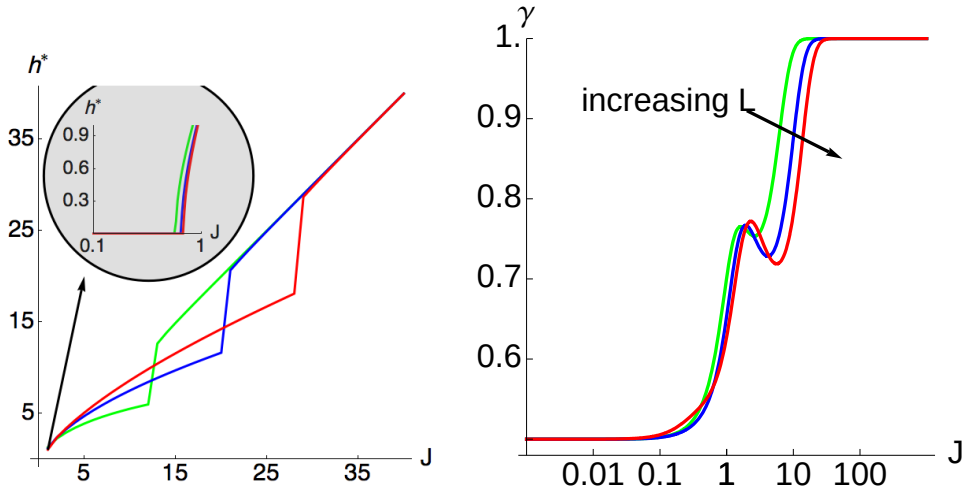

Figure 3.9: (Left): linear plot of the optimal field h^* maximizing the QCB metric as a function of J for $\beta = 1$. The inset shows the region of small J. (Right): log-linear plot of the ratio γ between the (maximized) QCB and Bures metrics as a function of J for $L = 2, 3, 4$ (green, blue and red lines respectively) and $\beta = 1$.

$\gamma = ds^2_{QCB}/d^2_B s$ at the (pseudo) critical point h^* (we take the maximum of both the metrics, which generally occurs at different values of the field). In the right panel of Fig. 3.9 we report γ as a function of J for $\beta = 1$ and $L = 2, 3, 4$. As it is apparent from the plot, for small J we have $ds^2_{QCB} \simeq \frac{1}{2} ds^2_B$, whereas for large J the two quantities become equal $ds^2_{QCB} \simeq ds^2_B$. The ratio is not monotone and the dependence on the size is weak. Upon exploiting the scaling in Eq. (3.106) we may easily see that the range of J for which the two metrics are almost equal increases with β. For vanishing temperature ($\beta \to \infty$) $ds^2_{QCB} \simeq ds^2_B$ everywhere and we recover the results of the previous Section. Conversely, for high temperature we have $ds^2_{QCB} \simeq \frac{1}{2} ds^2_B$ also for very large J. Also the transient region is shrinking for increasing temperature.

Large L

In the limit of large size L the behavior of the Chernoff metric follows the same scaling of Eq. (3.106) found for short chains. The optimal value of the field which maximizes the QCB metric is $h^* = J$ for any finite temperature, where the metric element has a cusp. We have studied the QCB metric in the quantum-critical region $\beta|J - h| \ll 1$ and for low temperature $T \to 0$. The classical elements of the metric vanish due to the factor $1/\cosh^2(\beta\Lambda_k/2)$ and we are left to analyze the nonclassical part g^{nc}_J as a function of T. Bounding the metric by functions that have the same scaling behavior in β [54], will ensure that the metric itself scales with the same exponent. The dispersion relation

is linear around $k = 0$ and we approximate $\Lambda_k \sim Jk$ at the critical point $J = h$. Upon defining

$$f(\beta, k) = \begin{cases} \beta^2 k^2/4 & 0 \leq k \leq 2/\beta \\ 1 & 2/\beta \leq k \leq \pi \end{cases},$$

we have, for all β and k, $\frac{1}{2} f(\beta, k) < \tanh^2(\beta J k/2) < f(\beta, k)$. For large L, the sum on the classical part of the QCB metric may be replaced by the integral $L \int dk$, thus leading to

$$g_J^{nc} \simeq \frac{L}{2\pi} \int_0^{2/\beta} dk \tanh^2(\beta J k/2) \frac{1}{J^2 k^2} + \frac{L}{2\pi} \int_{2/\beta}^{\pi} dk \tanh^2(\beta \Lambda_k/2) \frac{J^2 \sin^2(k)}{\Lambda_k^4}. \quad (3.107)$$

This is a good approximation in the limit $\beta \to \infty$ because the upper integration limit $2/\beta$ becomes arbitrarily close to 0. The first integral is bounded by $\frac{L}{2\pi} \int_0^{2/\beta} dk \frac{f(\beta,k)}{2} \frac{1}{J^2 k^2} \leq \frac{L}{2\pi} \int_0^{2/\beta} dk \tanh^2(\beta J k/2) \frac{1}{J^2 k^2} \leq \frac{L}{2\pi} \int_0^{2/\beta} dk f(\beta, k) \frac{1}{J^2 k^2}$. The bounding integrals scale as $L\beta$ and the first integral must scale in the same way for $\beta \to \infty$. The second term is upper bounded by $\frac{L}{2\pi} \int_{2/\beta}^{\pi} dk \tanh^2(\beta \Lambda_k/2) \frac{J^2 \sin^2(k)}{\Lambda_k^4} \leq \frac{L}{2\pi} \int_{2/\beta}^{\pi} dk \frac{1}{J^2 k^2} \sim L\beta$. Therefore, since the bounding integral scales as βL, g_J^{nc} must scale as βL to the highest order. Observe that in the quantum-critical region $g_J \sim L$ is extensive, whereas at the critical point it has a superextensive behavior $g_J \sim L^2$. The nonclassical element scales algebraically with temperature and in the zero temperature limit it diverges, matching the ground state behavior that we described in the previous section. These results remark that criticality provide a resource for quantum state discrimination, and that the discrimination of quantum states is indeed improved upon approaching the QCP.

3.5 Conclusions and Outlooks

In this chapter we have studied the quantum Ising model in a transverse magnetic field as a paradigmatic example of a system which undergoes a quantum phase transition.
We first exploited the equivalence between the quantum Fisher metric and the (ground or thermal) Bures metric and all the results recently obtained for the latter to estimate the coupling constant of the Hamiltonian. Specifically at zero temperature, the Bures metric scales with the system size L at regular points whereas it can increases as L^2 at or in the vicinity of quantum critical point. A similar enhancement takes place when temperature is considered. In turn it is possible to exploit this enhancement to dramatically improve the precision in a quantum estimation problem. Let us imagine that an experimenter would like to infer the value of a coupling constant of a physical system over which he has little or no control. Reasonably the experimenter has good control over the external fields he can apply to the system. The idea is then to tune the external field to a value close to the quantum critical point. At this value of the couplings, an improvement of order of L can be achieved in the precision of the estimation of the unknown coupling. To test these ideas in practice, we have worked out in detail a specific example, the 1D quantum Ising model. This model provides us with all the ingredients we need, a coupling constant J, an external field h, and a quantum critical point at $h = J$. The main accomplishments of our analysis are: i) At zero temperature we evaluated the precision in the estimation of the coupling, exactly for short chains of $L = 2, 3, 4$ sites and asymptotically for large L. We found that the optimal estimation is possible at values of the field exactly equal to the critical point, independently of L. For large L we indeed observe a $1/L$ enhancement of precision, and a quantum signal-to-noise ratio independent of the coupling. ii) At positive temperature the optimal value of the field is again given by the critical value when the system size is large or the temperature is low. In the other working regimes the optimal field maximizing the quantum Fisher information, defines a set of pseudo-critical points. In this case the optimal precision scales as TJ/L. iii) We obtained the optimal observable for estimation in terms of the symmetric logarithmic derivative and showed that already in the case $L = 2$ it does not correspond to an easily implementable measurement. iv) We have shown that measurements of the total magnetization allow to achieve ultimate precision. Using Monte Carlo simulated experiments and Bayesian analysis we proved that this is possible already after a limited number of measurements of the order of few hundreds.

Overall, we found that criticality is a resource for precise chracterization of interacting quantum systems (e.g. a quantum register), and may represent a relevant tool for the

development of integrated quantum networks.

We then addressed the problem of discriminating between two ground states or two thermal states of the quantum Ising model and found that at zero temperature both the error probability for single-copy discrimination, and the Chernoff information for n-copy discrimination in the asymptotic limit, are optimized by choosing the external field as the geometric mean of the two (pseudo) critical points. In this regime, the relevant parameter governing both quantities is the ratio between the two values of the coupling constant. On the other hand, the Chernoff metric is equal to the Bures metric and is maximized at the (pseudo) critical point. For finite temperature we have analyzed in some details the scaling properties of all the above quantities and have derived the optimal external field. We found that the effect of finite temperature is twofold. On the one hand, critical values of the field are optimal only for large values of the coupling constants. On the other hand, the ratio between the couplings is no longer the only relevant parameter for both the error probability and the Chernoff information, which also depends on the absolute difference. The ratio between the Chernoff metric and the Bures metric decreases continuously, but not monotonically, for increasing temperature and approaches 1/2 in the limit of high-temperature.

In conclusion, upon considering the one-dimensional Ising model as a paradigmatic example we have quantitatively shown how and to which extent criticality may represent a resource for state discrimination in many-body systems.

References

[1] Michael A. Nielsen and Isaac L. Chuang. *Quantum Computation and Quantum Information*. Cambridge University Press, 2000.

[2] Marco G. Genoni, Paolo Giorda, and Matteo G. A. Paris. Optimal estimation of entanglement. *Phys. Rev. A*, 78(3):032303, Sep 2008.

[3] Carmen Invernizzi, Michael Korbman, Lorenzo Campos Venuti, and Matteo G. A. Paris. Optimal quantum estimation in spin systems at criticality. *Phys. Rev. A*, 78(4):042106, Oct 2008.

[4] Alex Monras and Matteo G. A. Paris. Optimal quantum estimation of loss in bosonic channels. *Phys. Rev. Lett.*, 98(16):160401, Apr 2007.

[5] Vittorio Giovannetti, Seth Lloyd, and Lorenzo Maccone. Quantum metrology. *Phys. Rev. Lett.*, 96(1):010401, Jan 2006.

[6] Denes Petz. *Quantum Information Theory and Quantum Statistics*. Springer: Berlin, 2008.

[7] John Preskill. *Lecture Notes for Physics 229: Quantum Information and Computation*. www.theory.caltech.edu/people/preskill/ph229.

[8] Asher Peres. *Quantum Theory: Concepts and Methods*. Kluwer Academic Publishers, 2002.

[9] Naimark M. A. *Izv. Akad. Nauk SSSR Ser. Mat.*, 5:227, 1940.

[10] K. Kraus. General state changes in quantum theory. *Ann. Physics*, 64:311–335, 1971.

[11] K. Kraus. *States, Effects and Operations: Fundamental Notions of Quantum Theory.* Springer-Verlag, 1983.

[12] C.A. Fuchs and J. van de Graaf. Cryptographic distinguishability measures for quantum-mechanical states. *Information Theory, IEEE Transactions on*, 45(4):1216 –1227, May 1999.

[13] W. K. Wootters. Statistical distance and hilbert space. *Phys. Rev. D*, 23(2):357–362, Jan 1981.

[14] C. W. Helstrom. *Quantum Detection and Estimation Theory.* Academic Press: New York, 1976.

[15] C. A. Fuchs. *Distinguishability and Accessible Information in Quantum Theory.* e-print arXiv:quant-ph/9601020., 1995.

[16] A. Uhlmann. Geometric phases and related structures. *Rep. Math. Phys.*, 36:461–481, 1995.

[17] R. Jozsa. Fidelity for mixed quantum states. *J. Mod. Opt.*, 41:2315, Dec 1994.

[18] G. Fubini. *Atti Inst. Veneto*, 6:501, 1903.

[19] E. Study. *Ann. Math.*, 60:321, 1905.

[20] A. Uhlmann. *Rep. Math. Phys.*, 9:273, 1976.

[21] A. Uhlmann. *The metric of Bures and the geometric phase.* Groups and Related Topics, Kluwer Academic Publishers: Dordrecht, 1992.

[22] J. Twamley. Bures and statistical distance for squeezed thermal states. *Journal of Physics A: Mathematical and General*, 29:3723–3731, July 1996.

[23] D. J. C. Bures. *Trans. Am. Math. Soc.*, 135:199, 1976.

[24] H.-J. Sommers and K. Zyczkowski. Bures volume of the set of mixed quantum states. *Journal of Physics A: Mathematical and General*, 36(39):10083–10100, Oct 2003.

[25] Samuel L. Braunstein and Carlton M. Caves. Statistical distance and the geometry of quantum states. *Phys. Rev. Lett.*, 72(22):3439–3443, May 1994.

[26] V. Vedral and M. B. Plenio. Entanglement measures and purification procedures. *Phys. Rev. A*, 57(3):1619–1633, Mar 1998.

[27] W. K. Wootters and W. H. Zurek. A single quantum cannot be cloned. *Nature*, 299(5886):802–803, 1982.

[28] H. P. Robertson. The uncertainty principle. *Phys. Rev.*, 34(1):163–164, Jul 1929.

[29] G. M. D'Ariano and H. P. Yuen. Impossibility of measuring the wave function of a single quantum system. *Phys. Rev. Lett.*, 76(16):2832–2835, Apr 1996.

[30] A. S. Holevo. *Statistical Structure of Quantum Theory*. Springer-Verlag, 2001.

[31] C. W. Helstrom. *Physics Letters A*, 25:1012, 1967.

[32] C. Helstrom and R. Kennedy. Noncommuting observables in quantum detection and estimation theory. *Information Theory, IEEE Transactions on*, 20(1):16 – 24, January 1974.

[33] Alex Monras. Optimal phase measurements with pure gaussian states. *Phys. Rev. A*, 73(3):033821, Mar 2006.

[34] Akio Fujiwara. Quantum channel identification problem. *Phys. Rev. A*, 63(4):042304, Mar 2001.

[35] Alex Monras and Matteo G. A. Paris. Optimal quantum estimation of loss in bosonic channels. *Phys. Rev. Lett.*, 98(16):160401, Apr 2007.

[36] E. S. Polzik, J. Carri, and H. J. Kimble. Spectroscopy with squeezed light. *Phys. Rev. Lett.*, 68(20):3020–3023, May 1992.

[37] P. Grangier, R. E. Slusher, B. Yurke, and A. LaPorta. Squeezed-light–enhanced polarization interferometer. *Phys. Rev. Lett.*, 59(19):2153–2156, Nov 1987.

[38] S. Boixo and A. Monras. Operational interpretation for global multipartite entanglement. *Phys. Rev. Lett.*, 100(10):100503, Mar 2008.

[39] Paolo Zanardi, Matteo G. A. Paris, and Lorenzo Campos Venuti. Quantum criticality as a resource for quantum estimation. *Phys. Rev. A*, 78(4):042105, Oct 2008.

[40] Samuel L. Braunstein, Carlton M. Caves, and G. J. Milburn. Generalized uncertainty relations: Theory, examples, and lorentz invariance. *Annals of Physics*, 247(1):135–173, April 1996.

[41] H. Cramer. *Mathematical Methods of Statistics*. Princeton University Press, 1946.

[42] Matteo G. A. Paris. Quantum estimation for quantum technology. *Int. J. Quant. Inf.*, 7:125, 2009.

[43] M. Hubner. *Physics Letters A*, 163:239, 1992.

[44] P. B. Slater. *J. Phys. A*, 29:L271, 1996.

[45] M. J. W. Hall. *Physics Letters A*, 242:123, 1998.

[46] Dittmann J. *J. Phys. A*, 32:2663, 1999.

[47] H. Chernoff. A measure of asymptotic efficiency of tests of a hypothesis based on the sum of observations. *Ann. Math. Stat.*, 23:493, 1952.

[48] K. M. R. Audenaert, J. Calsamiglia, R. Muñoz Tapia, E. Bagan, Ll. Masanes, A. Acin, and F. Verstraete. Discriminating states: The quantum chernoff bound. *Phys. Rev. Lett.*, 98(16):160501, Apr 2007.

[49] Michael Nussbaum and Arleta Szkola. The chernoff lower bound for symmetric quantum hypothesis testing. *Ann. Stat.*, 37(2):pp. 1040–1057, 2009.

[50] J. Calsamiglia, R. Muñoz Tapia, Ll. Masanes, A. Acin, and E. Bagan. Quantum chernoff bound as a measure of distinguishability between density matrices: Application to qubit and gaussian states. *Phys. Rev. A*, 77(3):032311, Mar 2008.

[51] Stefano Pirandola and Seth Lloyd. Computable bounds for the discrimination of gaussian states. *Phys. Rev. A*, 78(1):012331, Jul 2008.

[52] Măd ălina Boca, Iulia Ghiu, Paulina Marian, and Tudor A. Marian. Quantum chernoff bound as a measure of nonclassicality for one-mode gaussian states. *Phys. Rev. A*, 79(1):014302, Jan 2009.

[53] Iulia Ghiu, Gunnar Björk, Paulina Marian, and Tudor A. Marian. Probing light polarization with the quantum chernoff bound. *Phys. Rev. A*, 82(2):023803, Aug 2010.

[54] Damian F. Abasto, N. Tobias Jacobson, and Paolo Zanardi. Quantum chernoff bound metric for the xy model at finite temperature. *Phys. Rev. A*, 77(2):022327, Feb 2008.

[55] Carmen Invernizzi and Matteo G. A. Paris. The discrimination problem for two ground states or two thermal states of the quantum ising model. *Journal of Modern Optics*, 57:198, 2010.

[56] János Bergou, Ulrike Herzog, and Mark Hillery. 11 discrimination of quantum states. In Matteo Paris and Jaroslav Rehcek, editors, *Quantum State Estimation*, volume 649 of *Lecture Notes in Physics*, pages 417–465. Springer Berlin / Heidelberg, 2004.

[57] I. D. Ivanovic. How to differentiate between non-orthogonal states. *Physics Letters A*, 123(6):257 – 259, 1987.

[58] M. Hellman and J. Raviv. Probability of error, equivocation, and the chernoff bound. *Information Theory, IEEE Transactions on*, 16(4):368 – 372, July 1970.

[59] T. M. Cover and J. A. Thomas. *Elements of Information Theory*. Wiley, New York, 1991.

[60] K. Audenaert, M. Nussbaum, A. Szkola, and F. Verstraete. Asymptotic error rates in quantum hypothesis testing. *Communications in Mathematical Physics*, 279:251–283, 2008. 10.1007/s00220-008-0417-5.

[61] Fumio Hiai and Dénes Petz. The proper formula for relative entropy and its asymptotics in quantum probability. *Communications in Mathematical Physics*, 143:99–114, 1991. 10.1007/BF02100287.

[62] T. Ogawa and H. Nagaoka. Strong converse and steins lemma in the quantum hypothesis testing. *Information Theory, IEEE Transactions on*, 46:2428 –2443, 2000.

[63] T. Ogawa and M. Hayashi. On error exponents in quantum hypothesis testing. *Information Theory, IEEE Transactions on*, 50:1368, 2004.

[64] V. Vedral. The role of relative entropy in quantum information theory. *Rev. Mod. Phys.*, 74(1):197–234, Mar 2002.

[65] Masahito Hayashi. Two quantum analogues of fisher information from a large deviation viewpoint of quantum estimation. *Journal of Physics A: Mathematical and General*, 35(36):7689, 2002.

[66] S. Amari and H. Nagaoka. *Methods of Information Geometry*. Translations of Mathematical Monographs, vol. 191, Oxford University Press, 2000.

[67] M. G. A. Paris A. Ferraro, S. Olivares. *Gaussian States in Quantum Information*. Bibliopolis, Napoli, 2005.

[68] M. B. Plenio J. Eisert. Introduction to the basics of entanglement theory in continuous-variable systems. *Int. J. Quant. Inf.*, 1:479, 2003.

[69] K. E. Cahill and R. J. Glauber. Ordered expansions in boson amplitude operators. *Phys. Rev.*, 177(5):1857–1881, Jan 1969.

[70] K. E. Cahill and R. J. Glauber. Density operators and quasiprobability distributions. *Phys. Rev.*, 177(5):1882–1902, Jan 1969.

[71] J. Williamson. *Am. J. of Math.*, 58:141, 1936.

[72] G. Adam. *J. Mod. Opt.*, 42:1311, 1995.

[73] A. Serafini, F. Illuminati, and S. De Siena. Symplectic invariants, entropic measures and correlations of gaussian states. *J. Phys. B*, 37(2):L21, Jan 2004.

[74] Reinhard F. Werner. Quantum states with einstein-podolsky-rosen correlations admitting a hidden-variable model. *Phys. Rev. A*, 40(8):4277–4281, Oct 1989.

[75] R. Simon. Peres-horodecki separability criterion for continuous variable systems. *Phys. Rev. Lett.*, 84(12):2726–2729, Mar 2000.

[76] G. Vidal and R. F. Werner. Computable measure of entanglement. *Phys. Rev. A*, 65(3):032314, Feb 2002.

[77] Paolo Giorda and Matteo G. A. Paris. Gaussian quantum discord. *Phys. Rev. Lett.*, 105(2):020503, Jul 2010.

[78] J. Eisert and M. M. Wolf. Gaussian quantum channels. *arXiv:quant-ph/0505151*, 2005.

[79] D. F. Walls and G. J. Milburn. *Quantum Optics*. Springer: Berlin, 1994.

[80] A. Vourdas. Superposition of squeezed coherent states with thermal light. *Phys. Rev. A*, 34(4):3466–3469, Oct 1986.

[81] Michael J. W. Hall. Gaussian noise and quantum-optical communication. *Phys. Rev. A*, 50(4):3295–3303, Oct 1994.

[82] Ziad H. Musslimani, Samuel L. Braunstein, A. Mann, and M. Revzen. Destruction of photocount oscillations by thermal noise. *Phys. Rev. A*, 51(6):4967–4973, Jun 1995.

[83] Roy S. Bondurant and Jeffrey H. Shapiro. Squeezed states in phase-sensing interferometers. *Phys. Rev. D*, 30(12):2548–2556, Dec 1984.

[84] Carlton M. Caves. Quantum-mechanical radiation-pressure fluctuations in an interferometer. *Phys. Rev. Lett.*, 45(2):75–79, Jul 1980.

[85] Carlton M. Caves. Quantum-mechanical noise in an interferometer. *Phys. Rev. D*, 23(8):1693–1708, Apr 1981.

[86] Bernard Yurke, Samuel L. McCall, and John R. Klauder. Su(2) and su(1,1) interferometers. *Phys. Rev. A*, 33(6):4033–4054, Jun 1986.

[87] A Bandilla, H Paul, and H H Ritze. Realistic quantum states of light with minimum phase uncertainty. *Quantum Optics: Journal of the European Optical Society Part B*, 3(5):267, 1991.

[88] Z Hradil. Phase measurement in quantum optics. *Quantum Optics: Journal of the European Optical Society Part B*, 4(2):93, 1992.

[89] Matteo G. A. Paris. Small amount of squeezing in high-sensitive realistic interferometry. *Physics Letters A*, 201(2-3):132 – 138, 1995.

[90] Kirk McKenzie, Daniel A. Shaddock, David E. McClelland, Ben C. Buchler, and Ping Koy Lam. Experimental demonstration of a squeezing-enhanced power-recycled michelson interferometer for gravitational wave detection. *Phys. Rev. Lett.*, 88(23):231102, May 2002.

[91] Samuel L. Braunstein and H. J. Kimble. Teleportation of continuous quantum variables. *Phys. Rev. Lett.*, 80(4):869–872, Jan 1998.

[92] A. Furusawa, J. L. Sørensen, S. L. Braunstein, C. A. Fuchs, H. J. Kimble, and E. S. Polzik. Unconditional quantum teleportation. *Science*, 282(5389):706–709, 1998.

[93] Nicolas Treps, Nicolai Grosse, Warwick P. Bowen, Claude Fabre, Hans-A. Bachor, and Ping Koy Lam. A quantum laser pointer. *Science*, 301(5635):940–943, 2003.

[94] Henning Vahlbruch, Simon Chelkowski, Boris Hage, Alexander Franzen, Karsten Danzmann, and Roman Schnabel. Demonstration of a squeezed-light-enhanced power- and signal-recycled michelson interferometer. *Phys. Rev. Lett.*, 95(21):211102, Nov 2005.

[95] Samuel L. Braunstein. Squeezing as an irreducible resource. *Phys. Rev. A*, 71(5):055801, May 2005.

[96] H Vahlbruch, S Chelkowski, K Danzmann, and R Schnabel. Quantum engineering of squeezed states for quantum communication and metrology. *New Journal of Physics*, 9(10):371, 2007.

[97] Roberto Gaiba and Matteo G.A. Paris. Squeezed vacuum as a universal quantum probe. *Physics Letters A*, 373(10):934 – 939, 2009.

[98] G. J. Milburn and Samuel L. Braunstein. Quantum teleportation with squeezed vacuum states. *Phys. Rev. A*, 60(2):937–942, Aug 1999.

[99] A. N. Chaba, M. J. Collett, and D. F. Walls. Quantum-nondemolition-measurement scheme using a kerr medium. *Phys. Rev. A*, 46(3):1499–1506, Aug 1992.

[100] Mark F. Bocko and Roberto Onofrio. On the measurement of a weak classical force coupled to a harmonic oscillator: experimental progress. *Rev. Mod. Phys.*, 68(3):755–799, Jul 1996.

[101] B. Yurke and D. Stoler. Generating quantum mechanical superpositions of macroscopically distinguishable states via amplitude dispersion. *Phys. Rev. Lett.*, 57(1):13–16, Jul 1986.

[102] A. D. Wilson-Gordon, V. Buek, and P. L. Knight. Statistical and phase properties of displaced kerr states. *Phys. Rev. A*, 44(11):7647–7656, Dec 1991.

[103] Kasivishvanathan Sundar. Amplitude-squeezed quantum states produced by the evolution of a quadrature-squeezed coherent state in a kerr medium. *Phys. Rev. A*, 53(2):1096–1111, Feb 1996.

[104] Oliver Glöckl, Ulrik L. Andersen, and Gerd Leuchs. Verifying continuous-variable entanglement of intense light pulses. *Phys. Rev. A*, 73(1):012306, Jan 2006.

[105] A. Imamoḡlu, H. Schmidt, G. Woods, and M. Deutsch. Strongly interacting photons in a nonlinear cavity. *Phys. Rev. Lett.*, 79(8):1467–1470, Aug 1997.

[106] Lene Vestergaard Hau, S. E. Harris, Zachary Dutton, and Cyrus H. Behroozi. Light speed reduction to 17 metres per second in an ultracold atomic gas. *Nature*, 397(6720):594–598, 1999.

[107] Hoonsoo Kang and Yifu Zhu. Observation of large kerr nonlinearity at low light intensities. *Phys. Rev. Lett.*, 91(9):093601, Aug 2003.

[108] Magdalena Stobińska, G. J. Milburn, and Krzysztof Wódkiewicz. Wigner function evolution of quantum states in the presence of self-kerr interaction. *Phys. Rev. A*, 78(1):013810, Jul 2008.

[109] G. J. Milburn, Wen-Yu Chen, and K. R. Jones. Hyperbolic phase and squeeze-parameter estimation. *Phys. Rev. A*, 50(1):801–804, Jul 1994.

[110] B. C. Sanders and G. J. Milburn. Optimal quantum measurements for phase estimation. *Phys. Rev. Lett.*, 75(16):2944–2947, Oct 1995.

[111] G Mauro D'Ariano, Matteo G A Paris, and Paolo Perinotti. Optimal quantum estimation of the coupling between two bosonic modes. *Journal of Optics B: Quantum and Semiclassical Optics*, 3(5):337, 2001.

[112] G. Chiribella, G. M. D'Ariano, and M. F. Sacchi. Optimal estimation of squeezing. *Phys. Rev. A*, 73(6):062103, Jun 2006.

[113] S. Personick. Application of quantum estimation theory to analog communication over quantum channels. *Information Theory, IEEE Transactions on*, 17(3):240 – 246, May 1971.

[114] Dorje C. Brody and Lane P. Hughston. Statistical geometry in quantum mechanics. *Proceedings of the Royal Society of London. Series A: Mathematical, Physical and Engineering Sciences*, 454(1977):2445–2475, 1998.

[115] Marco G. Genoni, Carmen Invernizzi, and Matteo G. A. Paris. Enhancement of parameter estimation by kerr interaction. *Phys. Rev. A*, 80(3):033842, Sep 2009.

[116] Paulina Marian and Tudor A. Marian. Squeezed states with thermal noise. i. photon-number statistics. *Phys. Rev. A*, 47(5):4474–4486, May 1993.

[117] Paulina Marian and Tudor A. Marian. Squeezed states with thermal noise. ii. damping and photon counting. *Phys. Rev. A*, 47(5):4487–4495, May 1993.

[118] H.-P. Breuer and F. Petruccione. *The Theory of Open Quantum Systems*. Oxford University Press, Oxford, 2002.

[119] A. Serafini, M. G. A. Paris, F. Illuminati, and S. De Siena. Quantifying decoherence of continuous variable systems. *J. Phys. B*, 7:R19–R36, 2005.

[120] V D'Auria, C de Lisio, A Porzio, S Solimeno, and Matteo G A Paris. Transmittivity measurements by means of squeezed vacuum light. *Journal of Physics B: Atomic, Molecular and Optical Physics*, 39(5):1187, 2006.

[121] Wojciech Hubert Zurek. Decoherence, einselection, and the quantum origins of the classical. *Rev. Mod. Phys.*, 75(3):715–775, May 2003.

[122] J. B. Brask, I. Rigas, E. S. Polzik, U. L. Andersen, and A. S. Sørensen. Hybrid long-distance entanglement distribution protocol. *Phys. Rev. Lett.*, 105(16):160501, Oct 2010.

[123] K. Jensen, W. Wasilewski, H. Krauter, T. Fernholz, B. M. Nielsen, M. Owari, M. B. Plenio, A. Serafini, M. M. Wolf, and E. S. Polzik. Quantum memory for entangled continuous-variable states. *Nat Phys*, 7(1):13–16, 2011.

[124] M. Brune, J. Bernu, C. Guerlin, S. Deléglise, C. Sayrin, S. Gleyzes, S. Kuhr, I. Dotsenko, J. M. Raimond, and S. Haroche. Process tomography of field damping and measurement of fock state lifetimes by quantum nondemolition photon counting in a cavity. *Phys. Rev. Lett.*, 101(24):240402, Dec 2008.

[125] H. Wang, M. Hofheinz, M. Ansmann, R. C. Bialczak, E. Lucero, M. Neeley, A. D. O'Connell, D. Sank, J. Wenner, A. N. Cleland, and John M. Martinis. Measurement of the decay of fock states in a superconducting quantum circuit. *Phys. Rev. Lett.*, 101(24):240401, Dec 2008.

[126] Anthony Chefles. Quantum state discrimination. *Contemporary Physics*, 41:401, 2000.

[127] Vladislav Kargin. On the chernoff bound for efficiency of quantum hypothesis testing. *The Annals of Statistics*, 33(2):pp. 959–976, 2005.

[128] S. L. Braunstein and A. K. Pati. *Quantum Information Theory with Continuous Variables*. Kluwer Academic, Dordrecht, 2003.

[129] V. D'Auria, S. Fornaro, A. Porzio, S. Solimeno, S. Olivares, and M. G. A. Paris. Full characterization of gaussian bipartite entangled states by a single homodyne detector. *Phys. Rev. Lett.*, 102(2):020502, Jan 2009.

[130] Hannah Venzl and Matthias Freyberger. Quantum estimation of a damping constant. *Phys. Rev. A*, 75(4):042322, Apr 2007.

[131] G. Adesso, F. Dell'Anno, S. De Siena, F. Illuminati, and L. A. M. Souza. Optimal estimation of losses at the ultimate quantum limit with non-gaussian states. *Phys. Rev. A*, 79(4):040305, Apr 2009.

[132] Alex Monras and Fabrizio Illuminati. Information geometry of gaussian channels. *Phys. Rev. A*, 81(6):062326, Jun 2010.

[133] Alex Monras and Fabrizio Illuminati. Measurement of damping and temperature: Precision bounds in gaussian dissipative channels. *Phys. Rev. A*, 83(1):012315, Jan 2011.

[134] Harold Ollivier and Wojciech H. Zurek. Quantum discord: A measure of the quantumness of correlations. *Phys. Rev. Lett.*, 88(1):017901, Dec 2001.

[135] Wojciech Hubert Zurek. Quantum discord and maxwell's demons. *Phys. Rev. A*, 67(1):012320, Jan 2003.

[136] Marco Piani, Paweł Horodecki, and Ryszard Horodecki. No-local-broadcasting theorem for multipartite quantum correlations. *Phys. Rev. Lett.*, 100(9):090502, Mar 2008.

[137] A. Ferraro, L. Aolita, D. Cavalcanti, F. M. Cucchietti, and A. Acín. Almost all quantum states have nonclassical correlations. *Phys. Rev. A*, 81(5):052318, May 2010.

[138] H Scutaru. Fidelity for displaced squeezed thermal states and the oscillator semigroup. *Journal of Physics A: Mathematical and General*, 31(15):3659, 1998.

[139] Stefano Olivares, Matteo G. A. Paris, and Ulrik L. Andersen. Cloning of gaussian states by linear optics. *Phys. Rev. A*, 73(6):062330, Jun 2006.

[140] Paulina Marian, Tudor A. Marian, and Horia Scutaru. Distinguishability and nonclassicality of one-mode gaussian states. *Phys. Rev. A*, 69(2):022104, Feb 2004.

[141] J Jordan and Wigner E. *Z. Phys.*, 47:631, 1928.

[142] Antonella De Pasquale and Paolo Facchi. xy model on the circle: Diagonalization, spectrum, and forerunners of the quantum phase transition. *Phys. Rev. A*, 80(3):032102, Sep 2009.

[143] Elliott Lieb, Theodore Schultz, and Daniel Mattis. Two soluble models of an antiferromagnetic chain. *Ann. Phys*, 16:407, 1961.

[144] Subir Sachdev. *Quantum Phase Transitions*. Cambridge: University Press, 1999.

[145] Paolo Zanardi, Lorenzo Campos Venuti, and Paolo Giorda. Bures metric over thermal state manifolds and quantum criticality. *Phys. Rev. A*, 76(6):062318, Dec 2007.

[146] L. Campos Venuti, C. Degli Esposti Boschi, M. Roncaglia, and A. Scaramucci. Local measures of entanglement and critical exponents at quantum phase transitions. *Phys. Rev. A*, 73(1):010303, Jan 2006.

[147] Paolo Zanardi, Paolo Giorda, and Marco Cozzini. Information-theoretic differential geometry of quantum phase transitions. *Phys. Rev. Lett.*, 99(10):100603, Sep 2007.

[148] Tobias J. Osborne and Michael A. Nielsen. Entanglement in a simple quantum phase transition. *Phys. Rev. A*, 66(3):032110, Sep 2002.

[149] G. Vidal, J. I. Latorre, E. Rico, and A. Kitaev. Entanglement in quantum critical phenomena. *Phys. Rev. Lett.*, 90(22):227902, Jun 2003.

[150] L.-A. Wu, M. S. Sarandy, and D. A. Lidar. Quantum phase transitions and bipartite entanglement. *Phys. Rev. Lett.*, 93(25):250404, Dec 2004.

[151] Thiago R. de Oliveira, Gustavo Rigolin, Marcos C. de Oliveira, and Eduardo Miranda. Multipartite entanglement signature of quantum phase transitions. *Phys. Rev. Lett.*, 97(17):170401, Oct 2006.

[152] Luigi Amico, Rosario Fazio, Andreas Osterloh, and Vlatko Vedral. Entanglement in many-body systems. *Rev. Mod. Phys.*, 80(2):517–576, May 2008.

[153] Paolo Zanardi and Nikola Paunković. Ground state overlap and quantum phase transitions. *Phys. Rev. E*, 74(3):031123, Sep 2006.

[154] Marco Cozzini, Paolo Giorda, and Paolo Zanardi. Quantum phase transitions and quantum fidelity in free fermion graphs. *Phys. Rev. B*, 75(1):014439, Jan 2007.

[155] Marco Cozzini, Radu Ionicioiu, and Paolo Zanardi. Quantum fidelity and quantum phase transitions in matrix product states. *Phys. Rev. B*, 76(10):104420, Sep 2007.

[156] Lorenzo Campos Venuti and Paolo Zanardi. Quantum critical scaling of the geometric tensors. *Phys. Rev. Lett.*, 99(9):095701, Aug 2007.

[157] P. Buonsante and A. Vezzani. Ground-state fidelity and bipartite entanglement in the bose-hubbard model. *Phys. Rev. Lett.*, 98(11):110601, Mar 2007.

[158] Min-Fong Yang. Ground-state fidelity in one-dimensional gapless models. *Phys. Rev. B*, 76(18):180403, Nov 2007.

[159] K. Huang. *Statistical Mechanics*. John Wiley and Sons, New York, 1987.

[160] X. G. Wen and Q. Niu. Ground-state degeneracy of the fractional quantum hall states in the presence of a random potential and on high-genus riemann surfaces. *Phys. Rev. B*, 41(13):9377–9396, May 1990.

[161] Paolo Zanardi, Marco Cozzini, and Paolo Giorda. Ground state fidelity and quantum phase transitions in free fermi systems. *Journal of Statistical Mechanics: Theory and Experiment*, 2007(02):L02002, 2007.

[162] Huan-Qiang Zhou and John Paul Barjaktarevi. Fidelity and quantum phase transitions. *Journal of Physics A: Mathematical and Theoretical*, 41(41):412001, 2008.

[163] Samuel L. Braunstein, Carlton M. Caves, and G. J. Milburn. Generalized uncertainty relations: Theory, examples, and lorentz invariance. *Annals of Physics*, 247(1):135 – 173, 1996.

[164] Richard Jozsa. Fidelity for mixed quantum states. *Journal of Modern Optics*, 41(12):2315 – 2323, 1994.

[165] Dorje C. Brody and Lane P. Hughston. Statistical geometry in quantum mechanics. *Proceedings of the Royal Society of London. Series A: Mathematical, Physical and Engineering Sciences*, 454(1977):2445–2475, 1998.

[166] A. Sun-Ichi and H. Nagaoka. *Methods of Information Geometry*. American Mathematical Society, Providence, 2000.

[167] L. LeCam. *Asymptotic Methods in Statistical Decision Theory*. Springer-Verlag, New York, 1986.

[168] Carmen Invernizzi and Matteo G. A. Paris. The discrimination problem for two ground states or two thermal states of the quantum ising model. *Journal of Modern Optics*, 57(3):198, 2010.

[169] B. Bauer, M. Troyer, V. W. Scarola, and K. B. Whaley. Distinguishing phases with ansatz wave functions. *Phys. Rev. B*, 81(8):085118, Feb 2010.

[170] Huan-Qiang Zhou, Roman Orús, and Guifre Vidal. Ground state fidelity from tensor network representations. *Phys. Rev. Lett.*, 100(8):080601, Feb 2008.